

2011

Ru-Ni-Al₂O₃ CATALYSTS FOR SUPERCRITICAL WATER GASIFICATION OF GLUCOSE

Md. Zakir Hossain

Follow this and additional works at: <https://ir.lib.uwo.ca/digitizedtheses>

Recommended Citation

Hossain, Md. Zakir, "Ru-Ni-Al₂O₃ CATALYSTS FOR SUPERCRITICAL WATER GASIFICATION OF GLUCOSE" (2011). *Digitized Theses*. 3491.
<https://ir.lib.uwo.ca/digitizedtheses/3491>

This Thesis is brought to you for free and open access by the Digitized Special Collections at Scholarship@Western. It has been accepted for inclusion in Digitized Theses by an authorized administrator of Scholarship@Western. For more information, please contact wlsadmin@uwo.ca.

Ru-Ni-Al₂O₃ CATALYSTS FOR SUPERCRITICAL WATER GASIFICATION OF GLUCOSE

(Spin Title: Supercritical Water Gasification)

(Thesis format: Integrated-Article)

by

Md. Zakir Hossain

Graduate Program in Engineering Science

Department of Chemical and Biochemical Engineering

A thesis submitted in partial fulfillment

of the requirements for the degree of

Master of Engineering Science

The School of Graduate and Postdoctoral Studies

The University of Western Ontario

London, Ontario, Canada

© Md. Zakir Hossain 2011

THE UNIVERSITY OF WESTERN ONTARIO
SCHOOL OF GRADUATE AND POSTDOCTORAL STUDIES

CERTIFICATE OF EXAMINATION

Supervisor

Prof. Paul A. Charpentier

Supervisory Committee

Prof. Madhumita B. Ray

Prof. George Nakhla

Examiners

Prof. Cedric Briens

Prof. Andy Sun

Prof. George Nakhla

The thesis by

Md. Zakir Hossain

Entitled:

Ru-Ni-Al₂O₃ Catalysts for Supercritical Water Gasification of Glucose

is accepted in partial fulfillment of the
requirements for the degree of
Master of Engineering Science

Date

Chair of Thesis Examination Board

ABSTRACT & KEYWORDS

Application of biomass and waste for renewable energy sources is gaining an important role in the world's future energy policy as we are facing a tremendous challenges related to energy and the environment, in particular energy sustainability while reducing carbon emissions from fossil fuels. Supercritical water gasification (SCWG) presents an innovative technology for complete and efficient destruction of biomass or wastes without formation of harmful by-products. The major products formed during supercritical water gasification of biomass are hydrogen, carbon monoxide, methane and carbon dioxide with clean water effluents. Catalysts enhance the overall gasification efficiency as well as the organic carbon destruction in the liquid effluents to enable drinking quality water as the effluent. Since SCWG is a hydrothermal process and catalyst deactivation always occurs in high temperature processes due to coke deposition on the catalyst surface, the aim of this study is to prepare noble and non-noble metal based catalyst on alumina support to reduce the graphitic coke formation during supercritical water gasification. Usually non-noble metal based catalysts are used in high temperature gasification because of their ready availability and low cost but this study showed that introduction of a small amount of noble metal onto non-noble based catalysts greatly influenced the catalyst performance while reducing the graphitic coke formation. In this research, supercritical water gasification (SCWG) of a model biomass compound was studied to produce hydrogen rich gas at moderate temperatures (400-500°C). The catalysts were synthesized by different procedures, evaluated and characterized (fresh and spent) to study the catalyst role in SCWG. The catalysts studied were synthesized by

incipient wetness impregnation and a sol-gel method with and without various templates, respectively to compare the catalytic performance based on their synthetic procedures.

It was found that the templating synthesis of catalysts increased the surface area as well as pore volume & strong metal support interactions in the catalysts which play an important role in SCWG. The aerogel catalyst prepared from sol-gel synthesis with supercritical CO₂ drying also enabled a catalyst to be produced with a large surface area and strong metal support interaction. The most important finding of this study was to reduce graphitic coke formation during gasification because of the presence of ruthenium metal in the catalyst structure.

To the best of our knowledge, the resulting hydrogen yield, total organic carbon (TOC) destruction and gasification efficiency were significantly higher using the novel aerogel and templated Ru-Ni-Al₂O₃ catalysts than any other reported results for SCWG of any biomass compound at moderate temperatures (~500 °C) and pressures (~25 MPa).

A global kinetic model for TOC destruction in supercritical water was developed using non-linear regression, which convincingly fit the experimental results showing the significant effect of water in SCWG of model biomass compound.

Key Words: Supercritical water gasification, Catalysts, Supercritical CO₂ drying, Coke deposition, Kinetics of TOC destruction.

Co-Authorship

Title: Ru-Ni-Al₂O₃ catalysts for the supercritical water gasification of glucose (Chapter 3).

Authors: Md. Zakir Hossain, Muhammad B.I. Chowdhury, and Paul A. Charpentier.

The catalysts development, experimental works and the liquid analysis were conducted by myself under the guidance of advisor Dr. Paul A. Charpentier. Dr. Muhammad B.I. Chowdhury provided guidance in catalyst preparation and characterization. The draft of this manuscript was written by Md. Zakir Hossain. Modifications were carried out under close supervision of Dr. Paul A. Charpentier. The final version of this article was submitted to the journal Applied Catalysis A: General.

Title: Kinetic analysis for TOC destruction of glucose by supercritical water gasification (Chapter 4).

Authors: Md. Zakir Hossain, Muhammad B.I. Chowdhury, and Paul A. Charpentier.

A global kinetic model for TOC destruction in supercritical water was developed by myself using Dr. Muhammad B.I. Chowdhury's MATLAB program for non-linear regression of the model. The draft of this manuscript was written by myself and modifications were carried out under close supervision of advisor Dr. Paul A. Charpentier. The final version of this article was submitted to the journal Industrial Engineering and Chemistry Research.

Title: Synthesis, characterization & evaluation of catalytic properties of Ni & Ru supported on ordered mesoporous alumina (Chapter 5).

Authors: Md. Zakir Hossain, Qasem Alsharari, and Paul A. Charpentier.

Metal supported mesoporous alumina catalysts were synthesized using different templates by myself under the guidance of advisor Dr. Paul A. Charpentier. Qasem Alsharari helped with developing the synthetic methodology. The draft of this manuscript was written by myself and modifications were carried out by advisor Dr. Paul A. Charpentier. The final version of this article was submitted to the journal Microporous and Mesoporous Materials.

Dedication

To my parents:

Late Md. Hossain Uddin
&
Angura Khathon

ACKNOWLEDGEMENT

First and foremost I would like to convey my grateful appreciation to my supervisor Prof. Paul A. Charpentier, who has been my supervisor, mentor, and friend throughout my entire graduate education. His meticulous supervision not only ensured the successful fulfillment of this study but also brought great improvement of my comprehension skills, which I will enjoy for ever. I gratefully acknowledge to my committee members, Prof. Madhumita B. Ray & Prof. George Nakhla for their guidance and support.

I am indebted to all the people whose knowledge and experience have been so valuable to the success of my work. I would like to thank Dr. Emhemmed A. Youssef & Dr. Muhammad B.I. Chowdhury for assembling the SCW reactors, Dr. Muhammad B.I. Chowdhury for his contribution, especially catalyst preparation and characterization, Qasem Alsharari for his help to synthesize mesoporous catalysts. I have been indebted to Dr. Yaocihuatl Medina, Dr. Edward S. Xiao, Dr. Behnaz Hojjati & Dr. SM Zahangir Khaled, my former colleagues of the research group, for sharing their scientific and technical knowledge and experiences on initiating my research.

I'd like to express my passion to all the colleagues in my group: Nasrin, Jeff, Sahar, Lin, Rajib, Mehernaz, Sepideh, Jenna, Golam, Mumin, Farida, Adria, Gu and Tang. Thanks for your assistance in the lab, being a place to bounce ideas off of and keeping it light and fun in the lab & office. You guys were an inspiration.

I'd like to express my sincere gratitude to the university machine services and Mr. Chris Vandelaar for troubleshooting of SCW unit, Dr. Pastor Solano-Flores for TOC, Dr. Hossein Kazemian for XRD, and Prof. Richard Gardiner for TEM & Dr. Tim Goldhawk for SEM analysis.

In addition, I wish to thank the Canadian Foundation for Innovation-Leading Edge (CFI-LE) program for infrastructure funding, the National Science and Engineering Research Council (NSERC) and the Agricultural Biorefinery Innovation Network (ABIN) program for operational funding.

TABLE OF CONTENTS

Certificate of Examination	ii
Abstract and Keywords	iii
Co-Authorship	v
Dedication	vii
Acknowledgements	viii
Table of contents	x
List of Tables	
List of figures	
CHAPTER ONE	1
General Introduction	1
1.1 Motivation for Choosing Biomass as Energy Source	1
1.2 Composition of Biomass	3
1.3 Biomass Processing Technology	6
1.4 Uses of Catalyst	10
1.5 Synthesizing Aerogel Catalyst	14
1.6 Synthesis of Ordered Mesoporous Catalyst	14
1.7 Selection of Model Compound	15
1.8 Objectives	16
1.9 Organization of Thesis	16
References	18

CHAPTER TWO	25
Literature Review	25
2.1 Introduction	25
2.2 Supercritical Water	27
2.3 Kinetics	29
2.4 Catalytic Supercritical Water Gasification	32
2.4.1 Carbon Catalysts	34
2.4.2 Alkaline Catalysts	35
2.4.3 Metal & Metal Oxide Catalysts	36
2.4.4 Other Catalysts	39
2.4.5 Catalyst Supports	39
2.5 Process Parameters & Their Effects	40
2.5.1. Effect of Temperature	41
2.5.2. Effect of Pressure	43
2.5.3 Effect of Residence Time	44
2.5.4 Effect of Solution Concentration	45
2.6 Brief Reaction Mechanism	46
2.7 Effect of Catalyst Preparation	48
2.8 Synthesis of Ordered Mesoporous Materials	49
2.9 Challenges	52
References	54

CHAPTER THREE	67
Ru-Ni-Al ₂ O ₃ catalysts for the supercritical water gasification of glucose	67
3.1 Introduction	67
3.2 Experimental	71
3.2.1 Materials	71
3.2.2 Catalyst preparation	71
3.2.3 Catalyst characterization	73
3.2.4 Catalyst testing	75
3.3. Results and discussion	77
3.3.1 Optimization of ruthenium concentration	77
3.3.2 Characterization of Synthesized Catalysts	79
3.3.3 Catalyst Evaluation	87
3.3.4 Characterization of spent catalysts	91
3.4 Conclusions	96
References	97
CHAPTER FOUR	103
Kinetic analysis for TOC destruction of glucose by supercritical water gasification	103
4.1 Introduction	103
4.2 Experimental	106
4.2.1 Materials	106

4.2.2 Methods	106
4.3 Results & Discussion	107
4.3.1 Effect of Reaction Time and Temperature	107
4.3.2 Effect of concentration	111
4.4 Reaction Kinetics of TOC destruction	113
4.4.1 Model one	113
4.4.2 Model two	117
4.5 Conclusion	122
References	123
CHAPTER FIVE	126
Synthesis and characterization of mesoporous alumina with nickel & ruthenium incorporated for use in glucose gasification in supercritical water	126
5.1 Introduction	126
5.2 Experimental	129
5.2.1 Materials	129
5.2.2 Preparation & Characterization	130
5.2.3 Catalyst Testing	132
5.3 Results & Discussion	134
5.3.1 Characterization of mesoporous catalysts	134
5.3.2 Catalyst Evaluation	150
5.3.3 Characterization of spent catalysts	154

5.4 Conclusion	159
References	161
CHAPTER SIX	166
Conclusion	166
Reference	168
APPENDIX	169
CURRICULUM VITAE	184

LIST OF THE TABLES

Table 1.1. Moisture content in several common biomass wastes.	8
Table 1.2. A comparison of energy conversion efficiency of different options for biomass conversion.	9
Table 3.1. BET surface area, pore size and pore volume of the catalysts.	79
Table 3.2. Pulse chemisorption data.	83
Table 4.1. Summary of experimental TOC data.	112
Table 4.2. Summary of TOC data for model one.	116
Table 4.3. Summary of TOC data for model two.	120
Table 5.1. BET surface area, pore size and pore volume of the synthesized mesoporous materials.	134
Table 5.2. Pulse chemisorption data.	142
Table 5.3. Comparing different catalysts activity for producing hydrogen & carbon monoxide yield, TOC destruction and CGE at 500°C.	151

LIST OF FIGURES

Fig. 1.1. Share of bioenergy in the world primary energy mix.	3
Fig. 1.2. Structure of Glucose.	4
Fig. 1.3. Structures of the main components of hemicellulose.	4
Fig. 1.4. Chemical Structure of the main components of lignin.	5
Fig. 1.5. Number of hits in ISI database for “supercritical water” + “catal*”.	11
Fig. 2.1. Schematic phase diagram of water.	28
Fig. 2.2. Simplified reaction scheme of liquefaction and/or gasification of biomass model compound.	30
Fig. 2.3. Variation of product yields with temperature for glucose hydrolysis at 24.6 MPa. Experimental conditions: $1.02 \pm 0.02 \times 10^{-3}$ mol/L glucose, 6.1 ± 0.3 s reactor residence time. No catalyst.	42
Fig. 2.4. Gas product yields as a function of reactor temperature on 0.6 M glucose gasification in SCW at 28 MPa and a 30 s reactor residence time. No catalyst.	43
Fig. 2.5. Effect of pressure over 5wt. % Ru/Al ₂ O ₃ catalyst with 10 wt % Ethanol.	44
Fig. 2.6. Time dependence of the yields of all products for ethanol reaction in a batch reactor at a density of 0.20 g/cm ³ at 500°C.	45
Fig. 2.7. Schematic showing reaction pathways (gasification and dehydration) for the hydrothermal treatment of glucose.	47

Fig. 3.1. Effect of ruthenium concentration on (a) hydrogen & (b) methane yield, Feed=0.25M Glucose, t=30 minutes, T=500°C, P=25 MPa, catalyst 1.0 gm.	78
Fig. 3.2. N ₂ adsorption–desorption isotherms of aerogel and impregnation catalysts.	80
Fig. 3.3. (a) ATR-FTIR analysis results of as prepared and calcined aerogel catalyst. (b) TG-DTA profiles of as prepared drying aerogel.	82
Fig. 3.4. XRD patterns of impregnation and aerogel catalysts.	84
Fig. 3.5. H ₂ -TPR profile of impregnation & aerogel catalysts.	86
Fig. 3.6. Temperature effect on product distribution during non-catalytic & catalytic gasification of glucose in supercritical water, (a) without catalyst (b) impregnation catalyst (c) aerogel catalyst; t=30 min, Feed= 0.25M Glucose, Catalyst 1.0 gm.	89
Fig. 3.7: Effect of catalysts on (a) TOC destruction and (b) CGE; t=30 min, Feed= 0.25M Glucose, Catalyst 1.0 gm.	91
Fig. 3.8. TPO profiles of spent catalysts.	93
Fig. 3.9. Comparison of XRD pattern of fresh & spent catalysts.	94
Fig.3.10. SEM & TEM micrographs of catalysts, (a&c) & (b&d): fresh & spent impregnation (crushed) and (e&g) & (f&h): fresh & spent aerogel catalysts respectively.	95

calcined samples synthesized by P-123, surfactant & without P-123/surfactant respectively. (ii) TG-DTA profiles of as prepared mesoporous catalysts. 139

Fig. 5.3. XRD patterns of mesoporous catalysts. (a), (c) & (e): fresh and (b), (d) & (f): reduced samples synthesized by P-123, surfactant & without P-123/surfactant respectively. (○ Al₂O₃, ▲ nickel, ■ NiO, ● RuO₂, □ Ru). 143

Fig. 5.4. TPR curves of synthesized catalysts by (a) P-123 (b) surfactant (c) non-templating respectively. 146

Fig. 5.5. SEM images of mesoporous catalysts. (a), (c) & (e) and (b), (d) & (f): fresh & reduced catalysts synthesized by P-123, surfactant and without P-123/surfactant. 148

Fig. 5.6. TEM images of mesoporous catalysts. (a), (c) & (e) and (b), (d) & (f): fresh & reduced catalysts synthesized by P-123, surfactant and without P-123/surfactant. 149

Fig. 5.7. Gasification of glucose in supercritical water using mesoporous catalysts, (a) & (c) synthesized by P-123 (b) & (d) synthesized by surfactant; t=30 min, Feed= 0.25M Glucose, Catalyst 1.0 gm. 150

Fig. 5.8. TG-DTA & TPO curves of spent catalysts. 156

Fig. 5.9. XRD (a&c: fresh reduced and b&d: spent mesoporous catalysts synthesized by P-123 & surfactant respectively) & Raman spectra of spent catalysts. 157

Fig. 5.10. SEM & TEM images of spent catalysts (a&c: reduced catalyst synthesized by P-123 & b&d: reduced catalysts synthesized by surfactant).

158

Fig. 5.11. Pore size distribution & TPR curves for spent catalysts.

159

CHAPTER ONE

General Introduction

1.1 Motivation for Choosing Biomass as Energy Source

Energy, Environment, and the Economy – the three big E's are so interrelated that it is almost impossible to explain any one independently without examining the other two. Dependency on fossil fuels has raised tremendous concerns for long-term environmental impacts, energy security, and the rising costs of living. This has made renewable sources of energy an attractive alternative to address environmental issues as well as to reduce our dependence on imported oil. Among the renewable sources of energy, a substantial focus of research is currently being directed towards the use of biomass. Biomass for energy has many positive attributes that contribute to both a healthy environment and economy. Biomass utilization helps mitigate climate change, reduces risk to life and property, and helps provide a secure and cost competitive energy source.

Biomass is a broad term which identifies organic matter from living and dead plant material to human waste, which is available on a renewable basis, including crops, trees, algae and other plants, as well as agricultural and forest wastes and residues. It also includes many materials that are considered as wastes by our society including food processing effluents, sludges, manures, industrial (organic) by-products and the organic fraction of household waste. Many of these wastes, such as agricultural residues and sewage sludge, have been employed in thermochemical conversion processes to produce fuels (gases and liquids) from biomass, and simultaneously eliminate residues.

There are many other advantages associated with using biomass due to its widespread abundance. Its use does not increase the net amount of CO₂ in the atmosphere. The combustion of carbon based fuels (which includes fossil fuels like oil, coal and gas, but also biomass) releases carbon dioxide into the atmosphere, which acts as a 'greenhouse' gas and its increased concentration is believed to result in global warming and climate change. The crucial difference between fossil fuels and biomass lies in the time frame over which carbon dioxide is released. Burning fossil fuels releases the carbon that has been locked up for millions of years. Burning biomass, however, can be a part of the natural process called the carbon cycle i.e. plants take up carbon dioxide when they grow to construct the organic biological molecules that make up the bulk of their dry mass, and when the plants are eaten, burned or decomposed, the carbon is released again and returned to the pool of carbon dioxide in the atmosphere.

At present, forestry, agricultural and municipal residues and wastes are the main feedstocks for the generation of electricity and heat from biomass. In addition, small amounts of sugar, grain, and vegetable oil crops are used as feedstocks for the production of liquid biofuels. Today, biomass supplies some 50 EJ globally, which represents 10% of global annual primary energy consumption.

This is mostly traditional biomass used for cooking and heating (Figure 1.1) [1].

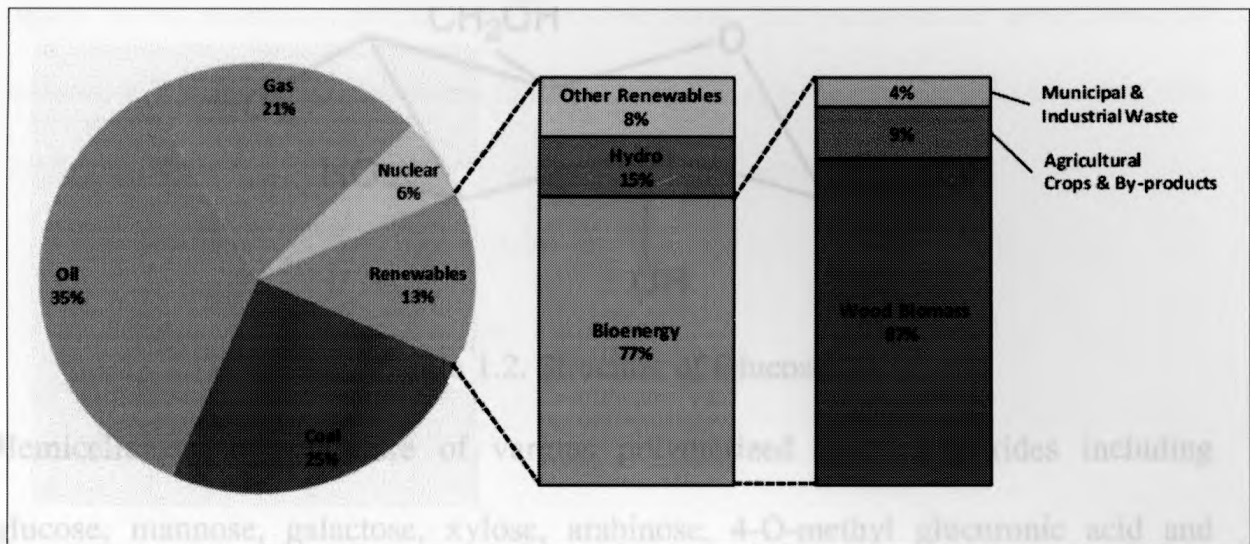


Figure 1.1. Share of bioenergy in the world primary energy mix.

1.2 Composition of Biomass

The chemical structure and major organic components in biomass are extremely important in the development of processes for producing derived fuels and chemicals [2]. Biomass is typically composed of cellulose, hemicellulose, lignin, and small percentages of other substances including minerals and organic molecules [3-5]. Cellulose and hemicellulose are high molecular weight compounds, present in hardwoods (78.8%) and softwoods (70.3%), with lignin present more in softwoods (29.2%) rather than hardwoods (21.7%) [6].

Cellulose is a linear biopolymer composed of D-glucose units connected by β -glycosidic bonds, which usually appears as a highly crystalline material [7]. Glucose anhydride, which is formed via the removal of water from each glucose residue, is polymerized into long cellulose chains that contain 5000-10000 glucose units. The basic repeating unit of the cellulose polymer consists of two glucose anhydride units, called a cellobiose unit [8]. The chemical structure of glucose is shown in Figure 1.2 [9].

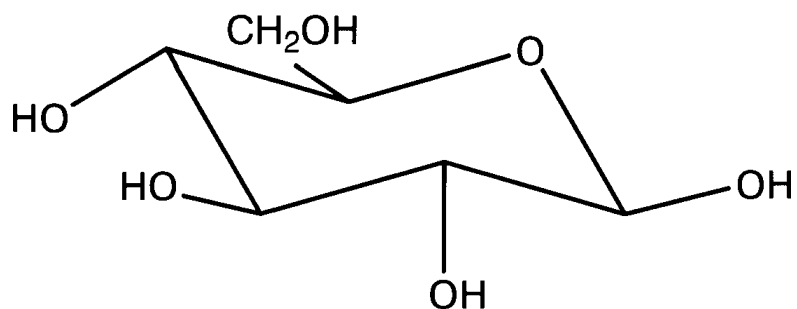


Figure 1.2. Structure of Glucose.

Hemicellulose is a mixture of various polymerized monosaccharides including glucose, mannose, galactose, xylose, arabinose, 4-O-methyl glucuronic acid and galacturonic acid residues [8]. Hemicellulose has low degrees of polymerization (50-300). The main components of hemicellulose are shown in Figure 1.3 [9].

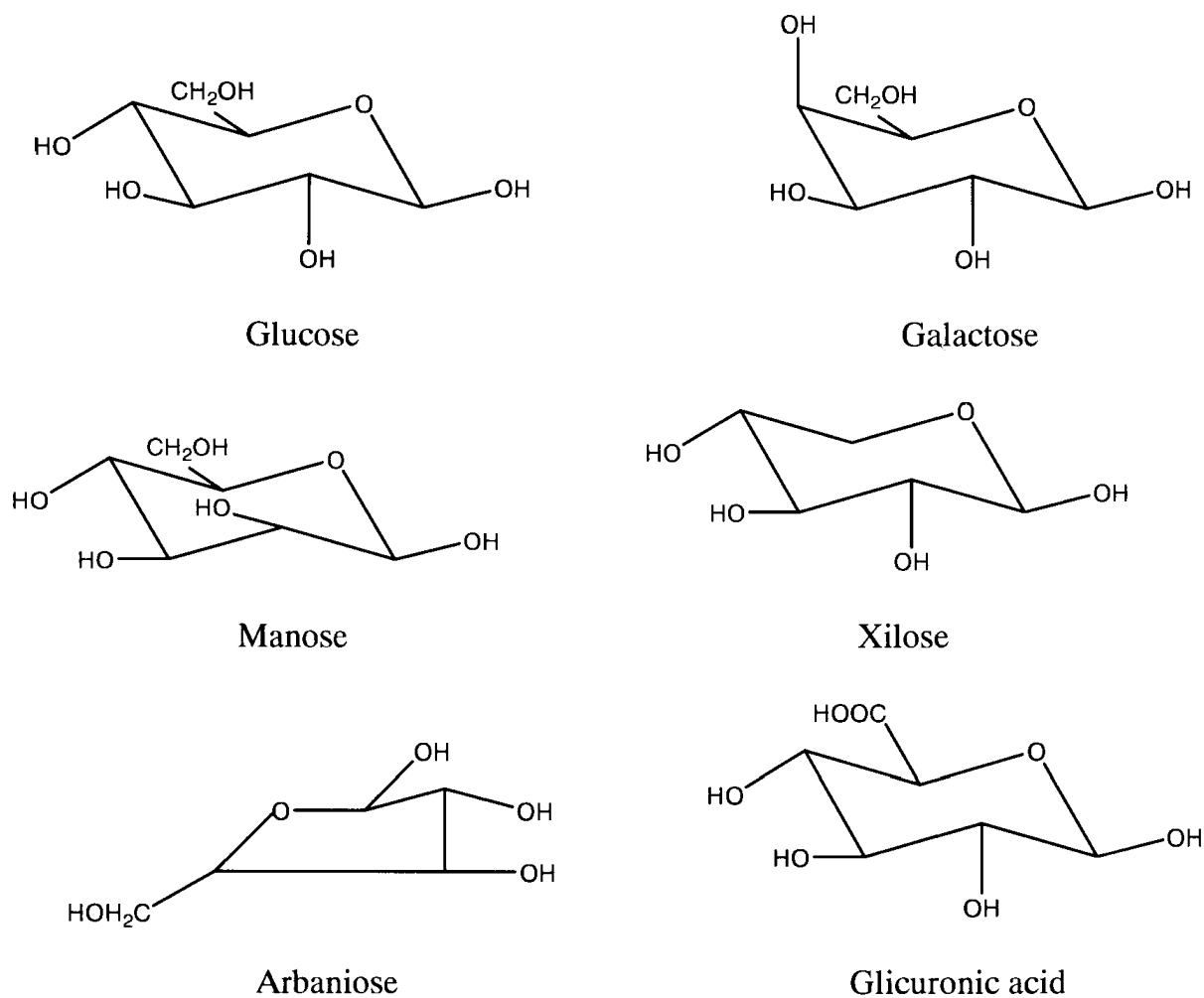


Figure 1.3. Monosaccharide Structures of the main components of hemicellulose.

Lignin is an aromatic polymer synthesised from phenylpropanoid precursors. Its structure in a three-dimensional macromolecular network provides high chemical stability [3, 9], with the main components lignin are shown in Figure 1.4.

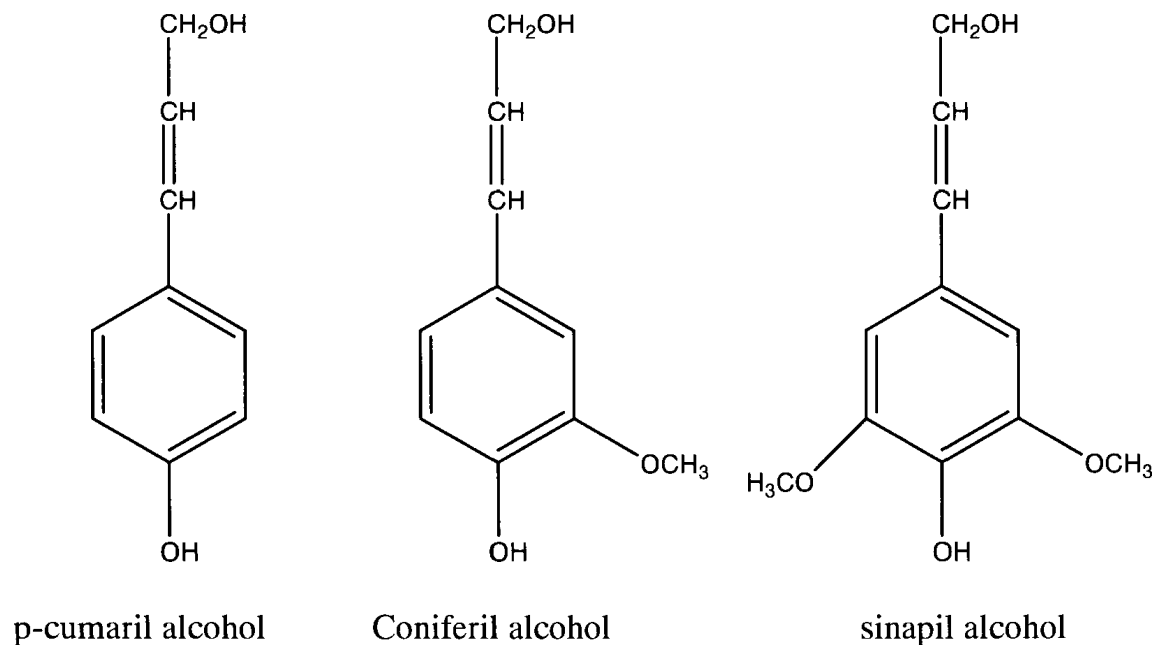


Figure 1.4. Chemical Structure of the main components of lignin.

To understand the complex nature of biomass gasification reactions, model compounds, which represent basic structures found within the biomass components, must first be studied. Glucose represents the basic building block of cellulose and was the focus of this research. Once the glucose conversion is understood, more feedstocks representing higher degrees of polymerization will need to be studied.

The most important difference between biomass and fossil fuels, in terms of their compositions, is oxygen content. Biomass feedstocks often contain 40-60 wt% oxygen compared to conventional fuels which are mostly hydrocarbons. There are some advantages and disadvantages to the use of biomass containing oxygen. For fossil fuels, the steam reforming reactions of hydrocarbons for H₂ production are endothermic. Conventional steam reforming of petroleum depends on heat provided by the combustion of additional hydrocarbons. In contrast, oxygenated compounds

such as the biomass components are able to form alkanes through exothermic reaction pathways, meaning that the energy required for the aqueous-phase reforming may be produced internally. In this respect, the formation of a mixture of H₂ and alkanes from aqueous-phase reforming of glucose is essentially neutral energetically, with little additional energy required to drive the reaction [10].

On the other hand, hydrocarbons are usually better quality fuels. For instance, for oils, high oxygen content can impart a number of undesirable qualities to the oil product, such as lower energy content, poor thermal stability, lower volatility, higher corrosivity, and a tendency to polymerize. For this reason, when producing fuels from biomass, one overall objective is to remove oxygen and create fuels with as high of a H: C ratio as possible [11].

1.3 Biomass Processing Technology

Various technologies have been used to obtain fuel/energy from biomass. Normally these processes differ on how much O₂ is present in the reactor. For instance, in combustion there is an excess of O₂ relative to the amount necessary for stoichiometric oxidation of the feedstock. In this case the energy (heat) is obtained directly in one step, but if there are plans of using biomass as a source of energy for the transportation sector, the fuel needs to be in a form suitable for use in engines or fuel cells.

In pyrolysis, a non-reactive gas is used in the reactor (absence of O₂) to avoid oxidation and allow the heat to break the large molecules into smaller ones. In the context of biomass, pyrolysis commonly refers to a lower temperature thermal process producing liquids as the primary product. In addition to liquid fuels, pyrolysis can also yield gasses, charcoal, and useful chemical and food products. Traditional slow

pyrolysis has been used to produce charcoal for many years. Fast or flash pyrolysis uses a moderate temperature and much shorter residence time to obtain liquid yields up to 70% and char yields below 5% [12]. However both slow and fast pyrolysis processes require drying of wet feedstocks, adding considerable expense to the overall process.

Gasification is a technology that employs a reaction medium with O₂ content below the stoichiometric amount required for combustion. O₂ (or air) causes partial combustion and maintains the high reaction temperatures (> 700°C) [13], so that the biomass feedstock decomposes by pyrolysis reactions into lighter compounds such as H₂, CH₄, CO₂ and CO [11, 14, 15]. Once produced, applications for the obtained gases are very wide, for example, they can be used in gas turbines, fuel cells or in the synthesis of chemicals [16]. The present work focuses on gasification.

Biomass gasification has been facing several technical difficulties which prevent its utilization at large scale. Much of the biomass resource is composed of material with higher levels of moisture, typically 50 wt % or higher often consisting of wet biomass or biomass in water slurries at 85 % moisture or higher. Examples are sewage sludge, cattle manure and food industry waste (Table 1.1). For water contents above 40 %, the thermal efficiency of a conventional gasification plant decreases dramatically [17] due to the energy required to dry the feedstock.

Table 1.1. Moisture content in several common biomass wastes [18].

Biomass Type	Moisture Content (% wet basis)
Wheat straw	8-20
Sawdust	25-55
RDF pellet	25-35
Wood bark	30-60
Corn Stalk	40-60
Rice Straw	50-80
Food Waste	70
Cattle Manure	88
Water hyacinth	95.3

As shown in Table 1.2, at above 31% moisture content, the energy conversion efficiency of supercritical water gasification (SCWG) is always higher than that of thermal gasification, pyrolysis, liquefaction, and anaerobic digestion. Gasification of biomass in supercritical water offers an attractive alternative to avoid the energy intensive drying process, particularly when the water content is above 30%.

Table 1.2. A comparison of energy conversion efficiency of different options for biomass conversion [16].

Moisture content in feed	5%	31%	55%	75%
Biomass conversion means	Energy conversion efficiency (%)			
Pyrolysis	57	53	45	27
Thermal gasification	61	55	47	27
Liquefaction	39	37	36	34
Anaerobic digestion	31	31	31	31
Supercritical water gasification	55	55	55	55

SCWG is an attractive method for converting wet biomass [15, 17, 19-25] or aqueous organic wastes [26-28] completely into combustible gases without a drying procedure as a pretreatment of the feedstock. An objective of SCWG operation is to produce hydrogen-rich gas while gasification at subcritical water temperatures (less than 374 °C) results in a product gas rich in methane [29]. It is known that the formation of hydrogen predominates over that of methane at high temperature [30]. For example, Antal and co-workers [15, 17, 19] achieved complete gasification of a variety of organic compounds including whole biomass such as water hyacinth, banana tree stem, sewage sludge, wood sawdust, and sugar cane bagasse in supercritical water under conditions with temperatures above 600 °C, pressures of 28-34.5 MPa, and reactor residence times of less than 1 min. Major products formed in their continuous flow system were hydrogen and carbon dioxide with clean water effluents. The

current status of SCWG technology and research development is summarized by Kruse [30] and Matsumura et al. [31].

The potential applicability of supercritical water to treat biomass or its components is mainly due to the unique thermophysical properties of supercritical water. The major properties of supercritical water, such as density, viscosity, dielectric constant, and hydrogen bonding are quite different from those of steam or liquid water. Supercritical water behaves like a nonpolar organic solvent under gasification conditions, and many kinds of organic compounds and gases are completely dissolved in supercritical water, resulting in a single phase [32]. On the other hand, the solubility of inorganic compounds decreases dramatically in supercritical water [33]. Furthermore, water in SCWG processes is not only a solvent but also a major reactant providing a significant influence on the gasification chemistry [15].

Although supercritical water provides a unique environment for the gasification of organic compounds, both the extent of gasification and the composition of gaseous products are very sensitive to reactor walls made of nickel composites [19]. Furthermore, the composition of gaseous effluent from SCWG of glucose significantly depends on the reactant concentration and temperature [17]. These findings have motivated studies of new catalysts to obtain hydrogen-rich gas from the complete gasification of concentrated biomass in supercritical water.

1.4 Uses of Catalyst:

Research into catalysis for SCWG has grown steadily over the last 20 years. Fig. 1.5 shows the number of articles and reviews published every two years since 1986, the first year that the ISI database indicated a hit from a search on “supercritical water” and “catal*”. Since the search terms will also return some papers that make a point of

doing reactions with no added catalyst, the absolute numbers in Figure 1.5 overestimate the number of studies on catalysis in SCW. However, this data does illustrate the trend with time. It is clear that this field has grown nearly exponentially from essentially no archival publications before 1986 to one or two per year in the late 1980s, to over 50 publications annually in recent years.

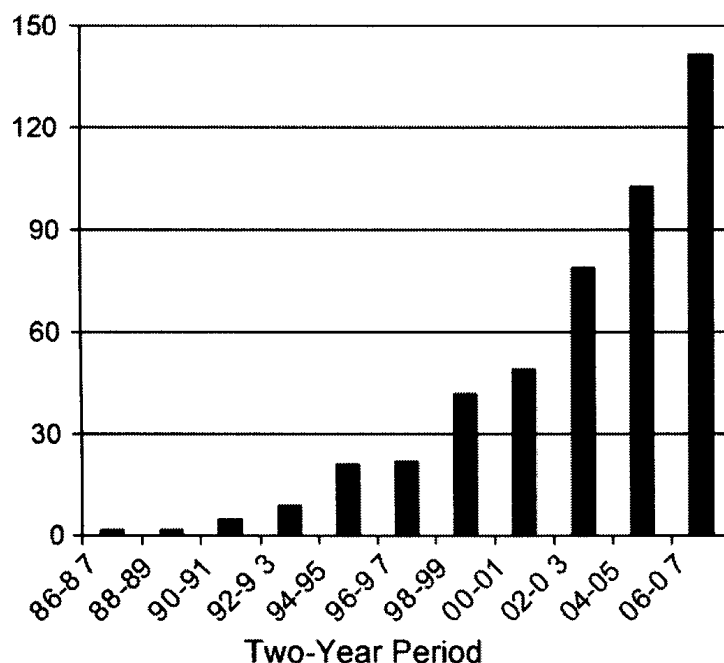


Figure 1.5. Number of hits in ISI database for “supercritical water” + “catal*” [34].

Amin et al. [35] demonstrated experimentally that supercritical water can suppress the char formation during the decomposition of glucose. Char is known to be a refractory byproduct formed in significant amounts during atmospheric steam gasification of biomass [36], or hydrothermal treatments of glucose [35, 37] and cellulose [37, 38] in pressurized liquid-phase water (subcritical water) at temperatures up to 350°C unless an appropriate catalyst is used. The advances in this area have been driven by the need to produce char or tar-free product gas from the gasification of biomass, since the removal of tars and chars and the reduction of the methane content increases the

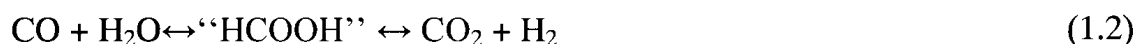
economic viability of the biomass gasification process. The criteria for the catalyst are fundamentally the same and may be summarised as follows:

1. The catalyst must be effective in the removal of tars.
2. If the desired product is syngas, the catalysts must be capable of reforming methane.
3. The catalyst should provide a suitable syngas ratio for the intended process.
4. The catalyst should be resistant to deactivation as a result of carbon fouling and sintering.
5. The catalyst should be easily regenerated.
6. The catalyst should be stable to SCW conditions.
7. The catalyst should be inexpensive.

The effect of alkali metal catalysts (Na_2CO_3 , KHCO_3 , K_2CO_3 , NaOH , etc) on SCWG of biomass has been confirmed by many previous studies. The main characteristic of the catalyst is to improve the water-gas shift reaction.



Kruse et al. [39] reported the catalytic action of KOH on SCWG of pyrocatechol. When the content of KOH increased from 0 to 5%, the production of H_2 and CO_2 increased due to the catalytic effect on the water-gas shift reaction. Compared with KOH , LiOH had similar activity on the gas-phase composition but to a smaller extent. The catalytic effect of NaOH was realized by Watanabe et al. [40], who showed that the water-gas shift reaction was accelerated by adding NaOH . Formic acid was presumed to be the intermediate product in the reaction process, and the production of H_2 and CO_2 was due to decomposition of formic acid.



The yield of CO was inversely proportional to the OH⁻ concentration, which indicates that HCHO reactions are governed by the OH⁻ concentration. This research group conducted another catalytic supercritical water gasification (CSCWG) experiment on n-hexadecane and lignin with NaOH (400°C, 30 MPa). The addition of NaOH enhanced the output of H₂ 4 times greater than that without NaOH. The production of coke was also effectively inhibited [41].

Compared to homogeneous catalysts, heterogeneous catalysts have the advantages of high selectivity, recyclability, environment-friendly, etc, and are becoming of increased interest for SCWG.

Nickel based heterogeneous catalysts are commonly used for SCWG as the cost of nickel is relatively low, and has been applied extensively to many petrochemical industries. Catalytic SCWG of 0.6 M glucose was investigated with 16 wt % Ni/Activated carbon catalyst over a temperature range of 575 to 725°C at 28 MPa [42]. The Ni/Activated carbon was found to catalyze hydrogen production pathways such as the water gas shift reaction and to enhance the carbon gasification efficiency. However, nickel based catalysts enhance coke formation when they are exposed to high temperature. A recent study [43] showed that Ru-Al₂O₃ had much better coke resistance and a lower graphitization degree of deposited carbon than Ni-Al₂O₃ for methane conversion to synthesis gas. This catalyst resulted in high cell performance for a fuel cell when operating on methane-oxygen, methane-H₂O or methane-CO₂ gas mixtures, in the range 600 to 850°C. Byrd et. al. [44] also found that Ru/Al₂O₃ catalyst significantly enhanced the conversion and hydrogen yield from glucose at 700°C and 248 bar, while significantly reducing the coke and other heavier liquid product formation.

1.5 Synthesizing Aerogel Catalyst

Heterogeneous catalysis is one of the most demanding applications of solid state chemistry. It is essential to have good control, not only of the chemistry of the reaction at the catalyst's surface, but also of the physical phenomena linked to heat and mass transfer processes. 'Aerogel-like' solids can help to solve some of the pending questions in heterogeneous catalysis, i.e., the high dispersion of an active species on a carrier having a homogeneous surface, acceptable mechanical properties and a porous texture which allows the easy diffusion of reactants to active sites and products away from these sites. These unique properties allow aerogels to facilitate the WGS reaction [45-46].

1.6 Synthesis of Ordered Mesoporous Catalyst

Since ordered mesoporous silica was first reported in 1992 [47-48], interest in this research field has been explored for the potential application of these materials in catalysis. Compared to silica, alumina is more popular in catalysis for its broad application as industrial catalysts and catalyst supports employed in petroleum refineries, automobile emission control, and other areas. With the characteristics of mesoporous materials, such as highly uniform channels, large surface areas, narrow pore-size distributions, tunable pore sizes over a wide range, and so on, alumina with a controlled mesostructure should possess excellent properties for SCWG.

Alumina with ordered mesoporosity is commonly prepared through the sol-gel process with surfactants as structure-directing agents (SDAs) or by utilizing the nanocasting method with alumina as hard templates [49].

Sol-gel chemistry is widely used for the preparation of industrial heterogeneous catalysts. Developments of the preparative inorganic chemistry in organic media

opens new possibilities in catalyst synthesis, in particular for the preparation of high porosity volume solids, homogeneous mixed oxides and highly dispersed metallic catalysts. Gel formation and the drying process are discussed in this work in relation to catalyst morphology control and the solid-state reactivity of the resulting solids for supercritical gasification of glucose. Attention is given to improvement of the morphological properties of the aerogel structure and to the preparation of multicomponent gels, in particular highly dispersed supported bi-metallic catalysts as well as homogeneous mixed oxide carriers which remain stable at high temperature.

1.7 Selection of Model Compound

Using a model compound for the feedstock of interest provides several advantages including making it easier to understand the basic chemical pathways occurring during conversion with novel catalysts. This is critical for an unusual reaction medium such as supercritical water. As described earlier, biomass is typically composed of cellulose, hemicellulose, lignin, and other organic and inorganic components. Cellulose is known as one of the most unmanageable components for dissolving in hot water [50]. The complete conversion of cellulose to glucose and its oligomers can be achieved at temperatures as high as 400°C in supercritical water conditions [51]. Therefore glucose ($C_6H_{12}O_6$) serves as a useful model compound for the more complex sludge and cellulosic wastes for gasification in supercritical water.

1.8 Objectives

The objectives of this research are divided as follows:

- Synthesizing metallic Ni-Ru catalysts for producing hydrogen rich gas from glucose, minimization of coke formation on the catalyst surface and organic destructions (TOCs) in the liquid effluent so no subsequent wastewater treatment is necessary.
- Gaining a structural understanding of the synthesized fresh and spent catalysts for SCWG by using various physical and chemical characterization techniques including TPR, TPO, Chemisorption, Raman, SEM, TEM, FTIR, TGA, BET and XRD analysis.
- Synthesis, characterization and evaluation of the catalytic properties of Ru-Ni supported ordered mesoporous alumina during model biomass compound gasification in supercritical water.
- Synthesizing metal organic frameworks (MOF's) for the purification of product gases to obtain pure H₂/green fuel.

1.9 Organization of Thesis

Chapter 1: General Introduction. This chapter provides a general introduction and a brief background literature review on biomass gasification and processing technologies and the synthesis of mesoporous materials.

Chapter 2: Literature Review. This chapter provides a detailed literature review on biomass gasification and catalysts used in supercritical water, synthesizing ordered mesoporous materials.

Chapter 3: Ru-Ni-Al₂O₃ catalysts for the supercritical water gasification of glucose. This chapter provides the synthesis procedure of Ru-Ni-Al₂O₃ catalysts via both an incipient impregnation method and a sol-gel process followed by supercritical

drying, evaluation for supercritical water gasification (SCWG) of glucose and detailed characterization of the fresh and spent catalyst.

Chapter 4: Kinetic analysis for TOC destruction of glucose by supercritical water gasification. This chapter discusses the development of a kinetic model of TOC destruction of glucose in SCWG process using non-linear regression (MATLAB programming).

Chapter 5: Synthesis, characterization & evaluation of the catalytic properties of Ni & Ru supported on ordered mesoporous alumina. This chapter provides the synthesis of Ni & Ru decorated ordered mesoporous alumina and evaluation of its catalytic properties during glucose gasification in supercritical water.

Chapter 6: Conclusion. This chapter presents the overall conclusions and gives some recommendations for future work.

References:

1. *Survey of Energy Resources*. World Energy council, November, 2010. 22nd Edition: p. 360.
2. Balat, M., *Gasification of biomass to produce gaseous products*. Energy Sources, Part A: Recovery, Utilization, and Environmental Effects, 2009. **31**(6): p. 516-526.
3. Kruse, A., *Supercritical water gasification*. Biofuels, Bioproducts and Biorefining, 2008. **2**(5): p. 415-437.
4. Loppinet Serani, A., C. Aymonier, and F. Cansell, *Current and foreseeable applications of supercritical water for energy and the environment*. ChemSusChem, 2008. **1**(6): p. 486-503.
5. Demirbas, A., *Pyrolysis of biomass for fuels and chemicals*. Energy Sources, Part A: Recovery, Utilization, and Environmental Effects, 2009. **31**(12): p. 1028-1037.
6. Balat, M., *Gasification of biomass to produce gaseous products*. Energy Sources, Part A: Recovery, Utilization, and Environmental Effects, 2009. **31**(6): p. 516-526.
7. Demirbas, A., *Products from lignocellulosic materials via degradation processes*. Energy Sources, Part A: Recovery, Utilization, and Environmental Effects, 2008. **30**(1): p. 27-37.
8. Mohan, D., C.U. Pittman Jr, and P.H. Steele, *Pyrolysis of wood/biomass for bio-oil: a critical review*. Energy Fuels, 2006. **20**(3): p. 848-889.

9. Alves, S.S. and J.L. Figueiredo, *Pyrolysis kinetics of lignocellulosic materials by multistage isothermal thermogravimetry*. Journal of Analytical and Applied Pyrolysis, 1988. **13**(1-2): p. 123-134.
10. Taylor, J.D., et al., *Hydrogen production in a compact supercritical water reformer*. International Journal of Hydrogen Energy, 2003. **28**(11): p. 1171-1178.
11. Boukis, N., et al., *Methanol reforming in supercritical water*. Ind. Eng. Chem. Res, 2003. **42**(4): p. 728-735.
12. Bridgwater, A.V. and S.A. Bridge, *A review of biomass pyrolysis and pyrolysis technologies*. Biomass Pyrolysis Liquids Upgrading and Utilization, 1991: p. 11–92.
13. Osada, M., et al., *Water density effect on lignin gasification over supported noble metal catalysts in supercritical water*. Energy & fuels, 2006. **20**(3): p. 930-935.
14. Matsumura, Y., et al., *Supercritical water treatment of biomass for energy and material recovery*. Combustion Science and Technology, 178, 2006. **1**(3): p. 509-536.
15. Antal Jr, M.J., et al., *Biomass gasification in supercritical water*. Industrial & engineering chemistry research, 2000. **39**(11): p. 4040-4053.
16. Yoshida, Y., et al., *Comprehensive comparison of efficiency and CO₂ emissions between biomass energy conversion technologies--position of supercritical water gasification in biomass technologies*. Biomass and Bioenergy, 2003. **25**(3): p. 257-272.

17. Schmieder, H., et al., *Hydrothermal gasification of biomass and organic wastes*. The Journal of Supercritical Fluids, 2000. **17**(2): p. 145-153
18. Xu, X., et al., *Carbon-Catalyzed Gasification of Organic Feedstocks in Supercritical Water†*. Ind. Eng. Chem. Res, 1996. **35**(8): p. 2522-2530.
19. Yu, D., M. Aihara, and M.J. Antal Jr, *Hydrogen production by steam reforming glucose in supercritical water*. Energy & fuels, 1993. **7**(5): p. 574-577.
20. Penninger, J.M.L. and M. Rep, *Reforming of aqueous wood pyrolysis condensate in supercritical water*. International Journal of Hydrogen Energy, 2006. **31**(11): p. 1597-1606.
21. Lu, Y.J., et al., *Hydrogen production by biomass gasification in supercritical water: a parametric study*. International Journal of Hydrogen Energy, 2006. **31**(7): p. 822-831.
22. D'Jesus, P., et al., *Gasification of corn and clover grass in supercritical water*. Fuel, 2006. **85**(7-8): p. 1032-1038.
23. Yanik, J., et al., *Biomass gasification in supercritical water: Part 1. Effect of the nature of biomass*. Fuel, 2007. **86**(15): p. 2410-2415.
24. Furusawa, T., et al., *Hydrogen production from the gasification of lignin with nickel catalysts in supercritical water*. International Journal of Hydrogen Energy, 2007. **32**(6): p. 699-704.
25. Di Blasi, C., et al., *Supercritical gasification of wastewater from updraft wood gasifiers*. Biomass and Bioenergy, 2007. **31**(11-12): p. 802-811.

26. Yan, B., *Hydrogen generation from polyvinyl alcohol-contaminated wastewater by a process of supercritical water gasification*. Journal of Environmental Sciences, 2007. **19**(12): p. 1424-1429.
27. Garcia Jarana, M.B., et al., *Supercritical water gasification of industrial organic wastes*. The Journal of Supercritical Fluids, 2008. **46**(3): p. 329-334.
28. Sricharoenchaikul, V., *Assessment of black liquor gasification in supercritical water*. Bioresource technology, 2009. **100**(2): p. 638-643.
29. Elliott, D.C., *Catalytic hydrothermal gasification of biomass*, *Biofuels Bioprod. Biorefin*, 2008. **2**(3): p. 254–265.
30. Kruse, A., *Supercritical water gasification*. Biofuels, Bioproducts and Biorefining, 2008. **2**(5): p. 415-437.
31. Matsumura, Y., et al., *Biomass gasification in near-and super-critical water: Status and prospects*. Biomass and Bioenergy, 2005. **29**(4): p. 269-292.
32. Josephson, J., *Supercritical fluids*. Environ. Sci. Technol. ;(United States), 1982. **16**(10) : p. 548A-551A.
33. Wofford, W.T. and E.F. Gloyna, *Solubility of potassium hydroxide and potassium phosphate in supercritical water*. Journal of Chemical and Engineering Data, 1995. **40**(4): p. 968-973.
34. Savage, P.E., *A perspective on catalysis in sub-and supercritical water*. The Journal of Supercritical Fluids, 2009. **47**(3): p. 407-414.
35. Amin, S., R.C. Reid, and M. Modell. *Reforming and decomposition of glucose in an aqueous phase*. ASME, SAE, AIAA, ASMA, and AIChE, Intersociety Conference on Environmental Systems, San Francisco, California; United States; 21-24 July 1975. 1975.

36. Herguido, J., J. Corella, and J. Gonzalez-Saiz, *Steam gasification of lignocellulosic residues in a fluidized bed at a small pilot scale. Effect of the type of feedstock*. Industrial & engineering chemistry research, 1992. **31**(5): p. 1274-1282.
37. Fang, Z., et al., *Catalytic hydrothermal gasification of cellulose and glucose*. International Journal of Hydrogen Energy, 2008. **33**(3): p. 981-990.
38. Minowa, T. and Z. Fang, *Hydrogen production from cellulose in hot compressed water using reduced nickel catalyst: product distribution at different reaction temperatures*. Journal of chemical engineering of Japan, 1998. **31**(3): p. 488-491.
39. Kruse, A., et al., *Gasification of pyrocatechol in supercritical water in the presence of potassium hydroxide*. Industrial & engineering chemistry research, 2000. **39**(12): p. 4842-4848.
40. Watanabe, M., et al., *Acidity and basicity of metal oxide catalysts for formaldehyde reaction in supercritical water at 673 K*. Applied Catalysis A: General, 2003. **245**(2): p. 333-341.
41. Watanabe, M., et al., *Catalytic effects of NaOH and ZrO₂ for partial oxidative gasification of n-hexadecane and lignin in supercritical water* 1*. Fuel, 2003. **82**(5): p. 545-552.
42. Lee, I.G. and S.K. Ihm, *Catalytic gasification of glucose over Ni/activated charcoal in supercritical water*. Industrial & engineering chemistry research, 2008. **48**(3): p. 1435-1442.

43. Wang, W., R. Ran, and Z. Shao, *Combustion-synthesized Ru-Al₂O₃ composites as anode catalyst layer of a solid oxide fuel cell operating on methane*. International Journal of Hydrogen Energy, 2011. **36**: p. 755-764.
44. Byrd, A.J., K.K. Pant, and R.B. Gupta, *Hydrogen production from glucose using Ru/Al₂O₃ catalyst in supercritical water*. Ind. Eng. Chem. Res, 2007. **46**(11): p. 3574-3579.
45. Rolison, D.R., *Catalytic nanoarchitectures--the importance of nothing and the unimportance of periodicity*. Science, 2003. **299**(5613): p. 1698-1701.
46. Pierre, A.C. and G.M. Pajonk, *Chemistry of aerogels and their applications*. Chemical reviews, 2002. **102**(11): p. 4243-4266.
47. Kresge, C.T., et al., *Ordered mesoporous molecular sieves synthesized by a liquid-crystal template mechanism*. Nature, 1992. **359**(6397): p. 710-712.
48. Beck, J.S., et al., *A new family of mesoporous molecular sieves prepared with liquid crystal templates*. Journal of the American Chemical Society, 1992. **114**(27): p. 10834-10843.
49. Yuan, Q., et. al., *Facile Synthesis for Ordered Mesoporous γ -Aluminas with High Thermal Stability*. Journal of American Chemical Society, 2008, 130: p. 3465-3472.
50. Allen, S.G., et al., *Fractionation of sugar cane with hot, compressed, liquid water*. Industrial & engineering chemistry research, 1996. **35**(8): p. 2709-2715.
51. Sasaki, M.; Kabyemela, B.; Adschiri, T.; Malaluan, R.; Hirose, S.; Takeda, N.; Arai, K. In *Cellulose Hydrolysis in Spercritical Water*, The 4th International

Symposium on Supercritical Fluids, Sendai, Japan, 1997; Sendai, Japan, 1997;

p 583

CHAPTER TWO

Literature Review

2.1 Introduction

The principal drivers behind a sustainable energy vision of our future centre on the need to:

1) reduce global carbon dioxide emissions and improve local (urban) air quality, 2) ensure security of energy supply and move towards the use of sustainable local energy resources, and 3) create a new industrial and technological energy base, crucial for future economic prosperity.

All modern-day assessments of global energy take the view that growth in demand must be met by a diverse energy mix, including renewable or sustainable energy sources [1-3]. The growth of tangible environmental concerns is providing one of the major driving forces towards sustainable energy development. Foremost among these concerns is the issue of the release and accumulation into the atmosphere of carbon dioxide (CO₂) and other climate-changing gases. These emissions are far above pre-industrial levels and are deemed to be responsible for raising the world's (average) temperature through the greenhouse effect. Unless there are drastic reductions in the amount of carbon dioxide that we release from our activities, there will potentially be disastrous consequences for our global climate. Such concerns are undoubtedly transforming the way we assess and use energy and its carriers, shifting the balance away from our traditional hydrocarbon base towards renewable or sustainable sources of energy. One promising component towards achieving this goal could come from the direct gasification of biomass, which is a CO₂-neutral process with the carbon by-product (CO₂) and energy originating from the atmosphere via photosynthesis.

Supercritical fluids (SCFs) have been researched extensively as media for catalyzed chemical transformations. Their physical and transport properties typically fall between those of a gas and a liquid, so a fluid in its supercritical state may provide a more optimal reaction environment than a fluid in either its liquid or gaseous state. That is, the best balance between competing demands for solvent properties (e.g., high heat capacity for efficient heat transfer, high diffusivity for rapid mass transfer) may be achieved in the supercritical state with its intermediate properties between gases and liquids. Moreover, the properties of a SCF can be adjusted by manipulating density, so the opportunity exists to tune the fluid properties without altering the chemical composition of the solvent. In liquid media, the only way to alter the properties is by changing the solvent identity or composition, which can lead to poor physical properties. In addition, operating a chemical reaction at conditions that exceed the critical properties of the reacting mixture ensures the existence of a single fluid phase. This feature can be very attractive for reactions with permanent gases (e.g., hydrogenation, oxidation) as it eliminates inter-phase mass transport limitations which would exist for a gas–liquid system. Also, concentrations of the gaseous reactant can be much higher in a SCF phase than in a liquid-phase reaction medium, where its solubility in the liquid limits the highest concentration available. Often, SCFs are considered as “green” reaction media because the molecules (e.g., CO₂, H₂O) are more environmentally benign than a competing organic solvent. Finally, SCFs make an interesting reaction medium because their use may facilitate downstream separation of products simply by depressurization. In these instances, separating the products from solvent is simpler than in conventional liquid-phase processes where distillation or liquid–liquid extraction might be required [4].

Water has received a great deal of attention as a reaction medium because it is safe, non-toxic, readily available, inexpensive, and environmentally benign. One of the approaches being used in implementing green chemistry practices is to use water as a solvent and reaction medium wherever possible.

2.2 Supercritical Water

Supercritical water is an attractive reaction medium to reform biomass due to its solubilization and transport properties, as well as its ability to suppress tar and coke formation [5]. Furthermore, water is a benign and environmental friendly solvent and is naturally present to various extents in all types of biomass. Water above its critical temperature, 374°C, and critical pressure, 22.1 MPa is known as ‘Supercritical water’ (SCW). Water below its critical temperature, 374°C but at a pressure above its saturation pressure is referred to as ‘Subcritical water’. Below its saturation pressure and critical temperature water is called ‘Subcritical steam’. Similarly, below the critical pressure, water will be called subcritical steam even if its temperature is above the critical temperature. Figure 2.1 illustrates these definitions. Above the critical pressure, instead of having a ‘boiling point’ like at subcritical pressure, water would have a ‘pseudo-critical’ temperature, where water experiences a transition from liquid-like to gas-like behavior.

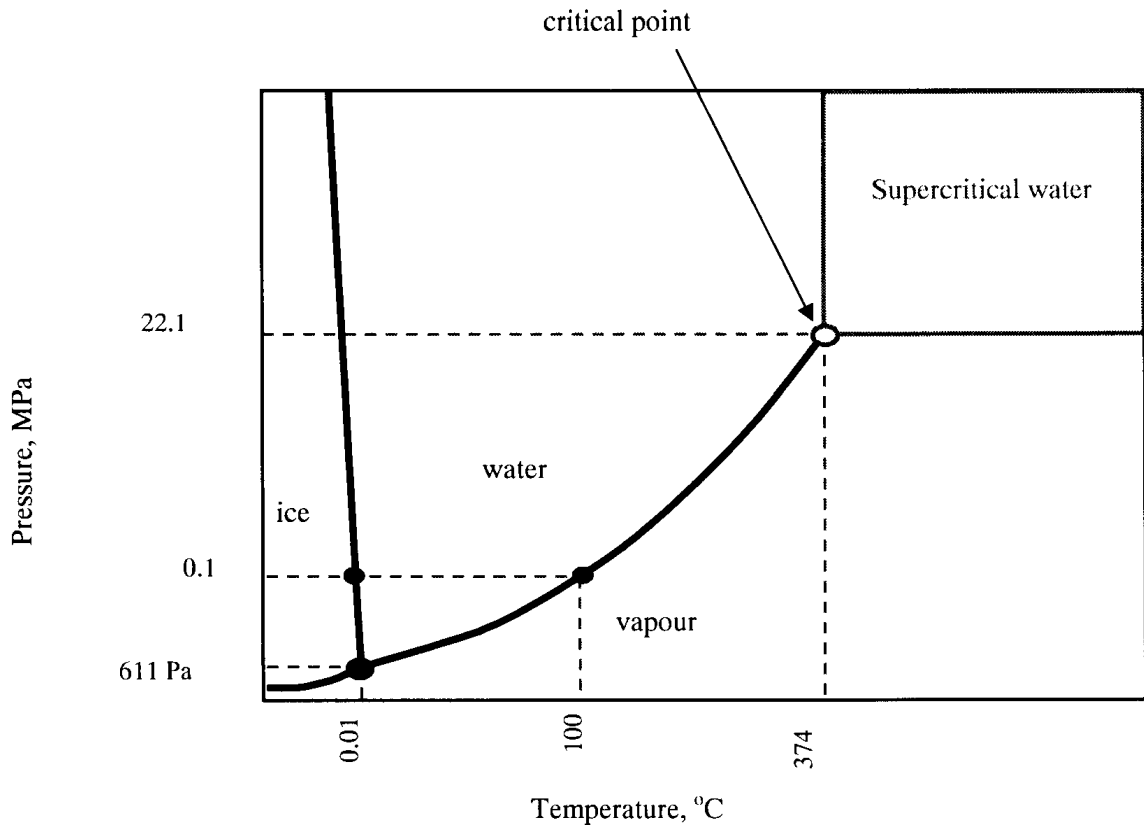


Figure 2.1. Schematic phase diagram of water.

As water is heated past its critical temperature, 374°C, at pressures greater than 22.1 MPa (3205 Psig), its physical properties undergo a significant change. Water's ionic character and ability to hydrogen bond is lowered due to a significant decrease in its dielectric constant which results in enhanced solubility of non-polar organic molecules and higher reactivity. A breakdown in the hydrogen bonding network, as well as a decrease in the hydrogen bonding lifetime, leads to an increase in mobility for single water molecules, and results in increased collision frequencies between reactant and solvent, thus resulting in greater reactivity [6]. A decrease in coke and tar formation is due to a reduced chance that a reactant or intermediate will react with one another and polymerize. Moreover, at temperatures greater than 600°C, supercritical water is a strong oxidizer and will react with carbon to produce CO and CO₂. For biomass gasification, supercritical water provides a homogeneous reaction

medium eliminating mass transport limitation characteristics in multiphase reactions. Conversely, because of the significant decrease in its dielectric constant, supercritical water is a poor solvent for inorganic salts. However, depending on the desired application the physical properties of supercritical water including solubility and reactivity can be tuned by adjusting its temperature and pressure [7]. Transport properties in supercritical water benefit from an increase in diffusion rates and a decrease in fluid viscosity compared to liquid water, and an increase in heat transfer compared to steam [8]. Several characteristics of supercritical water including miscibility with non-polar compounds and gas, enhanced transport properties, and the ability to suppress coking reactions, make it an ideal reaction medium to reform biomass.

2.3 Kinetics

A kinetic analysis of the decomposition rate in SCWG is important to design the reactor system for potential industrial implementation. Kruse and Gawlik [9] studied the sub and supercritical conversion of biomass and concluded that the following simplified reaction pathways of liquefaction and/or gasification for the biomass (Figure 2.2) are occurring.

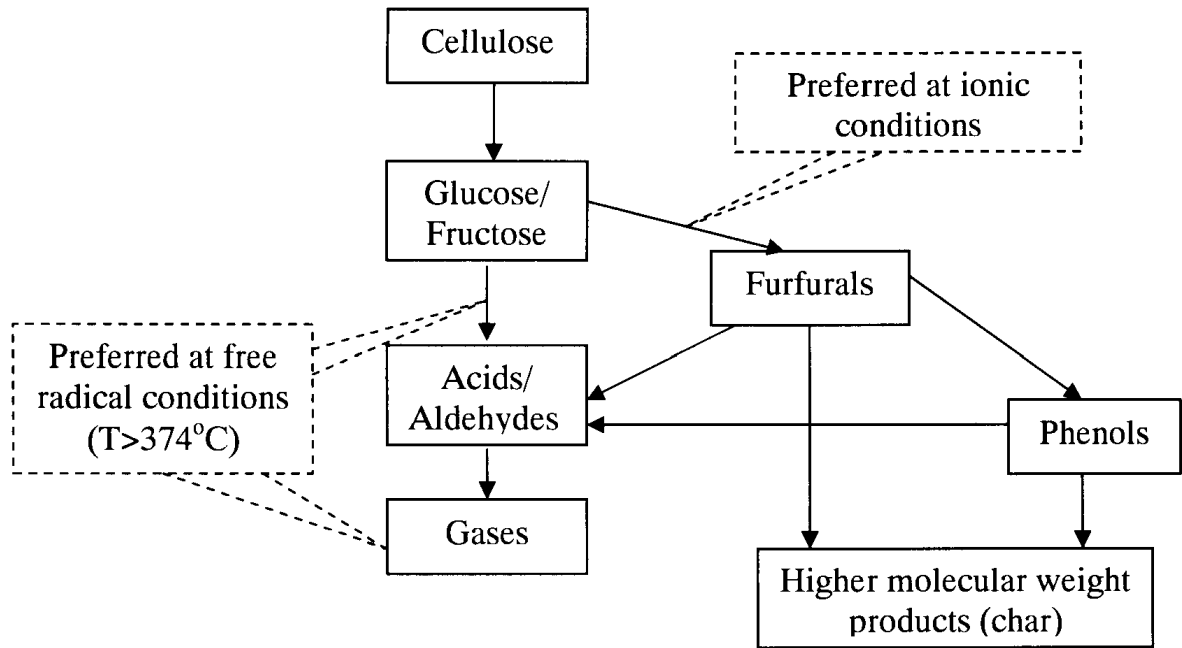
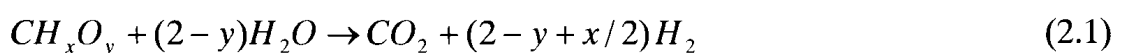


Figure 2.2. Simplified reaction scheme of liquefaction and/or gasification of biomass model compound.

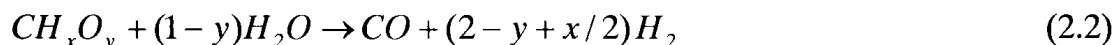
They showed two parallel paths of conversion; the left path is through a free radical reaction process which is preferred at supercritical conditions while the right path is through ionic reactions, preferred at subcritical conditions. From the properties of SCW, it may be inferred that the intermediate decomposition products are dissolved in SCW as a result of its high solvent power for organic compounds. This allows faster reaction rates while minimizing the formation of tar and chars.

The overall biomass gasification reaction in supercritical water for the production of hydrogen is represented as follows [10]:



where x and y are the elemental molar ratios of H/C and O/C in biomass, respectively. In addition to gasification, three major competing reactions occur during the gasification of biomass in supercritical water as follows:

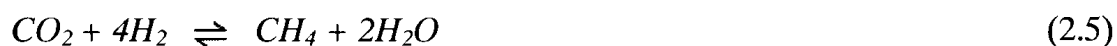
Steam reforming:



Water gas shift reaction:



Methanation reaction:



As the primary objective of biomass gasification in supercritical water gasification is hydrogen production, reactions (2.4) and (2.5) must be restrained while CO reacting with water to form CO_2 and H_2 is desired in reaction (2.3). Other than the products mentioned above, other intermediate products (i.e. char and tar) are also formed during SCW gasification.

The detailed kinetics of biomass gasification, even using the model compound glucose is still unavailable due to multi-component intermediate reactants and products involved in this complex reaction mechanism. More than thirty components in the liquid product stream were detected during gasification of glucose in SCW [11]. Kabyemela et al. [12] studied glucose and fructose decomposition in sub and supercritical water at residence times down to 2 sec in a tubular reactor, finding first order reaction kinetics. The main products of glucose decomposition reported were fructose, erythrose, glycolaldehyde, dihydroxyacetone, glyceraldehyde, 1,6-anhydroglucose, and pyruvaldehyde. The reactions involved were three types, namely

isomerization, bond cleavage, and dehydration. On the other hand, Lee et al. [13] studied the conversion of glucose without catalysts in a tubular reactor at 480-750° C, 28 MPa, 10-50 sec. They found that below 600°C the hydrogen yield increases with increased residence time when gasifying glucose in supercritical water. They did not study the liquid phase in detail, rather performed a kinetic analysis of COD (chemical oxygen demand) destruction assuming pseudo first order reaction during the gasification of glucose in supercritical water. Their kinetic investigation leads to the following first order reaction rates:

Glucose as a function of its concentration, C_g :

$$-r_g = 10^{3.09 \pm 0.26} \exp(-67.6 \pm \frac{3.9}{RT}) C_g \quad (2.6)$$

The COD as a function of the corresponding concentration C_c :

$$-r_c = 10^{2.95 \pm 0.23} \exp(-71.0 \pm \frac{3.9}{RT}) C_c \quad (2.7)$$

Jesus et al. [14] developed a model for corn silage using a mathematical approximation based on zero-order kinetics as follows:

$$Y = 10^2 \exp(\frac{47.9[KJ]}{RT[K]}) \tau(\text{min}^{-1}) + 10^{-2.8} \exp(6.1 \times 10^{-3} T[K]) \quad (2.8)$$

Jin et al. [15] studied the TOC (Total organic carbon) kinetics of oxidation of food wastes. They found a fast reaction rate at an early stage of reaction (within 50 seconds) and slow reactions afterwards.

2.4 Catalytic Supercritical Water Gasification

Supercritical water gasification of biomass has several advantages compared to traditional gasification including the direct use of wet biomass feedstocks, a single reactor for biomass hydrolysis and gasification, additional H₂ generation through

reforming, and a compressed gas product convenient for storage and transportation. Three temperature regions have been identified for SCWG in the literature as follows [16, 17]:

- 1) Region I (500–700°C supercritical water) biomass decomposes and activated carbon catalyst is used to avoid char formation or alkali catalysts can facilitate the water-gas shift reaction.
- 2) Region II (374–500°C, supercritical water) biomass hydrolyzes and metal catalysts facilitate gasification.
- 3) Region III (below 374°C, sub critical water) biomass hydrolysis is slow and catalysts are required for gas formation.

In region II, biomass gasification was operated at supercritical temperatures (374–500°C), which will produce more hydrogen and less methane [18]. Catalytic gasification by supercritical water is an attractive alternative to high temperature biomass reforming because it reduces the minimum reaction temperature necessary for gasification while maintaining useful kinetics. This reduces the overall process cost since the majority of the energy input into supercritical water gasification goes into heating up a large excess of water in relation to biomass in the feed and also reduces corrosion on the reactor walls, which allows the use of less costly alloys [17]. As a result of the harsh reaction environment, the catalyst system must be highly active and stable in supercritical water. Furthermore, the catalyst system should be able to suppress coke and char formation to avoid catalyst deactivation. Catalysts considered for biomass gasification by supercritical water include carbon catalysts, alkaline catalysts, and transition metal catalysts.

2.4.1 Carbon Catalysts

Activated carbon has potential as an effective catalyst for biomass gasification in supercritical water as it has been shown to improve gas yields and H₂ selectivity. Matsumura's group [19], Antal's group [20] and Xu et al. [21] have identified activated carbon as a catalyst for hydrothermal gasification under supercritical water (600°C) conditions. Matsumura's group showed SCWG of a pretreated chicken manure feedstock with a suspended activated carbon catalyst. In this processing mode, the plugging in the reactor was avoided for up to 4 h of operation at 600 °C and 25 MPa. Recovery and reuse of the catalyst is perceived as a simple process step. Antal's group and Xu et. al. catalytically gasified glucose with an activated carbon catalyst, and were able to achieve greater than 90% carbon gasification efficiency (CGE), or carbon recovered in the gas, for a 22wt% glucose feed solution at temperatures ranging from 600 to 750°C. Furthermore, Antal et al [20] gasified real biomass feedstocks including cornstarch, potato starch, sawdust, and potato waste, and were able to achieve greater than 70 % CGE for feed concentrations ranging from 8.9 wt% to 13.7 wt % at temperatures greater than 700°C. Both groups concluded that gas composition and gas yield were a strong function of reactor temperature and increased H₂ yields were due to the promotion of the water gas shift reaction:



Although carbon catalysts have been shown to improve CGE and the H₂ yield for biomass gasification, two technical issues need to be addressed. The first is reactor plugging. Antal et al. [20] reported that all feed solutions with greater than 15 wt% organic material plugged the reactor within 1-2 hours of on stream time. For feed concentrations less than 15 wt % they observed a prolonged time on stream, but

eventually the reactor would plug due to a buildup of ash and char in the heating zone. The second problem observed was catalyst deactivation. Xu et al. [21] observed a decrease in catalytic activity after 4 hours of operation, but noted that catalyst deactivation was prolonged when swirl flow was initiated in the entrance of the reactor, essentially increasing the rate of heat transfer to the fluid.

2.4.2 Alkaline Catalysts

Alkaline catalysts benefit biomass gasification in supercritical water by increasing gasification efficiency and H₂ yield [10, 22, 23], and are used in alkaline lignocellulosic biomass pre-treatment processes for bioconversion of cellulose to ethanol [24, 25]. Sinag et al. [23] observed a nearly two times increase in the H₂ yield and a significant decrease in the CO concentration for glucose gasification at 500°C with a K₂CO₃ catalyst. They attributed the improved H₂ yield to an increase in the kinetics of the forward water gas shift reaction via formate formation. They also determined that the addition of K₂CO₃ led to an increase in acid formation, and a decrease in furfural formation. This is important because the polymerization of furfurals with other liquid intermediates is thought to be one of the causes of char and coke formation [26, 27]. Ultimately, less furfural formation will improve the CGE since furfural is more difficult to gasify than small organic acids. Guo et al. [28] used Ca(OH)₂ to gasify glucose to H₂ and CH₄, with both gases being formed with enhanced yields compared to experiments with no catalyst. However, due to the formation of CaCO₃ from CO₂ and Ca(OH)₂, there was little to no CO₂ or CO found in the product gas. Kruse et al. [29] showed that KOH could enhance the gasification of lignin. The group gasified pyrocatechol, a lignin model compound, at 600°C and

400 MPa with KOH and achieved a 99% carbon gasification efficiency for a 6.6 wt% feed solution.

Generally, alkaline catalysts have improved biomass gasification in supercritical water by catalyzing biomass gasification reactions and promoting the water gas shift reaction, however, Kruse et al. [26] and Sinag et al. [23] observed a solid residue accumulate in batch and continuous flow reactors during gasification experiments. In one case the solid residue accounted for up to 8% of the carbon fed to the reactor. Additionally, alkaline catalysts are thought to increase corrosion of the reactor material. Energy dispersive x-ray (EDX) analysis performed by Sinag et al. [23] on solid particles filtered from the liquid products indicated the presence of Ni, Mo, and Cr, all of which were primary constituents of their Inconel reactor.

2.4.3 Metal & Metal Oxide Catalysts

Metal and metal oxides are a third class of catalyst used for biomass gasification by supercritical water. Metal catalysts and catalyst supports are limited to materials that are stable in the strongly oxidizing environment of supercritical water. Currently, metal catalysts investigated for biomass gasification in supercritical water include Ru, Rh, Pd, Pt, and Ni. Typically, biomass gasification over metal catalysts at temperatures ranging from 350°C to 500°C produces gas rich in CH₄, CO₂, and H₂, with small amounts of CO and C₂+ hydrocarbons. Osada's group reported gasification of alkyl-phenols with several noble metal catalysts at 400°C [30]. Their results confirmed that ruthenium and rhodium were the most active metals with high levels of methane production after only 15 minutes at temperature, while platinum and palladium produced almost no gas with lower levels of methane and higher levels of hydrogen formation. They also studied the stability of three ruthenium catalysts

[31] at 400°C using lignin as the feedstock and found the titania (anatase)-supported catalyst to be stable. The carbon supported catalyst showed evidence of metal crystal growth with a resulting loss of activity. An alumina-supported catalyst was destroyed in the process as the alumina changed phase from γ - to α - and ruthenium was dissolved into the supercritical water.

Vogel's group has compared ruthenium catalysis with nickel using synthetic liquefied wood mixture as the feedstock [32]. The skeletal nickel metal catalyst was found to sinter rapidly at 400°C, even when stabilized by ruthenium doping, while a Ru on carbon catalyst was stable during 220 h of testing. Osada et al. [22] produced gas containing up to 41 mole % CH₄ from lignin gasification at 400°C with a Ru/TiO₂ catalyst, compared to Guo et al. [10] who measured around 10 mole % CH₄ for non-catalytic continuous gasification of lignin in a Hastelloy tubular reactor at temperatures ranging from 500-775°C.

Nickel based catalysts are widely used for biomass gasification in supercritical water because of their high activity and low cost. However, nickel catalysts promote the water-gas shift reaction [23], methanation [13, 33-35] and hydrogenation reactions [36]. The use of nickel catalysts in SCWG are expected to lead to higher yields of gas products, especially hydrogen and methane. Yoshida et al. [37] conducted SCWG of lignin, cellulose and their mixture in the presence of a nickel catalyst at 400°C and obtained methane and carbon dioxide as the major gaseous products. Minowa and Ogi [38] studied the effect of reduced Ni catalyst on gasification of cellulose in subcritical water and reported that the yield of CH₄ was enhanced whereas the yield of H₂ was suppressed by the methanation reaction in the presence of Ni.





High biomass CGE can be achieved with metallic catalysts for long reaction times, but generally depends on the activity of the catalyst system, water density, temperature, and feedstock. Sato et al. [39] was able to gasify lignin with a 20 wt % Ni / MgO catalyst at 400°C in a batch reactor, however, 360 min reaction time was necessary for 78% CGE. Sato et al. [30] ranked several transition metal catalysts and supports in order of catalytic activity for supercritical water gasification of alkylphenols at 400°C as: Ru / γ -Al₂O₃ > Ru / Carbon > Rh / Carbon > Pt / γ -Al₂O₃ > Pd / Carbon > Pd / γ -Al₂O₃. However, CGE's were low, ranging from 0.2%-15%. Hao et al. [40] observed a similar trend for the gasification of cellulose and sawdust at 500°C and ranked catalytic systems based on catalytic activity as: Ru/Carbon > Pd/Carbon > CeO₂ particles > CeO₂ nano particles > (CeZr)_xO₂. The observed CGE's were as high as 94% for cellulose, and 77% for sawdust with a Ru/carbon catalyst. Yamaguchi et al. [41] investigated several metal catalysts on titania and activated carbon supports and, similar to the previous reports, concluded Ru had the highest catalytic activity followed by Rh > Pt > Pd > Ni. Furthermore, for Ru/carbon catalysts Osada et al. [42] determined that gasification efficiency was a function of reactor pressure, and were able to increase CGE's for lignin gasified at 400°C up to 47% by optimizing the water density.

Although metallic catalysts designed for low temperature biomass gasification by supercritical water have demonstrated the potential to lower the activation energy for gasification reactions and increase selectivity for the gas products, the stability of these catalyst system needs to be addressed before this technology can come to fruition [31, 43-47]. Metal catalysts are typically expensive, thus the lifetime of a

catalyst and support becomes an important factor when optimizing a catalytic process. Osada et al. [31] concluded that $\gamma\text{-Al}_2\text{O}_3$ and carbon supports demonstrated poor stability due to a change in morphology in $\gamma\text{-Al}_2\text{O}_3$, and a decrease in surface area for the carbon support. TiO_2 was the most stable support, but CGE decreased after the third subsequent use. Additional studies by Byrd and Gupta [43] and Lu et al. [48] investigated the stability of adding CeO_2 to $\gamma\text{-Al}_2\text{O}_3$ as a catalyst support. Although CeO_2 was found to stabilize the $\gamma\text{-Al}_2\text{O}_3$ support by inhibiting carbon formation on the catalyst, the improvement was only incremental and the catalyst eventually became deactivated due to the formation of carbon on the catalyst surface and sintering. Catalyst stability is a critical issue that needs to be improved before low temperature catalytic gasification by supercritical water can be considered as a viable thermochemical conversion technology for biomass.

2.4.4 Other Catalysts

The majority of the published research concentrates on the catalysts previously mentioned [49-53], but some groups have tested less common catalysts in SCWG. Yanik et al. [54] reported that iron can be an effective catalyst for the gasification of red-mud (a by-product of the electrochemical process of aluminum production). Arita [55] has reported that the addition of copper wires accelerates gasification of ethanol considerably.

2.4.5 Catalyst Supports

The effectiveness of catalysts in hydrothermal gasification can be greatly improved by the use of support materials with long-term stability in hot liquid water. Many alumina and silica based materials commonly used for catalyst formulations in the petroleum and gas processing industries are less useful for hydrothermal gasification.

The better supports for SCWG include activated carbon, mono-clinic zirconia, titania, and α -alumina [17].

Nickel, for instance, has high activity and generates more CH_4 with a magnesia support than without the support [26, 56]. Ruthenium has been evaluated on many supports [30, 57]. Ruthenium on rutile titania extrudate is particularly effective in this process. It is easily reduced to its active form and maintains its activity for long periods of operation [58]. Osada [42] obtained high carbon gasification yields with ruthenium on titania for repetitive uses. In general, γ -alumina as a support leads to higher gas yields than carbon [30]. But it is not a useful catalyst support for more than a few hours in aqueous systems as it did not survive in long-term processing using SCWG [30, 59].

2.5 Process Parameters & Their Effects

The SCWG process parameters affect various performance aspects like efficiency, product gas quality, energy and energy inputs. Many of the literature studies have been undertaken to investigate the optimum parameters to obtain maximum hydrogen yields or syngas.

Moghtaderi [60] conducted a study to gain a fundamental understanding about the catalytic steam gasification of some species under low temperature conditions. He particularly focused on the role and relative importance of controlling parameters, such as reaction temperature and the heating rate on the composition of the products. In the experimental study, temperatures were changed from 200 to 800°C and investigated both with catalyst and without a catalyst, with the residence time changed at 20 mins or 2 mins. Addition of catalyst particles was found to change the selectivity of gasification reaction enhancing hydrogen production while reducing the levels of

methane produced at temperatures above 500°C. At lower temperatures (200°C<T<450°C) the catalysts appeared to have no significant impact on hydrogen yield although they increased the yield of methane. A relatively low reaction temperature of 600°C and a high steam content of about 90% showed the strongest tendency for maximizing the hydrogen production.

Garcia Jarana et al. [61] tested a SCWG on a laboratory-scale continuous-flow system with two different industrial wastewaters, using cutting oil wastes, oleaginous wastewater from metalworking industries, and vinasse, and alcohol distillery wastewater. The influence of the temperature, amount of oxidant and catalyst addition on the yield and composition of the gas phase was studied. Experiments were carried out in the temperature range 450–550°C, the amount of oxidant ranged from the absence of oxygen (oxygen coefficient, $n=0$) to 20% of stoichiometric oxygen ($n=0.2$), and 25 MPa of pressure in all cases. A maximum of 0.19 mol H₂ per initial COD_m (COD_m was given as mol O₂ consumed for total oxidation) was obtained in the gas phase under the best conditions.

2.5.1. Effect of Temperature

The effect of temperature on hydrogen production in SCW has been studied with and without catalysts. The reaction temperature has been found to highly affect the conversion, yield and by-product formation. Holgate et al. [11] studied the effect of temperature on the hydrolysis of glucose in a plug flow reactor made of Inconel-625. Figure 2.3 shows the product yield for glucose hydrolysis for temperatures between 400°C and 650°C. Hydrogen and carbon dioxide were the main gaseous species detected, indicating the presence of the water gas shift reaction. Interestingly, acetaldehyde and CO disappeared at temperatures above 575°C, and formation of

simple hydrocarbons (such as methane and ethane) and hydrogen were favoured at higher temperatures. These observations are generally consistent with the results reported by Yu et al. [58] and Lee et al. [13]. The results of Lee et al [13] are shown in Figure 2.4, where it is seen that without a catalyst, hydrogen yield and the yield of other by-products are strongly dependent on temperature. The gasification conversion reached 100% at 700°C and 28 MPa. As the temperature increases, the yield of hydrogen increases sharply, whereas the yield of carbon monoxide decreases above 650°C. For ethanol reforming in SCW, Byrd et al. [63] reported that ethanol conversion over commercial Ru/Al₂O₃ was not complete and C₂ species were detected at temperatures below 600°C. However, in the temperature range of 700-800°C, the product compositions were mainly H₂, CO, CO₂, and CH₄.

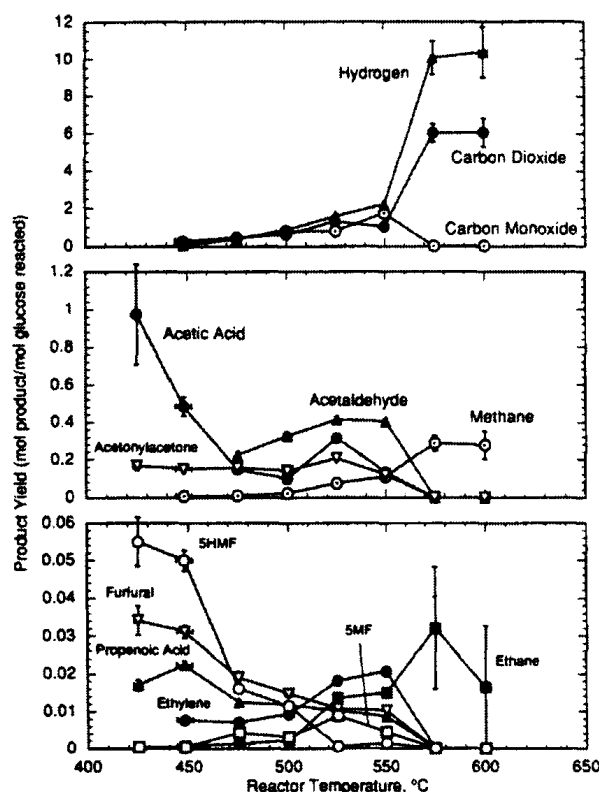


Figure 2.3. Variation of product yields with temperature for glucose hydrolysis at 24.6 MPa. Experimental conditions: $1.02 \pm 0.02 \times 10^{-3}$ mol/L glucose, 6.1 ± 0.3 s reactor residence time. No catalyst [11].

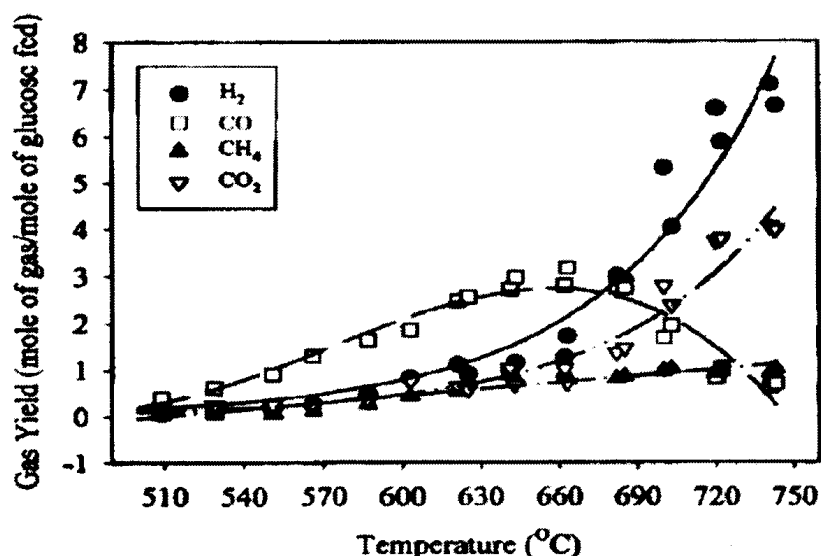


Figure 2.4. Gas product yields as a function of reactor temperature on 0.6 M glucose gasification in SCW at 28 MPa and a 30 s reactor residence time. No catalyst [13].

2.5.2. Effect of Pressure

There are only a few reported studies that have looked at the effect of pressure on hydrogen production in sub- and supercritical water. Gadhe and Gupta [64] investigated methanol reforming for pressures between 3.4 and 27.6 MPa and at a constant temperature of 700°C. They found that H₂, CO₂ and CO decreased with increasing pressure in the subcritical region, whereas methane increased significantly until the critical temperature was reached. Sato et al. [65] observed similar trends. Kruse and co-workers [29] reported that the hydrogen production from the gasification of pyrocatechol (C₆H₆O₂) at 700°C slightly decreased as the pressure increased from 20 MPa to 40 MPa. Their results matched the calculated equilibrium data. However, in a small pressure range slightly above the critical point of water, Byrd et al. [59] found that there was not much difference in ethanol conversion and product composition in the pressure range from 22.1 to 27.5 MPa, as shown in Figure 2.5.

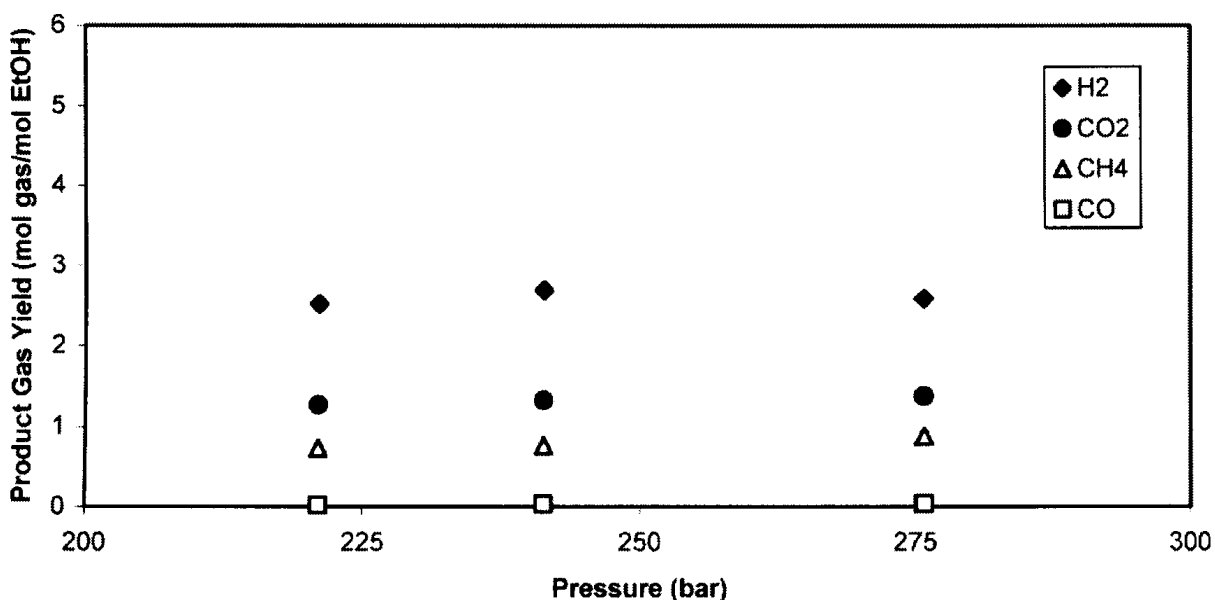


Figure 2.5. Effect of pressure over 5wt. % Ru/Al₂O₃ catalyst with 10 wt % Ethanol [59].

2.5.3 Effect of Residence Time

Thus far, because most of the studies on ethanol (or other organic materials) reforming in SCW involved non catalytic reactions, the influence of residence time on hydrogen production was reported [13, 40, 62, 64, 66]. They observed that the formation of hydrogen, carbon dioxide and methane increased with longer residence times, while carbon monoxide decreased. For catalytic reactions, Osada et al. [22] reported their results in terms of reaction time, with methane increasing by increasing the reaction time for all catalytic reactions investigated in a batch reactor. Interestingly, Arita et al. [55] showed that the hydrolysis of ethanol in a batch reactor led to higher conversions of hydrogen as the residence time increased, as shown in Figure 2.6.

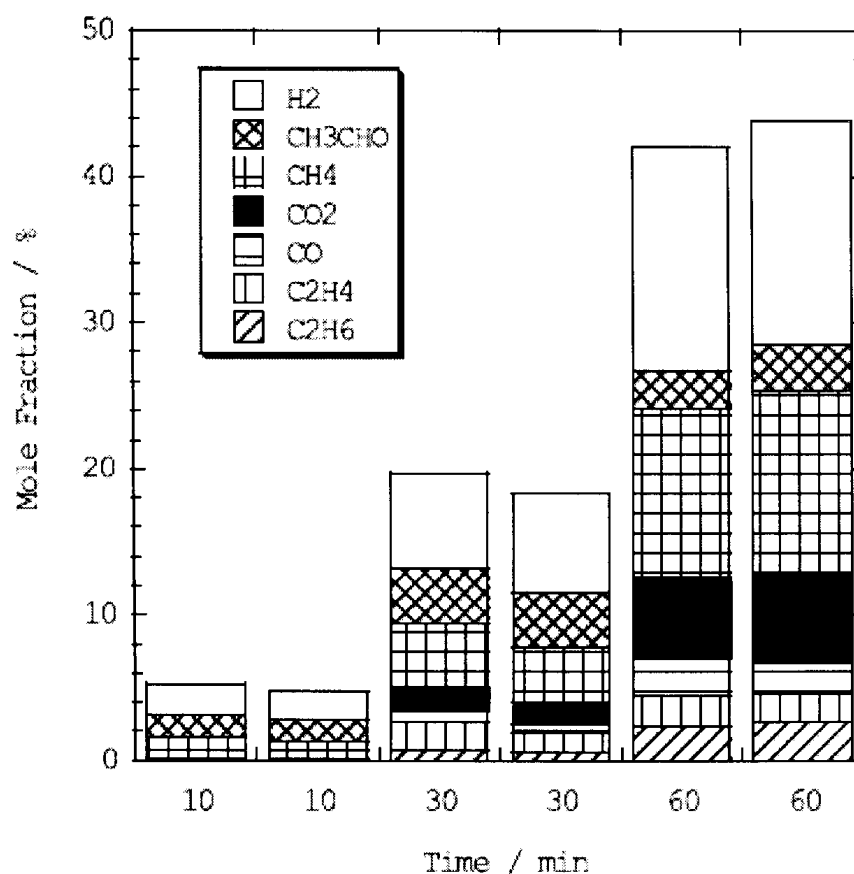


Figure 2.6. Time dependence of the yields of all products for ethanol reaction in a batch reactor at a density of 0.20 g/cm³ at 500°C [55].

2.5.4 Effect of Solution Concentration

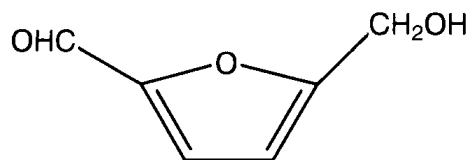
Solid biomass and water are the main components of the feedstock for SCWG. The solid concentration in the feedstock could be a major design issue for the commercial application of SCWG. When gasifying glucose as a model compound for biomass in SCW, Matsumura et al. [67] found that the yields of H₂, CH₄ and CO₂ decreased while CO increased with an increase in glucose concentration in the feedstock. Hao et al. [40] showed that the percentages of H₂ and CO₂ in the total product gas increased with increasing glucose concentration in the range of 0.1 M to 0.9 M, but that the CO and CH₄ fractions were reduced while the gasification efficiency (GE) decreased. Kersten et al. [68] found that at 700 °C and 30 MPa, H₂ and CO₂ decreased with

initial glucose concentration from 1 to 7wt% while CO and CH₄ remained almost constant. Nearly complete gasification was achieved with the lowest concentration at 650 °C or above.

The experiments with real biomass gasification in SCW [28, 69] also showed that both gasification efficiency (GE) and carbon conversion efficiency (CGE) decreased with an increase in feed concentration. The yields of H₂, CH₄ and CO₂ also decreased with feed concentration, while the yield of CO increased.

2.6 Brief Reaction Mechanism

The chemistry of hydrothermal glucose reactions is rather complex. Most of the published studies agree that dehydration reactions of glucose occur in aqueous solutions producing various amounts of 5-HMF (C₆H₆O₃) and other furan derivatives [70-71]:



5-hydroxymethylfurfural (5-HMF)

The generation of these undesirable byproducts is considered to be the main obstacle in the hydrothermal gasification of biomass. Hashaikeh, et. al. [72] proposed a mechanism for catalytic hydrothermal glucose gasification. There are two competing reaction pathways that glucose tends to take: (i) the desired gasification to H₂ on the surface of the catalyst (reaction 2.12) and (ii) the undesired precipitation within the voids of the close packed catalyst bed (reaction 2.13):



The schematic also shown in Figure 2.7 illustrates possible pathways for hydrothermal treatment of glucose.

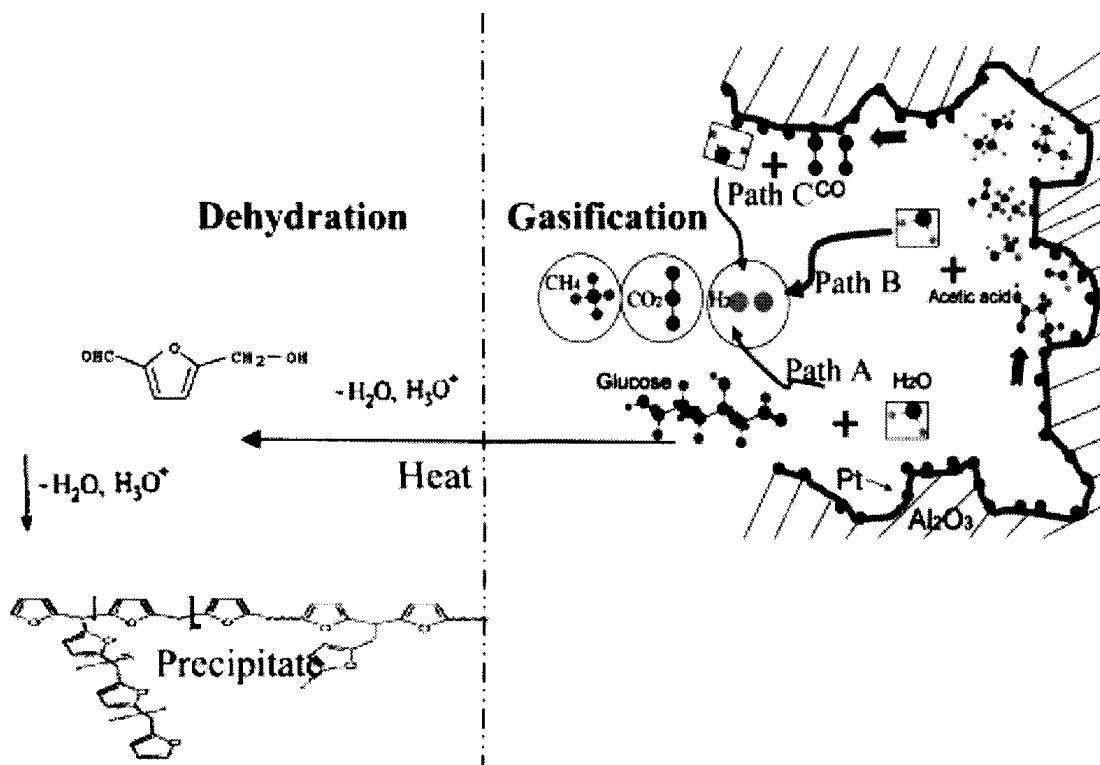
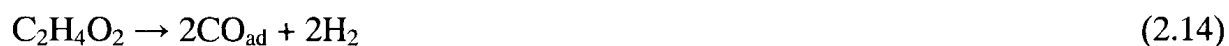


Figure 2.7. Schematic showing reaction pathways (gasification and dehydration) for the hydrothermal treatment of glucose [72].

The gasification process of glucose requires glucose adsorption on the catalyst. This is the first and most important step. Decomposition of glucose to intermediates (e.g., acetic acid, methanol, propanol, propionic acid, and butyric acid) is believed to be the main catalytic decomposition step. It leads to subsequent direct dehydrogenation producing hydrogen gas and acetic acid (path A, Fig. 2.7). The produced acetic acid is then dehydrogenated (reaction 2.14) producing hydrogen gas and leaving behind carbon monoxide adsorbates at the surface of the catalyst (path B, Fig. 2.7):



Finally, the gasification mechanism involves carbon monoxide gasification (reaction 2.15) generating hydrogen and carbon dioxide through the water-gas shift reaction (path C, Fig.2.7):



The precipitate formation observed during the hydrothermal treatment of aqueous glucose is caused mainly by 5-HMF polymerization and condensation reactions including branching and cross linking to form linear and cyclic oligomers. The trouble is that both processes (reactions 2.12 and 2.13) could occur at about the same temperature, and the challenge is to selectively promote the first reaction and suppress the second one.

2.7 Effect of Catalyst Preparation

The catalyst preparation method (precipitation, co-precipitation, impregnation, sol gel, etc.), calcination and reduction steps, all have an impact on the catalyst activity. To the best of our knowledge, most of the researchers have used either commercial catalysts or those prepared by conventional techniques like precipitation or impregnation for biomass gasification in supercritical water. There is also a lack of literature, particularly for supercritical water gasification, concerning the relationship between catalyst preparation and carbon deposition. Deposition of carbon leads to catalyst deactivation and/or plugging the reactor when the catalyst is exposed to this high temperature and pressure environment. Several studies have investigated related fields such as CH₄-CO₂ reforming or steam reforming [73-79]. Haga et al. [80, 81] suggested that the product composition varied due to the crystallite size of Co/γ-Al₂O₃ for ethanol steam reforming. They found that the activity of the catalyst was independent from the starting precursor during preparation. However, Aupretre et al.

[82, 83] reported that the catalyst activity depended on the type of metal precursor, for example the catalyst prepared from metal chloride solution was more active compared to that from acetate solution for Rh/ γ -Al₂O₃ and Mg/Ni/Al₂O₃. The effect of catalyst preparation on product composition was also reported by Jiang et al. [76] & Kaddouri and Mazzocchia [84]. Jiang et al. [76] prepared different percentages of impregnation and aerogel Ni/Al₂O₃ catalysts and proved that Aerogel Ni/Al₂O₃ nanoparticle catalysts, which were prepared by a sol-gel method combined with a supercritical drying route showed better catalytic activity and stability than the impregnation catalyst. Characterization of spent catalysts revealed that only limited graphitic carbon with filamentous was found on the surface of the aerogel catalysts, however, massive graphitic carbon with filamentous morphology covered most of the surface of the impregnation catalyst and resulted in catalyst deactivation. Kaddouri and Mazzocchia [84] prepared Co/SiO₂ and Co/ γ -Al₂O₃ catalysts by incipient wetness, sol-gel and a combination of both techniques. They showed that the combination method provided better catalytic performance toward hydrogen production over the Co/SiO₂ catalyst. However, impregnation is the most popular method that has been used to prepare catalysts for biomass gasification, steam or carbon dioxide reforming etc.

2.8 Synthesis of Ordered Mesoporous Materials

Porous materials have been intensively studied with regard to technical applications as catalysts and catalyst supports. According to the IUPAC definition, porous materials are divided into three classes; microporous (pore size < 2nm), mesoporous (2–50nm), and macroporous (>50nm) materials [85]. In addition, the term “nanoporous” is also increasingly being used. However, it is not clearly defined and loosely refers to pores in the nanometer size range. Many kinds of porous materials

such as (pillared) clays, anodic alumina, carbon nanotubes and related porous carbons and so on, have been extensively described in the literature [86]. Among the family of microporous materials, aluminum oxides are largely studied because of their catalytic [87], optical [88], electronic [89], and biomedical properties [90]. There has been great interest in obtaining well-defined mesoporous aluminum oxides with high surface areas and pore volumes [87]. Porous aluminum oxides have been synthesized by high-temperature dehydration of bulk powders [88], aerosol generation of particles with the use of block copolymers [91], modified sol-gel in the presence of organic structural agents [92], cationic [93] and anionic surfactants [94], block copolymers [95], using ordered mesoporous carbon templates [96], colloidal precursors with amine structural agents [97], and evaporation-induced self assembly (EISA) with block copolymers [98]. Also, meso- and macroporous γ -Al₂O₃ was obtained under microwave irradiation in the presence of surfactants under acidic conditions [99]. It is noteworthy that the use of ordered mesoporous carbons as hard templates for the synthesis of mesoporous γ -alumina [96] was an important achievement as it initiated interest in the development of alumina materials with ordered and uniform mesopores. Even though the hard-templating synthesis route may afford crystalline aluminas with desired pore geometries and symmetries, this method has several drawbacks. First, it is time consuming because preparation of a carbon template adds additional steps to the synthesis procedure. Also, the nanocasting process consists of several cycles, which often results in a partial or complete loss of mesostructural ordering and a change of particle morphology.

Among the various investigated synthesis routes, those employing poly(ethylene oxide)-poly(propylene oxide)-poly(ethylene oxide) block copolymers

$[(EO)_x(PO)_y(EO)_x]$ as soft templates has attracted a lot of attention as they are inexpensive, commercially available, biodegradable, and afford materials with relatively large and uniform mesopores. The first successful synthesis of ordered mesoporous alumina (OMA) in the presence of block copolymers used as soft templates was reported by Niesz et al. [100]; however, this procedure required strict control of experimental conditions. A major leap in the preparation of $\gamma\text{-Al}_2\text{O}_3$ with ordered mesopores was achieved by self-assembly of the $(EO)_{20}(PO)_{70}(EO)_{20}$ triblock copolymer and alumina precursors in ethanolic solution in the presence of additives such as citric or nitric acid [99]. This route has been found to be reproducible and avoids the need for controlling hydrolysis conditions, such as the amount of water and humidity.

Alumina is an important support in catalysis, especially now that ordered mesoporous alumina (OMA) can be made in a facile and reproducible manner. Therefore, the successful preparation of OMA stimulates to extend this approach to the synthesis of alumina-supported metal oxides with well-developed mesoporosity, relatively high surface area, and crystalline pore walls. For instance, nickel aluminate (NiAl_2O_4) is used as a catalyst for several hydrogenation and dehydrogenation reactions: oxidative dehydrogenation of ethane to ethylene for petrochemical purposes [101], conversion of methane and carbon dioxide to syngas [102], and hydrogenation of nitriles [103]. Nickel aluminate is relatively inexpensive compared to other known active catalysts, has strong resistance to acids and bases, and has high thermal stability. Several methods have been employed for the synthesis of NiAl_2O_4 including wet impregnation of Al_2O_3 , pelletization and sintering of Al_2O_3 and NiO .

2.9 Challenges

Although the SCWG process seems to be very efficient for hydrogen production, some physical limitations and/or technical difficulties have been encountered. Due to the severe process conditions utilized (typically: $T = 600\text{ }^{\circ}\text{C}$, $P = 300\text{ bar}$ and a corrosive environment), experimental investigations using SCWG are expensive and time consuming. Chars from non-converted biomass and tars from unwanted reaction products are two major challenges in SCWG. Chars are linked to the conversion yields of the process, while tars are usually formed by pyrolysis of organic molecules. Because of sedimentation, these char and tars plug continuous reactors after several hours of running, while also limiting the amount of hydrogen produced. Although SCWG can lower the amount of chars and tars compared to low pressure processes, this drawback has to be carefully considered because of the rather small volume of laboratory reactors and tubing. Antal et al. [20] produced less than a few percent of such residual compounds in SCWG, whereas Corella and his coworkers [104] observed 10-20% chars and 4% tars in atmospheric pressure steam gasification.

Three major limitations considering the material of reactor construction should be considered; i.e. corrosion, pressure resistance and hydrogen aging. Antal et al. [20] showed that the inner walls of nickel alloy reactors were strongly corroded by the SCWG reaction. Only specific geometries and specific materials can be used due to the high pressures and temperatures used in SCWG. As an example, it is impossible to build whole titanium reactors with high corrosion resistance by comparison to classical stainless steels, due to the low allowable stress (pressure resistance) of titanium. The contact of metallic materials with hydrogen gas is well known for weakening the strength (pressure resistance) of the used materials. Combined with the

high pressure constraint, hydrogen aging can limit the duration of use of reactors and tubing. In this research a 600ml Hastelloy C-276 reactor was utilized to withstand these difficulties while preventing plugging from chars and tars.

Separation of hydrogen from the other formed gases, especially carbon dioxide, is another relevant problem. Matsumura et al. [105] proposed to mix the formed gas and sub-critical water, which dissolves most of the carbon dioxide.

References:

1. Johnson, S.R., et al., *Chemical Activation of MgH₂; a New Route to Superior Hydrogen Storage Materials*. ChemInform, 2005. **36**(39): p. no-no.
2. Dorian, J.P., H.T. Franssen, and D.R. Simbeck, *Global challenges in energy*. Energy Policy, 2006. **34**(15): p. 1984-1991.
3. Solomon, B.D. and A. Banerjee, *A global survey of hydrogen energy research, development and policy*. Energy Policy, 2006. **34**(7): p. 781-792.
4. Savage, P.E., *A perspective on catalysis in sub-and supercritical water*. The Journal of Supercritical Fluids, 2009. **47**(3): p. 407-414.
5. Calzavara, Y., et al., *Evaluation of biomass gasification in supercritical water process for hydrogen production*. Energy Conversion and Management, 2005. **46**(4): p. 615-631.
6. Kruse, A. and E. Dinjus, *Hot compressed water as reaction medium and reactant:: 2. Degradation reactions*. The Journal of Supercritical Fluids, 2007. **41**(3): p. 361-379.
7. Weingaertner, H. and E.U. Franck, *Supercritical water*. Angew. Chem., Int. Ed, 2005. **44**: p. 2672–2692.
8. Savage, P.E., *Heterogeneous catalysis in supercritical water*. Catalysis Today, 2000. **62**(2-3): p. 167-173.
9. Kruse, A. and A. Gawlik, *Biomass conversion in water at 330-410°C and 30-50 MPa. Identification of key compounds for indicating different chemical reaction pathways*. Industrial & engineering chemistry research, 2003. **42**(2): p. 267-279.

10. Guo, L.J., et al., *Hydrogen production by biomass gasification in supercritical water: a systematic experimental and analytical study*. *Catalysis today*, 2007. **129**(3-4): p. 275-286.
11. Holgate, H.R., J.C. Meyer, and J.W. Tester, *Glucose hydrolysis and oxidation in supercritical water*. *AIChE Journal*, 1995. **41**(3): p. 637-648.
12. Kabyemela, B. M.; Adschiri, T.; Malaluan, R. M.; Arai, K., Glucose and Fructose Decomposition in Subcritical and Supercritical Water: Detailed Reaction Pathway, Mechanisms, and Kinetics. *Ind. Eng. Chem. Res.* **1999**, 38, 2888.
13. Lee, I.G., M.S. Kim, and S.K. Ihm, *Gasification of glucose in supercritical water*. *Industrial & engineering chemistry research*, 2002. **41**(5): p. 1182-1188.
14. Jesus, P.; Boukis, N.; K., C. B.; E, D., Influence of process variables on gasification of corn silage in supercritical water, *Industrial Engineering Chemistry research*. *Ind. Eng. Chem. Res.* **2006**, 45, 1622.
15. Jin, F.; Kishita, A.; Moriya, T.; Enomoto, H., Kinetics of oxidation of food wastes with H₂O₂ in supercritical water. *J. Supercrit. Fluids* **2001**, 19, 251.
16. Osada, M., et al., *Catalytic gasification of wood biomass in subcritical and supercritical water*. *Combustion Science and Technology*, 178, 2006. **1**(3): p. 537-552.
17. Elliott, D.C., *Catalytic hydrothermal gasification of biomass*, *Biofuels Bioprod.* Biorefin, 2008. **2**(3): p. 254–265.

18. Lu, Y., et al., *Thermodynamic modeling and analysis of biomass gasification for hydrogen production in supercritical water*. Chemical Engineering Journal, 2007. **131**(1-3): p. 233-244.
19. Matsumura Y, Hara S, Minowa T, Noda Y and Shimizu Y, Catalyst-slurry supercritical water gasification (CS-SCWG) as a new wet biomass gasification technology, *15th European Biomass Conference and Exhibition: From Research to Market Deployment*. Berlin. **V2.1.I.60**. (2007).
20. Antal Jr, M.J., et al., *Biomass gasification in supercritical water*. Industrial & engineering chemistry research, 2000. **39**(11): p. 4040-4053.
21. Xu, X., et al., *Carbon-Catalyzed Gasification of Organic Feedstocks in Supercritical Water*. Ind. Eng. Chem. Res, 1996. **35**(8): p. 2522-2530.
22. Osada, M., et al., *Low-temperature catalytic gasification of lignin and cellulose with a ruthenium catalyst in supercritical water*. Energy Fuels, 2004. **18**(2): p. 327-333.
23. Sinag, A., A. Kruse, and J. Rathert, *Influence of the heating rate and the type of catalyst on the formation of key intermediates and on the generation of gases during hydrolysis of glucose in supercritical water in a batch reactor*. Industrial & engineering chemistry research, 2004. **43**(2): p. 502-508.
24. Mosier, N., et al., *Features of promising technologies for pretreatment of lignocellulosic biomass*. Bioresource technology, 2005. **96**(6): p. 673-686.
25. Hendriks, A. and G. Zeeman, *Pretreatments to enhance the digestibility of lignocellulosic biomass*. Bioresource technology, 2009. **100**(1): p. 10-18.
26. Kruse, A. and A. Gawlik, *Biomass conversion in water at 330-410°C and 30-50 MPa. Identification of key compounds for indicating different chemical*

- reaction pathways*. Industrial & engineering chemistry research, 2003. **42**(2): p. 267-279.
27. Chuntanapum, A. and Y. Matsumura, *Char formation mechanism in supercritical water gasification process: a study of model compounds*. Industrial & engineering chemistry research. **49**(9): p. 4055-4062.
28. Guo, L.J., et al., *Hydrogen production by biomass gasification in supercritical water: a systematic experimental and analytical study*. Catalysis Today, 2007. **129**(3-4): p. 275-286.
29. Kruse, A., et al., *Gasification of pyrocatechol in supercritical water in the presence of potassium hydroxide*. Ind. Eng. Chem. Res, 2000. **39**(12): p. 4842-4848.
30. Sato, T., et al., *Gasification of alkylphenols with supported noble metal catalysts in supercritical water*. Industrial & engineering chemistry research, 2003. **42**(19): p. 4277-4282.
31. Osada, M., et al., *Stability of supported ruthenium catalysts for lignin gasification in supercritical water*. Energy & fuels, 2006. **20**(6): p. 2337-2343.
32. Waldner, M.H., F. Krumeich, and F. Vogel, *Synthetic natural gas by hydrothermal gasification of biomass:: Selection procedure towards a stable catalyst and its sodium sulfate tolerance*. The Journal of Supercritical Fluids, 2007. **43**(1): p. 91-105.
33. Xu, J. and G.F. Froment, *Methane steam reforming: II. Diffusional limitations and reactor simulation*. AIChE Journal, 1989. **35**(1): p. 97-103.

34. Agnelli, M., et al., *CO Hydrogenation on a Nickel Catalyst* 1:: II. A Mechanistic Study by Transient Kinetics and Infrared Spectroscopy*. Journal of Catalysis, 1998. **175**(1): p. 117-128.
35. Tavares, M.T., et al., *Carbon formation and CO methanation on silica-supported nickel and nickel-copper catalysts in CO+ H₂ mixtures*. Journal of Catalysis. 1996. **158**: 402-410.
36. Fu, Y.C., et al., *Hydrogenation of model compounds in syngas-D₂O systems*. Energy & fuels, 1995. **9**(3): p. 406-412.
37. Yoshida, T. and Y. Matsumura, *Gasification of cellulose, xylan, and lignin mixtures in supercritical water*. Industrial & engineering chemistry research, 2001. **40**(23): p. 5469-5474.
38. Minowa, T. and T. Ogi, *Hydrogen production from cellulose using a reduced nickel catalyst*. Catalysis today, 1998. **45**(1-4): p. 411-416.
39. Sato, T., et al., *Effect of water density on the gasification of lignin with magnesium oxide supported nickel catalysts in supercritical water*. Industrial & engineering chemistry research, 2006. **45**(2): p. 615-622.
40. Hao, X.H., et al., *Hydrogen production from glucose used as a model compound of biomass gasified in supercritical water*. International Journal of Hydrogen Energy, 2003. **28**(1): p. 55-64.
41. Yamaguchi, A., et al., *Hydrogen production from woody biomass over supported metal catalysts in supercritical water*. Catalysis Today, 2009. **146**(1-2): p. 192-195.

42. Osada, M., et al., *Water density effect on lignin gasification over supported noble metal catalysts in supercritical water*. Energy & fuels, 2006. **20**(3): p. 930-935.
43. Byrd, A.J. and R.B. Gupta, *Stability of cerium-modified [gamma]-alumina catalyst support in supercritical water*. Applied Catalysis A: General, 2010. **381**(1-2): p. 177-182.
44. Furusawa, T., et al., *The evaluation of the stability of Ni/MgO catalysts for the gasification of lignin in supercritical water*. Applied Catalysis A: General, 2007. **327**(2): p. 300-310.
45. Tomita, K. and Y. Oshima, *Stability of manganese oxide in catalytic supercritical water oxidation of phenol*. Industrial & engineering chemistry research, 2004. **43**(24): p. 7740-7743.
46. Yu, J. and P.E. Savage, *Catalyst activity, stability, and transformations during oxidation in supercritical water*. Applied Catalysis B: Environmental, 2001. **31**(2): p. 123-132.
47. Aki, S.N.V.K., Z.Y. Ding, and M.A. Abraham, *Catalytic supercritical water oxidation: stability of Cr₂O₃ catalyst*. AIChE Journal, 1996. **42**(7): p. 1995-2004.
48. Lu, Y., et al., *Hydrogen production by biomass gasification in supercritical water over Ni/[gamma] Al₂O₃ and Ni/CeO₂-[gamma] Al₂O₃ catalysts*. International Journal of Hydrogen Energy, 2010. **35**(13): p. 7161-7168.
49. Tomishige, K. and K. Fujimoto, *Ultra-stable Ni catalysts for methane reforming by carbon dioxide*. Catalysis surveys from Japan, 1998. **2**(1): p. 3-15.

50. Tsyganok, A.I., et al., *Mg–Al layered double hydroxide intercalated with [Ni (edta)] 2- chelate as a precursor for an efficient catalyst of methane reforming with carbon dioxide*. Catalysis letters, 2001. **77**(1): p. 75-86.
51. S. Tang, L. Ji, J. Lin, H.C. Zeng, k.L. Tan, and K. Li, *CO₂ Reforming of methane to synthesis gas over Sol-gel made Ni/γ-Al₂O₃ catalysts from organometallic precursors*. J. of Catal. 2000. **194**: p.424.
52. Montoya, J.A., et al., *Methane reforming with CO₂ over Ni/ZrO₂-CeO₂ catalysts prepared by sol-gel*. Catalysis Today, 2000. **63**(1): p. 71-85.
53. Hwang, K.S., H.Y. Zhu, and G.Q. Lu, *New nickel catalysts supported on highly porous alumina intercalated laponite for methane reforming with CO₂*. Catalysis Today, 2001. **68**(1-3): p. 183-190.
54. Yanik, J., et al., *Biomass gasification in supercritical water: II. Effect of catalyst*. International Journal of Hydrogen Energy, 2008. **33**(17): p. 4520-4526.
55. Arita, T., et al., *Hydrogen generation from ethanol in supercritical water without catalyst*. Tetrahedron letters, 2003. **44**(5): p. 1083-1086.
56. Minowa, T. and T. Ogi, *Hydrogen production from cellulose using a reduced nickel catalyst*. Catalysis Today, 1998. **45**(1-4): p. 411-416.
57. Huber, G.W., J.W. Shabaker, and J.A. Dumesic, *Raney Ni-Sn catalyst for H₂ production from biomass-derived hydrocarbons*. Science, 2003. **300**(5628): p. 2075.
58. Matsumura, Y., et al., *Supercritical water treatment of biomass for energy and material recovery*. Combustion Science and Technology, 178, 2006. **1**(3): p. 509-536.

59. Cortright, R.D., R.R. Davda, and J.A. Dumesic, *Hydrogen from catalytic reforming of biomass-derived hydrocarbons in liquid water*. *Nature*, 2002. **418**(6901): p. 964-967.
60. Moghtaderi, B., *Effects of controlling parameters on production of hydrogen by catalytic steam gasification of biomass at low temperatures*. *Fuel*, 2007. **86**(15): p. 2422-2430.
61. Garcia Jarana, M.B., et al., *Supercritical water gasification of industrial organic wastes*. *The Journal of Supercritical Fluids*, 2008. **46**(3): p. 329-334.
62. Yu, D., M. Aihara, and M.J. Antal Jr, *Hydrogen production by steam reforming glucose in supercritical water*. *Energy & fuels*, 1993. **7**(5): p. 574-577.
63. Byrd, A.J., K.K. Pant, and R.B. Gupta, *Hydrogen production from ethanol by reforming in supercritical water using Ru/Al₂O₃ catalyst*. *Energy & fuels*, 2007. **21**(6): p. 3541-3547.
64. Gadhe, J.B. and R.B. Gupta, *Hydrogen production by methanol reforming in supercritical water: suppression of methane formation*. *Industrial & engineering chemistry research*, 2005. **44**(13): p. 4577-4585.
65. Sato, T., S. Kurosawa, and R.L. Smith, *Water gas shift reaction kinetics under noncatalytic conditions in supercritical water*. *The Journal of Supercritical Fluids*, 2004. **29**(1-2): p. 113-119.
66. Kruse, A. and E. Dinjus, *Hydrogen from methane and supercritical water*. *Angewandte Chemie International Edition*, 2003. **42**(8): p. 909-911.
67. Matsumura, Y., et al., *Biomass gasification in near-and super-critical water: Status and prospects*. *Biomass and Bioenergy*, 2005. **29**(4): p. 269-292.

68. Kersten, S.R.A., et al., *Gasification of model compounds and wood in hot compressed water*. Industrial & engineering chemistry research, 2006. **45**(12): p. 4169-4177.
69. Lu, Y.J., et al., *Hydrogen production by biomass gasification in supercritical water: a parametric study*. International Journal of Hydrogen Energy, 2006. **31**(7): p. 822-831.
70. Srokol, Z., et al., *Hydrothermal upgrading of biomass to biofuel; studies on some monosaccharide model compounds*. Carbohydrate research, 2004. **339**(10): p. 1717-1726.
71. Gandini, A. and M.N. Belgacem, *Furans in polymer chemistry*. PROG POLYM SCI(OXFORD), 1997. **22**(6): p. 1203-1379.
72. Hashaikeh, R., I.S. Butler, and J.A. Kozinski, *Selective promotion of catalytic reactions during biomass gasification to hydrogen*. Energy & fuels, 2006. **20**(6): p. 2743-2747.
73. Yang, M. and H. Papp, *CO₂ reforming of methane to syngas over highly active and stable Pt/MgO catalysts*. Catalysis Today, 2006. **115**(1-4): p. 199-204.
74. Therdthianwong, S., C. Siangchin, and A. Therdthianwong, *Improvement of coke resistance of Ni/Al₂O₃ catalyst in CH₄/CO₂ reforming by ZrO₂ addition*. fuel processing technology, 2008. **89**(2): p. 160-168.
75. Hao, Z., et al., *Characterization of aerogel Ni/Al₂O₃ catalysts and investigation on their stability for CH₄-CO₂ reforming in a fluidized bed*. Fuel Processing Technology, 2009. **90**(1): p. 113-121.

76. Jiang, H., et al., *Preparation of Ni/MgxTi1- α xO catalysts and investigation on their stability in tri-reforming of methane*. Fuel Processing Technology, 2007. **88**(10): p. 988-995.
77. Fatsikostas, A.N. and X.E. Verykios, *Reaction network of steam reforming of ethanol over Ni-based catalysts*. Journal of Catalysis, 2004. **225**(2): p. 439-452.
78. Homs, N., J. Llorca, and P.R. de la Piscina, *Low-temperature steam-reforming of ethanol over ZnO-supported Ni and Cu catalysts:: The effect of nickel and copper addition to ZnO-supported cobalt-based catalysts*. Catalysis today, 2006. **116**(3): p. 361-366.
79. Garcia, L., et al., *Catalytic steam reforming of bio-oils for the production of hydrogen: effects of catalyst composition*. Applied Catalysis A: General, 2000. **201**(2): p. 225-239.
80. Haga, F., et al., *Catalytic properties of supported cobalt catalysts for steam reforming of ethanol*. Catalysis letters, 1997. **48**(3): p. 223-227.
81. Haga, F., Nakajima, T., Yamashita, K., Mishima, S., *Nippon Kagaku Kaishi*. J. Chem. Soc. Japan. 1997, **1**, 33.
82. Aupretre, F., C. Descorme, and D. Duprez, *Bio-ethanol catalytic steam reforming over supported metal catalysts*. Catalysis Communications, 2002. **3**(6): p. 263-267.
83. Aupretre, F., C. Descorme, and D. Duprez, *Hydrogen production for fuel cells from the catalytic ethanol steam reforming*. Topics in catalysis, 2004. **30**(1): p. 487-491.

84. Kaddouri, A. and C. Mazzocchia, *A study of the influence of the synthesis conditions upon the catalytic properties of Co/SiO₂ or Co/Al₂O₃ catalysts used for ethanol steam reforming*. Catalysis Communications, 2004. **5**(6): p. 339-345.
85. Sing, K.S.W., et al., *Reporting physisorption data for gas/solid systems*. 1985.
86. Euzen, P., et al., *Handbook of Porous Solids, Vol. 3*, Schüth, F., Sing, KSW, Weitkamp, J. 2002, Wiley-VCH Verlag GmbH, Weinheim.
87. Marquez-Alvarez, C.; Zilkova, N.; Perez-Pariente, J.; Cejka, J. *Synthesis, Characterization and Catalytic Applications of Organized Mesoporous Aluminas*. Cat. Rev.-Sci. Eng., 2008. **50**(2): 222–286.
88. Fang, X.S., et al., *Synthesis and photoluminescence of -Al₂O₃ nanowires*. Journal of Physics: Condensed Matter, 2004. **16**: p. 4157-4163.
89. Kurien, S., et al., *Dielectric behavior and ac electrical conductivity of nanocrystalline nickel aluminate*. Materials chemistry and physics, 2006. **98**(2-3): p. 470-476.
90. Kim, S.E., et al., *Anodically nanostructured titanium oxides for implant applications*. Electrochimica Acta, 2008. **53**(14): p. 4846-4851.
91. Boissière, C., et al., *Nanocrystalline Mesoporous -Alumina Powders UPMCI Material” Gathers Thermal and Chemical Stability with High Surface Area*. Chemistry of materials, 2006. **18**(22): p. 5238-5243.
92. Zima, T.M., N.I. Baklanova, and N.Z. Lyakhov, *Mesoporous structure of Al₂O₃ prepared from poly (N-vinylpyrrolidone)-modified sols of hydrous metal oxides*. Inorganic Materials, 2008. **44**(2): p. 146-153.

93. Trueba, M.; Trasatti, S. P., *γ -Alumina as a Support for Catalysts: A Review of Fundamental Aspects*. Eur. J. Inorg. Chem. 2005, **17**, 3393–3403.
94. Vaudry, F., S. Khodabandeh, and M.E. Davis, *Synthesis of pure alumina mesoporous materials*. Chemistry of materials, 1996. **8**(7): p. 1451-1464.
95. Zhang, Z., et al., *Mesostructured forms of γ -Al₂O₃*. Journal of the American Chemical Society, 2002. **124**(8): p. 1592-1593.
96. Liu, Q., et al., *Ordered crystalline alumina molecular sieves synthesized via a nanocasting route*. Chemistry of materials, 2006. **18**(22): p. 5153-5155.
97. Zhang, Z. and T.J. Pinnavaia, *Mesostructured Forms of the Transition Phases- γ -Al₂O₃*. Angew. Chem. Int. Ed, 2008. **47**: p. 7501–7504.
98. Yuan, Q., et al., *Facile synthesis for ordered mesoporous γ -aluminas with high thermal stability*. Journal of the American Chemical Society, 2008. **130**(11): p. 3465-3472.
99. Ren, T.Z., Z.Y. Yuan, and B.L. Su, *Microwave-assisted preparation of hierarchical mesoporous-macroporous boehmite AlOOH and γ -Al₂O₃*. Langmuir, 2004. **20**(4): p. 1531-1534.
100. Niesz, K., P. Yang, and G.A. Somorjai, *Sol-gel synthesis of ordered mesoporous alumina*. Chem. Commun, 2005. **15**: p. 1986-1987.
101. Heracleous, E., et al., *Investigation of Ni-based alumina-supported catalysts for the oxidative dehydrogenation of ethane to ethylene: structural characterization and reactivity studies*. Journal of Catalysis, 2005. **231**(1): p. 159-171.

102. Zhang, S., et al., *One-pot synthesis of Ni-nanoparticle-embedded mesoporous titania/silica catalyst and its application for CO₂-reforming of methane*. *Catalysis Communications*, 2008. **9**(6): p. 995-1000.
103. Salagre, P., et al., *Characterization of nickel species on several [gamma]-alumina supported nickel samples*. *Journal of Molecular Catalysis A: Chemical*, 1996. **106**(1-2): p. 125-134.
104. Delgado, J.; Aznar, M.; Corella, J., Biomass gasification with steam in fluidized bed: effectiveness of CaO, MgO for hot raw gas cleaning. *Ind. Eng. Chem. Res.* **1997**, 36, 1535.
105. Matsumura, Y.; Minowa, T.; Xu, X.; Nuessle, F.; Adschiri, T.; Antal, J. M., High pressure carbon dioxide removal in supercritical water gasification of biomass. *Ind. Eng. Chem. Res.* **1996**, 864.

CHAPTER THREE

Ru-Ni-Al₂O₃ catalysts for the supercritical water gasification of glucose

3.1 Introduction

Increasing concerns regarding the emission of greenhouse gases such as CO₂ from the burning of fossil fuels, along with the projected decline in world oil production has led to a tremendous current interest in alternative energies [1]. Hydrogen is considered to be one of the most suitable long-term sustainable clean energy carriers as it emits only water vapour during its combustion or oxidation process. However, a renewable source of hydrogen is required with biomass being considered one of its most abundant and renewable sources [2]. One promising method for hydrogen production is the direct gasification of biomass which leads to zero net CO₂ emissions as CO₂ produced from gasification is fixed by photosynthesis during biomass growth. However, biomass contains a higher moisture content than solid fossil fuels, in the range of 90% or sometimes even higher. As direct combustion requires removing moisture from the biomass before gasification, the energy spent on water evaporation may cause a negative net energy production. Supercritical water gasification (SCWG) offers an emerging option for the gasification of high moisture content biomass without removing moisture while maintaining a high energy conversion efficiency [3].

SCWG is basically the hydrothermal conversion of biomass into gaseous products at conditions that exceed the critical point of water (374°C and 22.1 MPa). Supercritical water (SCW) shows low-viscosity and high-diffusivity values similar to those of

organic solvents which enhances the tendency to dissolve most organic substances present in biomass components. This allows for hydrolysis to break down the polymeric biomass structure as opposed to pyrolysis used in conventional gasification. A well designed SCWG system can recover 92% of the chemical energy from the biomass in the gaseous products, and produce 4.5 J of energy for every 1 J of energy lost in the system [4].

Catalysts play an important role in hydrogen production from biomass during SCWG by increasing hydrogen yield, reducing tar and char formation, and affecting organic matter gasification efficiencies, defined as the percentage of biomass converted into gas, of up to 98%. The most commonly used catalysts for SCWG described in the literature are activated carbon, metals, metal oxides and alkali [5]. Metal catalysts, such as the noble metals Pt, Pd, Ru, Rh [6] and metal Ni [7-12], have been examined in SCWG. Alkalis including NaOH, KOH etc have been examined as catalysts or promoters for SCWG [13-14]. Some researchers have also investigated activated charcoal [15] and metal oxides as catalysts in SCWG [16].

Nickel has been widely used as a catalyst in steam reforming reactions, and sub or SCWG because of its high activity and low cost. Elliot et al. obtained a CH₄ rich product gas by using different types of nickel catalysts at 400°C and 17–23 MPa with a batch reactor [17]. Minowa et al. found that a nickel catalyst catalyzed the steam reforming cellulose examining various supports in hot-compressed water [8-9]. Sato et al. investigated lignin and cellulose gasification in SCW using nickel catalysts with various supports [10]. Azadi et al. used transition metal chelates consisting of nickel(II) acetylacetonate (Ni(acac)₂), cobalt(II) acetylacetonate (Co(acac)₂), iron(III) acetylacetonate (Fe(acac)₃) and Raney nickel particles for hydrothermal gasification

of glucose and found that Raney-nickel was a more effective catalyst compared to homogeneous $\text{Ni}(\text{acac})_2$, $\text{Co}(\text{acac})_2$, and $\text{Fe}(\text{acac})_3$ catalysts [11]. Azadi et al. also used supported and unsupported metal catalysts consisting of Raney-nickel, Raney-cobalt, Raney copper, carbon-supported ruthenium, and alumina-supported ruthenium for gasification of glucose in near-critical water [12]. The authors used Ru and Ni supported alumina catalysts for hydrothermal gasification of glucose and found that Ru significantly reduced the graphitic coke formation on the catalyst surface.

From an industrial point of view, it may be more practical to develop Ni-based catalysts because of their low price and ready availability. However, One of the major problems of nickel based catalysts in a high temperature system is the high thermodynamic potential for coke formation [18]. Ronggang et al. suggested that carbon deposition was inevitable in the temperature range from 300 to 1000°C from a thermodynamic analysis [19]. Carbon deposition also depends on the physicochemical properties of the catalysts, including the particle sizes of the active metal, types of support and promoter, etc. [20-22].

It is well known that bimetallic catalysts may sometimes exhibit superior activity, selectivity and deactivation resistance compared to their corresponding monometallic analogs [23]. Noble metals (i.e Rh, Ru) can provide high activity's with a high coke resistance but they are also less attractive in view of their higher costs [24]. The strong improvement in the activity and stability observed in the case of Ni–Ru catalysts has been attributed to the formation of Ni–Ru bimetallic clusters with a surface mainly covered by nickel [25]. This leads to an increase in the metallic dispersion of Ni and favours the formation of a more reactive intermediate carbonaceous species, thus limiting the deactivation of the catalyst. Ruthenium itself

plays an important role in reducing coke formation on the catalyst surface when exposed to a high temperature environment. Ru-Al₂O₃ showed better coke resistance and a lower graphitization degree of deposited carbon than Ni-Al₂O₃ for a solid oxide fuel cell operating on methane [26]. Youssef et al. found the highest conversion and hydrogen yield from hog manure using Ru-Al₂O₃ rather than Ru-Ac, Ac, or NaOH [27]. Ru-Al₂O₃ also enhanced the conversion and hydrogen yield from glucose and ethanol reforming by SCW, while significantly reducing the coke and other heavier liquid products formation [28].

Since Ru ensures C–C bond rupture of formation of adsorbed intermediates during glucose gasification in SCW [28], the aim of this work was to investigate the promoting effect of incorporation of small amounts (0.5 wt%) of Ru into 11% Ni-Al₂O₃ for glucose gasification in SCW at moderate temperatures (400-500°C). Youssef et al. showed that the hydrogen yield was relatively insensitive on the pellet catalyst at nickel loading above 11 wt% as well as on different catalyst supports [29]. In this study we tried to reduce the graphitic coke deposition on the catalyst surface which mainly deactivates the catalyst by synthesizing and investigating a novel Ru-Ni-Al₂O₃ aerogel catalyst using a sol–gel technique combined with supercritical CO₂ drying. Al₂O₃ was chosen as the support as it provides a high thermal stability to the catalyst [30].

The properties of the aerogel catalysts were characterized by means of BET surface area analysis, FTIR analysis, TGA, X-ray diffraction (XRD), Hydrogen temperature programmed reduction (H₂-TPR), Pulse chemisorption, scanning electron microscopy (SEM), and transmission electron microscopy (TEM). The catalytic activities of the catalysts were investigated in SCW for glucose gasification in a batch reactor. After

the reaction in SCW, the catalysts surface was examined for coke deposition using several techniques, including conventional temperature-programmed oxidation (TPO), X-ray diffraction (XRD), and Raman spectroscopy.

3.2 Experimental

3.2.1 Materials

Aluminum isopropoxide ($C_9H_{21}O_3Al$) (98%) and Ruthenium chloride ($RuCl_3$) were obtained from Aldrich (Mississauga, Canada), Nickel nitrate hexahydrate ($NiNO_3 \cdot 6H_2O$) and glucose were obtained from Sigma–Aldrich (Oakville, Ontario, Canada), isopropanol (purity 99.5%) was obtained from Caledon Laboratories Ltd, Georgetown, ON, Canada. All of these chemicals were used as received. De-ionized water was obtained from a compact ultrapure water system (EASY pure LF, Mandel Scientific co, model BDI-D7381). For impregnation catalyst preparation, $\gamma-Al_2O_3$ pellets with 3 mm average particle diameter, $263\text{ m}^2/\text{gm}$ BET surface area and pore volume of $0.34\text{ cm}^3/\text{gm}$ were received from Aldrich (Mississauga, Canada).

3.2.2 Catalyst preparation

Two methods of synthesis: impregnation and supercritical sol-gel processing were investigated. The preparation procedure used for the impregnation method was similar to that described previously [31]. $\theta-Al_2O_3$ pellets were used as the catalyst support and obtained by calcining $\gamma-Al_2O_3$ at $1050\text{ }^\circ\text{C}$ for 1h at a rate of $10\text{ }^\circ\text{C}$ per min. For a typical synthesis, the required metal salt solution was prepared in a volume of pure water corresponding to 130 vol% of pore volume of alumina ($0.19\text{ cm}^3/\text{gm}$, measured by Tristar II 3020, Micromeritics Instrument Corporation) used for the catalyst support. The required amount of nickel was calculated from the nickel present in $NiNO_3 \cdot 6H_2O$. All alumina was dipped into the solution at once for uniform metal

dispersion. The catalyst was then placed in a beaker which was placed in a separate closed beaker of 10 vol% $\text{NH}_3\text{-H}_2\text{O}$ solutions for ammonia vapor treatment for 10 min at 60 °C inside the oven to convert metal salt into ammonium salt to increase the Ni dispersion. The pellets were then heated from 60 to 250 °C at rate of 2°C/min with most of the ammonium salts attached to the catalyst being removed by sublimation. Hydrogen reduction and thermal treatment at 600 °C for 1h at a rate of 3°C per minute was performed afterwards, in a stream of 5 vol% H_2 balanced with Ar. The reduced catalysts were weighed to measure the actual loading of nickel by the difference between support alumina and nickel loaded catalyst.

Aerogel catalysts were prepared by a combination of sol–gel synthesis and supercritical drying, similar to the preparation of simple metal oxide aerogel [32]. Aluminum isopropoxide was used as the aerogel support precursor. The required amount of aluminum isopropoxide (i.e. 20 gm for synthesizing 5 gm of catalyst) dispersed in isopropanol (80 ml) was placed in a 250 ml flask and the resultant mixture was kept under vigorous stirring at 75°C for one hour. To the cloudy sol, 0.3 ml of 1M nitric acid was added for peptization (formation of stable dispersion of colloidal particles) and the sol was refluxed with stirring at 75°C for 1h to obtain a clear sol. The appropriate amount of nickel nitrate and ruthenium chloride was dissolved in isopropanol with the individual solutions then added to the clear boehmite sol at 15 minutes intervals, with the resultant mixture refluxed at 75°C for 1 h with vigorous stirring. The sol was kept for three days at room temperature in a sealed flask for aging. After aging, the resultant gel was washed with acetone to remove any traces of solvent, nitric acid, etc. This washed gel was dried in scCO_2 at 4000 psi and 60 °C for 3 days to remove unreacted acid, alcohol and ester from the

gel formation. The rate of venting CO₂ was approximately 0.2ml/min to prevent collapse of nano-structured morphology. At the end of drying, a porous aerogel was obtained which was calcined and reduced at 600 °C for 1h at a rate of 3°C per minute, in a stream of 5 vol% H₂ balanced with Ar.

The textural properties of any material are largely dependent on the employed preparation method and conditions. Several synthetic strategies have been developed to obtain porous high-surface area alumina. The most common synthetic routes are based on sol–gel. In the sol–gel process, the method of solvent removal from the gel is very critical and determines the textural properties of the final product. While supercritical drying results in aerogel with unique textural properties including high surface areas and total pore volumes, conventional drying usually results in xerogel with lower surface areas and pore volumes [33].

3.2.3 Catalyst characterization

The Brunauer-Emmett-Teller (BET) surface area, pore diameter and pore volume of both impregnation and aerogel catalysts were determined from nitrogen adsorption and desorption isotherm data obtained at –193 °C in a constant-volume adsorption apparatus (Tristar II 3020, Micromeritics Instrument Corporation) using 99.995% pure N₂ gas obtained from Praxair (Oakville, Canada). The prepared samples were degassed at 200 °C for 12 hours before measurements to remove the moisture and other adsorbed gases from the catalyst surface.

Infrared analysis of the as prepared & calcined aerogel samples were analyzed using an ATR-FTIR spectroscope (Nicolet 6700 FTIR), connected to a computer, supported by Thermo Scientific OMNICTM software. After the crystal area was cleaned and background collected, a small amount of the as-prepared or calcined aerogel sample

was loaded on the small crystal area with the ATR probe positioned over the crystal/sample area and force applied to the sample for collection.

Thermogravimetric analysis of the as-prepared aerogel catalyst before calcination was measured by a TGA/SDT A851 model gravimetric analyzer with a heating rate of 10°C/min from ambient temperature to 1000°C. The as-prepared aerogel sample (ca. 10 mg) was loaded onto an alumina crucible using an empty alumina crucible as a reference and heated from room temperature to 1000°C at a rate of 10°C/min in air with a flow rate of 50 ml/min.

The phase structure of the catalysts and coke deposition was analyzed by using Powder X-ray diffractometry. A Rigaku rotating-anode XRD was used employing CuK α radiation ($\lambda=1.5408 \text{ \AA}$). The instrument was operated at 45kV and 160mA, using the normal scan rate of 10° per minute in the 2 θ range from 2° to 82°.

Temperature programmed reduction of hydrogen (H₂-TPR) was performed on a chemisorption apparatus (Micromeritics Autochem 2920). Before TPR measurements, 100-150 mg of the fresh catalyst was completely oxidized at 550 °C by flowing a stream of gas containing 5% O₂ in He. The TPR analysis was performed by circulating a stream of gas containing 10 % H₂ and balanced Ar at a rate of 50 mL/min. The temperature was raised from ambient to 950°C at a rate of 10°C/min. A thermal conductivity detector (TCD) was used to record the change of hydrogen concentration of the gas stream passing through the catalyst sample for calculating the amount of hydrogen consumed during the reduction process.

H₂ pulse chemisorption experiments were also conducted using a Micromeritics Autochem 2920 to determine the active metal surface area, the percent dispersion and the active particle size of the nickel crystallites on the alumina support.

The morphologies of both the fresh and spent catalysts were obtained from scanning electron microscopy (SEM) micrographs (model LEO1530) and transmission electron microscopy (TEM) images (model JEOL 2010F). Before TEM analysis, the powdered samples were dispersed in methanol by sonication and then placed and dried by normal evaporation on a copper grid covered with holey carbon film.

Temperature programmed oxidation (TPO) of the spent catalysts was performed to examine the characteristics of deposited carbonaceous products on the catalysts during reaction. TPO was done by heating the coked sample from room temperature to 800°C with a rate of 10°C/min. In the experiment, 5% O₂ balanced with He with a flow-rate of 50 ml/min was used. The coke deposition on the catalyst surface was also characterized by Raman spectroscopy using a Kaiser Optical Systems RXNI-785 with an excitation wavelength of 785 nm.

3.2.4 Catalyst testing

The evaluation of catalyst activity using SCWG was carried out in a reactor from Autoclave Engineers, Erie, Penn, U.S.A, which was constructed from Hastelloy C-276 with a capacity of 600 ml with operating pressure of 36 MPa rating at 500°C. The reactor was heated with a 1.5 kW electric furnace that surrounded its main body supplied by the same manufacturer. A detailed description of the experimental setup and procedure was reported elsewhere by Youssef et al. [29]. The glucose solution was prepared using purified water and kept well mixed until delivered to the reactor via a syringe pump (Isco 100D). Analysis of the product gases was performed using a gas chromatograph (Shimadzu, GC-2014) equipped with a thermal conductivity detector (TCD) and a 120/80 D Hayesep stainless steel packed column (Grace Davidson) having dimensions of 6.2m long, and 3.18mm inside diameter. Helium was

used as the carrier gas. The GC was calibrated using a standard gas mixture of known composition containing H₂, CO, CH₄, and CO₂. The analysis was performed manually using 1ml SGE gas tight syringe (Model number 008100, Reno, NV, USA) by collecting the sample from a Tedlar gas bag obtained from SKC Inc (PA, USA). Each experiment was repeated at least two times & the gas analysis was performed at least six times for each sample to minimize experimental error. The liquid effluents from the SCWG experiments were analyzed to measure the Total Organic Carbon (TOC) content using a TOC-VCPH (Shimadzu Instruments).

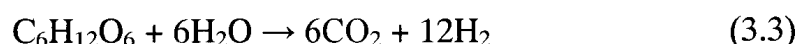
Calculation of product gas yield and carbon gasification efficiency (CGE) was performed by the same procedure used by Yu and Antal [34]. The aforementioned authors calculated the CGE as:

$$CGE = \frac{\text{mole carbon in gas}}{\text{mole carbon in feed}} \quad (3.1)$$

and

$$\text{Gas yields} = \frac{\text{mole of gas species produced}}{\text{mole of glucose in feed}} \quad (3.2)$$

Biomass gasification proceeds via several complex reactions, such as pyrolysis, hydrolysis, steam reforming, and water gas shift reaction, and methanation. For glucose reforming in supercritical water, a maximum theoretical yield of hydrogen can be calculated by converting the entire feed carbon to carbon dioxide with water as:



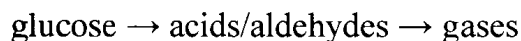
In the overall reaction scheme, CO₂ also undergoes hydrogenation reaction to form CO and CH₄ as



and



However, mechanistically glucose reforming via reaction intermediates can be shown as follows:



The TOC decomposition X , was used to evaluate the extent of decomposition, as defined by:

$$\text{TOC decomposition, } X = 1 - \frac{[\text{TOC}]_e}{[\text{TOC}]_0} \quad (3.6)$$

where, $[\text{TOC}]_0$ is the initial TOC and $[\text{TOC}]_e$ is the residual TOC after reaction and was selected as a parameter to track the liquid effluent quality and to optimize, together with maximum hydrogen yield in gasification of glucose in supercritical water.

3.3. Results and discussion

3.3.1 Optimization of ruthenium concentration

Sato et al. reported gasification of alkyl-phenols with several noble metal catalysts such as platinum, palladium, ruthenium & rhodium at 400°C [6]. Their results confirmed that ruthenium and rhodium were the most active metals with high levels of methane produced after only 15 minutes reaction time. Three different concentrations of Ru i.e 0.2, 0.5, and 1.9% were chosen in this study and used for glucose gasification in SCW and investigated for the production of H₂. As shown in Figure 3.1a, the 0.5% ruthenium containing catalyst showed the highest hydrogen yield. The hydrogen yield decreased with a higher concentration of ruthenium as a

major portion of hydrogen produced during glucose gasification was converted into methane (Figure 3.1b). The high concentration of ruthenium enhanced methanation reactions are described in detailed later. Hence the remainder of this study used the optimum ruthenium concentration (0.5%).

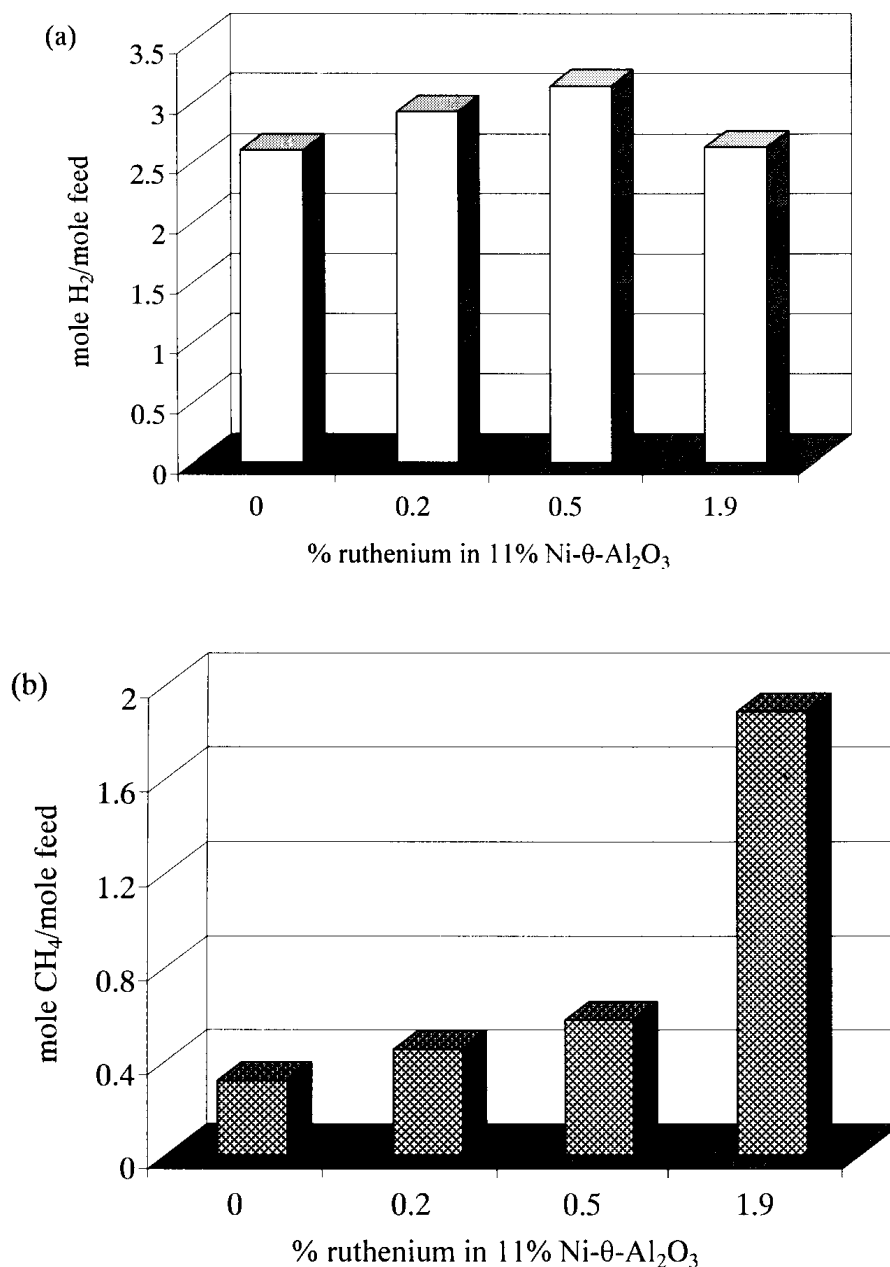


Figure 3.1. Effect of ruthenium concentration on (a) hydrogen & (b) methane yield, Feed=0.25M Glucose, t=30 minutes, T=500°C, P=25 MPa, catalyst 1.0 gm (impregnation).

3.3.2 Characterization of Synthesized Catalysts

Using the novel catalysts synthesized by the impregnation and aerogel procedures, Table 3.1 shows the BET surface area, pore volume and pore size of the 0.5%Ru-11%Ni-Al₂O₃ after calcination and reduction at 600°C. Compared to the catalyst prepared by the impregnation method, the aerogel catalyst shows a much higher BET surface area (380 m²/g), larger pore volume (0.75 cm³/g), and more pronounced mesoporosity attributed to the difference of the synthesis method.

Table 3.1. BET surface area, pore size and pore volume of the catalysts.

Catalyst	Total surface area (BET) (m ²)	Pore volume (cm ³ /g)	Average pore size (nm)
0.5%Ru-11%Ni- θ Al ₂ O ₃ (impregnation)	52	0.21	16.3
0.5%Ru-11%Ni-Al ₂ O ₃ (aerogel)	380	0.75	7.9

Figure 3.2 compares the N₂ adsorption-desorption isotherms of these novel aerogel and impregnation catalysts. During the drying of the gel, the capillary forces originated by the surface tension of the liquid phase, tend to densify the solid by closely packing together the elementary particles, destroying the most fragile part of the three-dimensional network and reducing the porous volume of the resulting solid. Supercritical drying minimizes the effects of the capillary forces during the drying step both by reducing the surface tension of the liquid phase organic solvent and by increasing the mechanical properties of the wet solid network. In the case of the conventional preparation process using impregnation, the dispersion of nickel species may block pores on the support resulting in the observed lower specific surface area

and smaller pore volume. Thus, the aerogel catalysts exhibit a significantly higher BET surface area as well as pore volume.

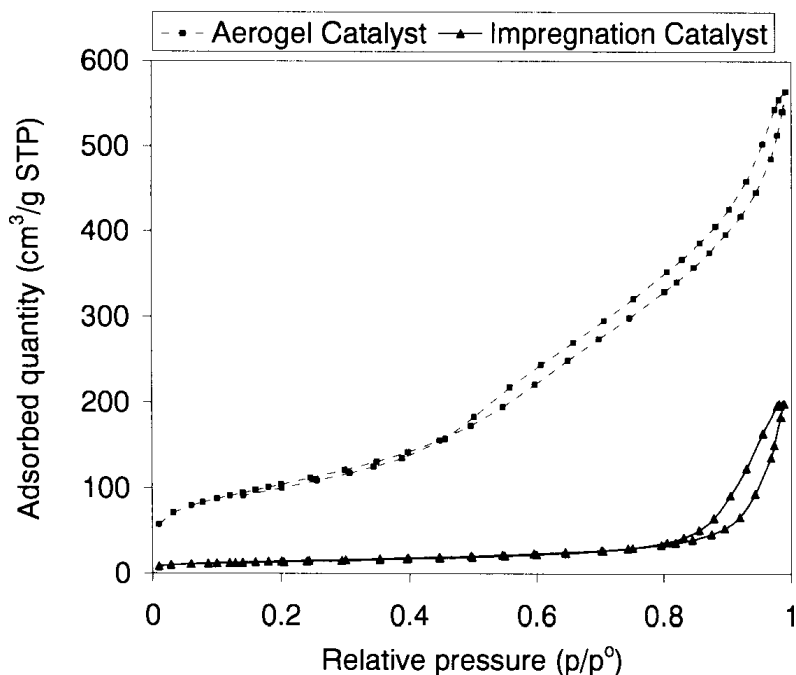


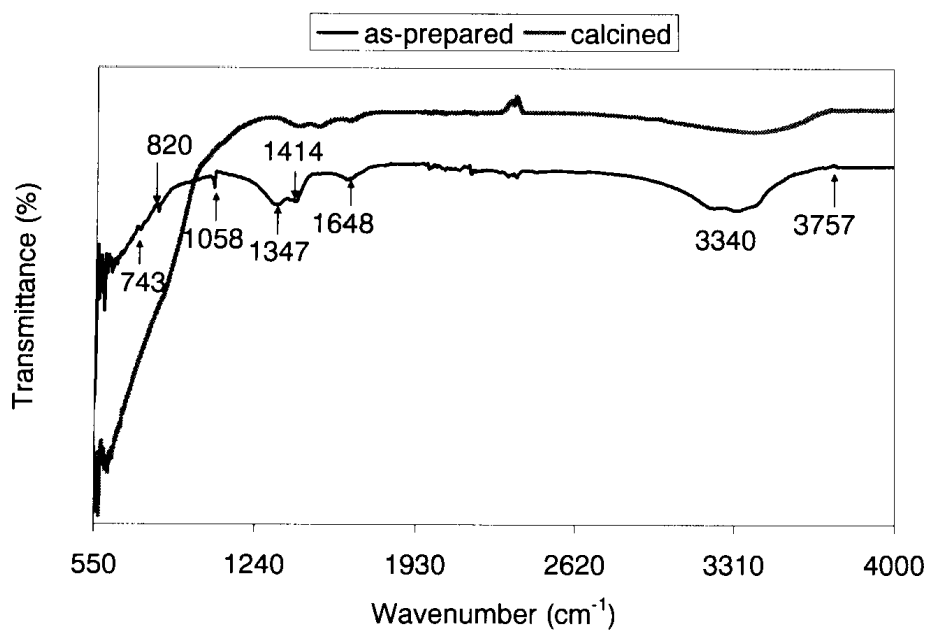
Figure 3.2. N_2 adsorption–desorption isotherms of aerogel and impregnation catalysts.

Figure 3.3a provides the ATR-FTIR traces of both the as-prepared and calcined alumina aerogel catalysts. There was a strong absorption band for the as-prepared sample at 1058 cm^{-1} which is responsible for alumina hydrate [35] which subsequently disappeared after calcination indicating the hydrolysis of aluminum isopropoxide. The peak at 820 cm^{-1} also belongs to the aerogel product representing the octahedrally coordinated aluminum [36]. The small peak at 1648 cm^{-1} is from C=O bond stretching. The small peaks at 1347 & 1414 cm^{-1} are due to C-H rocking & bending respectively which are shifted slightly to higher wavelengths after calcination. The small peak at 3757 cm^{-1} and the broad peak at 3340 cm^{-1} are attributed to the isolated and hydrogen-bonded Al-OH, respectively. In addition, the peak changes in the regions of $3400\text{-}3700 \text{ cm}^{-1}$ and below 1000 cm^{-1} can be observed with the gradual formation of oxo bonds. Analysis of the FTIR spectrum also shows a

product peak at 3340 cm^{-1} , which is attributed to production of the condensate (H_2O and $\text{CH}_3\text{CH}_2\text{OH}$) formed during synthesis [37]. There was no significant spectrum found for the impregnation catalyst (not shown).

Thermo gravimetric-differential thermal analysis (TG-DTA) of the aerogel catalyst was also carried out to examine the formation process of catalyst, as shown in Figure 3.3b. There was only one weight loss observed on heating to 1000°C , corresponding to an endothermic peak (around 110°C) & two exothermic peaks ($320\text{--}360$ & 875°C respectively) in the DTA curve (dashed line). Combined with the IR results, the weight losses in the TG profile and the corresponding broad endothermic peak in the DTA curve resulted from the loss of condensate molecules from the fresh aerogel sample. The first exothermic peak is attributed to either removal of physically bound adsorbed organic molecules or the decomposition of nitrates. Another exothermic peak observed at 875°C in the DTA profile is attributed to the phase change to δ -alumina [38]. Hence, the utilized calcination temperature (600°C) was appropriate for the aerogel catalyst.

(a)



(b)

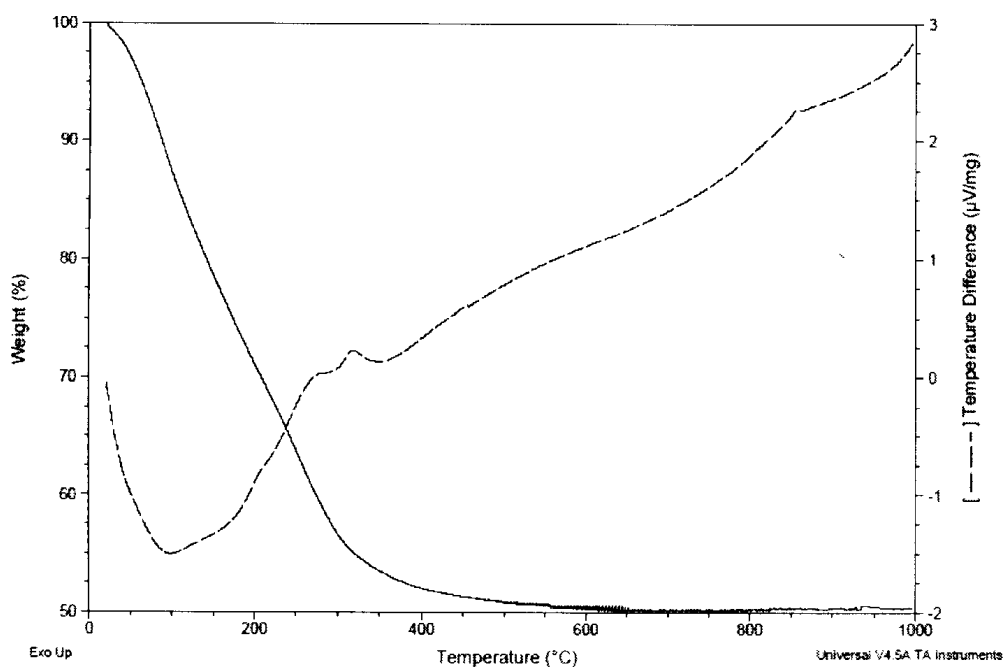


Figure 3.3. (a) ATR-FTIR analysis results of as-prepared and calcined aerogel catalyst. (b) TG-DTA profiles of as prepared drying aerogel.

H₂ pulse chemisorption analysis also supports that the sol-gel synthesis method of catalyst preparation makes strong metal-support interactions which enhances the metal dispersion of the catalyst providing small catalyst particle sizes (Table 3.2).

Table 3.2. Pulse chemisorption data.

Catalyst	Metal dispersion (%)	Active particle diameter (nm)	Cubic crystallite size (nm)
0.5%Ru-11%Ni- θ Al ₂ O ₃ (impregnation)	0.44	231.4	192.9
0.5%Ru-11%Ni-Al ₂ O ₃ (aerogel)	3.65	27.9	23.2

The coke forming tendency of Ni based catalysts may have a close relationship with the metal particle size [39]. As shown in Table 3.2, the impregnation catalyst gives a limited control of morphology and low metal dispersion i.e 0.44 vs. 3.65%. The aerogel catalyst also gives much smaller particle diameter and crystallite size.

The XRD patterns of the impregnation and aerogel catalysts after reduction at 600°C are depicted in Figure 3.4. No detectable crystalline NiO or RuO₂ peaks are observed except at around 44° in the case of the aerogel catalyst, which indicates that a large fraction of Ni or Ru form either very small clusters undetectable by XRD or are imbedded in the network of alumina [20]. The nickel and ruthenium metal likely react with the alumina support forming a Ru-Ni alloy. The other reason for the NiO or RuO₂ formation in the impregnation catalyst compared to the aerogel catalyst may be due to the inhomogeneous distribution of Ni or Ru species on the support surface. Compared to the impregnation catalyst, which showed the presence of well-developed metallic Ni and Ru crystalline phases, there was no noticeable sign of forming X-ray

detectable Ni & Ru crystalline particles in the aerogel catalyst, supporting the BET and pulse chemisorption experiments. The analysis of the XRD patterns of the bimetallic impregnation catalyst indicates that the positions of the diffraction lines of nickel are slightly shifted in relation to those of the monometallic catalyst [40]. The observed shifts provide evidence for bimetallic particle formation on the support surface. The diffraction peaks of the NiAl_2O_4 and the $\theta\text{-Al}_2\text{O}_3$ phases are observed for the impregnation catalyst. The presence of NiAl_2O_4 peak suggests that the addition of Ni species was combined with the Al_2O_3 support to form the spinel NiAl_2O_4 phase. During the process of catalyst preparation, nickel species might be isolated in the aluminum hydroxide matrix; thus aggregation of nickel species could be suppressed and the formation of structurally stable spinel phase NiAl_2O_4 favored.

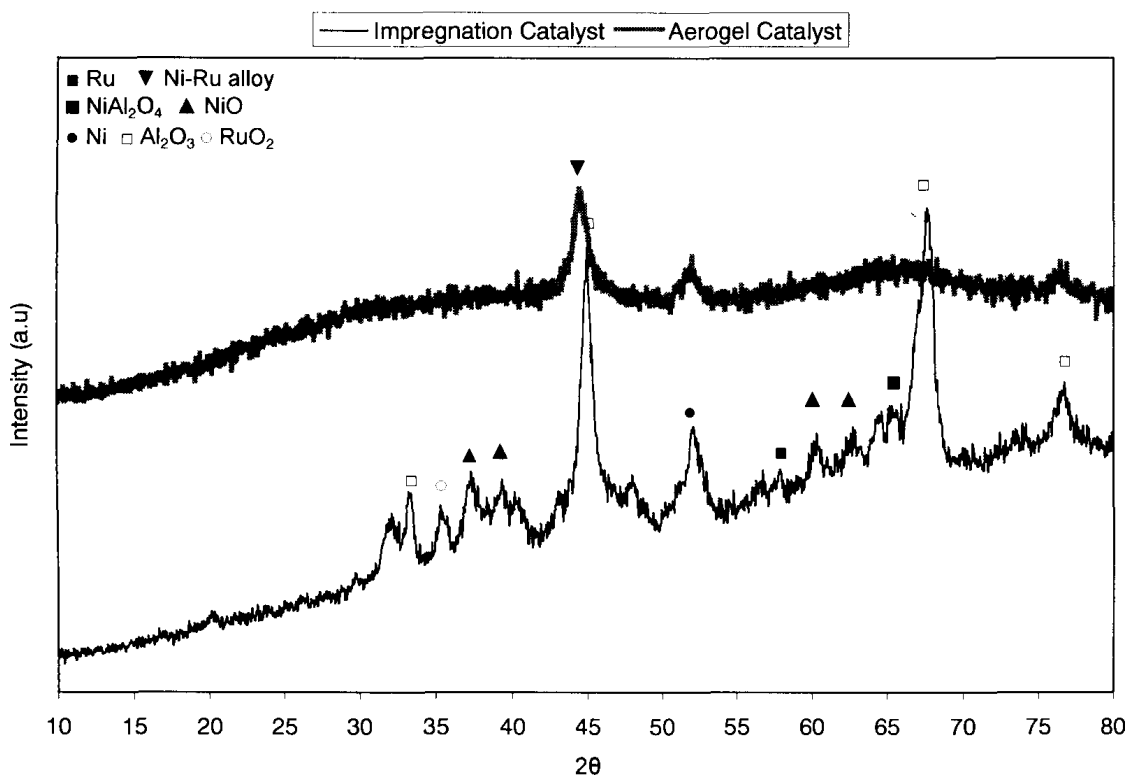


Figure 3.4. XRD patterns of impregnation and aerogel catalysts.

In order to determine the reducibility as well as the optimum reduction temperature for the investigated catalysts for subsequent glucose gasification in SCW, TPR-H₂ experiments were undertaken. In conjunction with the XRD data, it was also useful to determine the type of species present in the calcined catalysts. The TPR-H₂ profiles of the impregnation & aerogel catalysts calcined at 600°C are given in Figure 3.5, with the aerogel catalyst showing three reduction peaks around 93, 200 & 585°C while the impregnation catalyst shows five reduction peaks at 90, 165, 320, 460 & 770°C. It has been reported that the low temperature reduction peak between 81-96°C can be assigned to the reduction of well-dispersed RuO_x species containing mainly RuO₂ which was observed with both catalysts. The peaks around 160°C are attributed to the reduction of bulk RuO₂ species which indicates RuO₂ species having very weak interactions with the catalyst support [41]. The impregnation catalyst shows a sharp peak at around 165°C and the aerogel catalyst shows a broad peak around 200°C. The low reduction temperature of the impregnation catalyst compared to the aerogel catalyst and the high peak intensity shows that the impregnation catalyst contains more bulk RuO₂ species which are loosely bound with the support i.e the sol-gel synthesis method gives a strong metal-support interaction. The main reduction peak for the impregnation catalyst is observed at around 320°C along with two shoulders in the high temperature region i.e 460 & 770°C respectively. The sharp peak at 320°C is attributed to the reduction of RuO₂ & NiO present on the alumina surface which form Ni-Ru bimetallic particles. All peaks between 400-602°C represent only NiO reduction while peaks observed at 750-812°C represent reduction of NiAl₂O₄ [42]. The first shoulder of the impregnation catalyst at 460°C indicates the reduction of free NiO species. The second shoulder at 770°C can be assigned to complex NiO species,

possibly NiAl_2O_4 which may strongly interact with RuO_2 & Al_2O_3 due to the interaction among Ni, Ru and Al_2O_3 which makes ruthenium more reducible, which may help to produce mobile oxygen during glucose gasification, as described later.

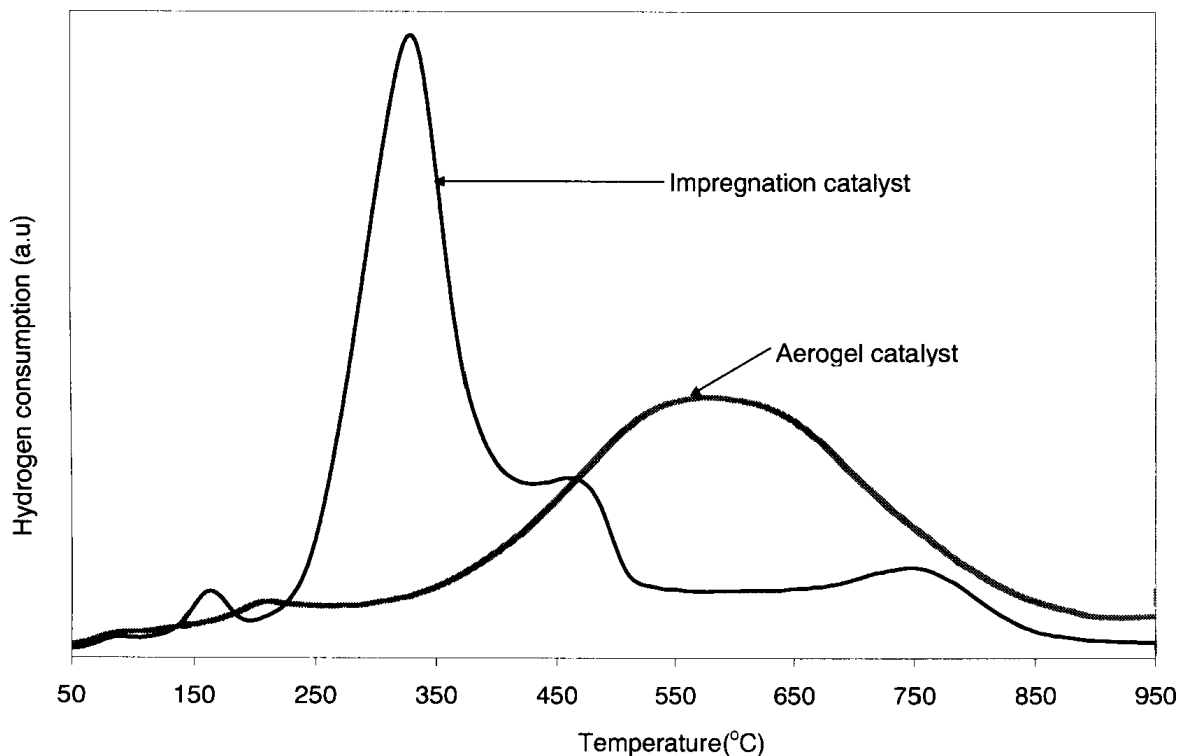


Figure 3.5. H_2 -TPR profile of impregnation & aerogel catalysts.

The main reduction peak for the aerogel catalyst is rather broad and observed at around 585°C . Since a lower amount of bulk and well dispersed RuO_2 (comparing peak intensities) was present in the aerogel catalyst, the residual RuO_2 is in intimate contact with NiO and enhances its reduction. Both Ru and Ni oxides are reduced simultaneously, thus we may assume that they form a strong interaction and possibly alloy with the Al_2O_3 support.

The sol-gel synthesis method also avoids the formation of spinel NiAl_2O_4 , which can lead to the disintegration of the catalyst structure [43]. The catalytic activity of alumina-supported Ni catalysts can be suppressed by the presence of NiAl_2O_4 spinel

because this tends to stabilize the nickel in the divalent oxidation state and makes it very hard to reduce. Therefore, for the gasification reaction it is desirable to develop a catalyst that has superior coke resistance and also the ability to minimize the formation of NiAl_2O_4 spinel.

The reduction temperature and peak width measured by TPR are indications of the ease of reduction and the degree of interaction between different metallic species, respectively. A high reduction temperature indicates difficulty in reduction whereas wide peaks indicate a higher degree of interaction between the species and the support. It is seen from the TPR- H_2 profile that both catalysts are completely reduced at higher temperatures. The impregnation & aerogel catalysts require a higher reduction temperature due to the presence of the NiAl_2O_4 species & Ni-Ru alloy respectively. However, the TPR- H_2 peaks for the impregnation catalyst were comparatively narrower than those for the aerogel catalyst implying a lower degree of interaction of metal species with Al_2O_3 .

3.3.3 Catalyst Evaluation

To study the effect of the investigated impregnation & aerogel catalysts on hydrogen yield as well as on the carbon gasification efficiency (CGE) and total organic carbon (TOC) destruction, catalytic experiments were firstly compared to the empty reactor experiments (without adding catalysts) under identical conditions. The gas yield is defined as the moles of product gases divided by the moles of glucose fed to the reactor. Typical product distributions are shown in Figure 3.6 for experiments without and with catalysts at 400, 450 & 500°C using 0.25 molar glucose feed (reaction time: 30 minutes and 1 gm catalyst used for each experiment). If we compare the non-catalytic and catalytic reactions at 500°C, the hydrogen yield increased by 72% &

90% with addition of 1 gm crushed impregnation & aerogel catalyst in the reactor respectively. The higher temperature is always favourable for high hydrogen yield with the hydrogen yield at 500°C without catalyst being less than the gasification reaction at lower temperature (400°C) with both catalysts. This shows the importance of the catalyst on decreasing the activation energy for glucose gasification to produce hydrogen in SCW. The addition of either catalyst greatly enhanced the gasification reaction of glucose for all three investigated temperatures. The impregnation catalyst enhanced the water gas shift reaction (Eqn. 3.4) i.e the hydrogen yield increased with increasing carbon dioxide and decreasing carbon monoxide concentrations. There was also a slight reduction of the methane production observed in the presence of the impregnation catalyst. The aerogel catalyst was more active while also producing a high hydrogen yield and carbonaceous product gases (CO & CO₂) compared to the impregnation catalyst. There was a significant increase in carbon monoxide, methane and carbon di-oxide yield observed in the presence of aerogel catalyst.

Compared to the previously prepared by Youssef et al., 11%Ni- θ Al₂O₃ catalyst with an optimum nickel impregnation loading [29], the hydrogen yield increased about 3 & 2.75 times at 500°C and 25 MPa using the novel synthesized impregnation and aerogel catalysts because of introducing ruthenium. This shows that ruthenium had a significant role in enhancing the water gas shift reaction giving a higher H₂ yield as well as decomposing the intermediate compounds, suppressing coke deposition on the catalyst surface.

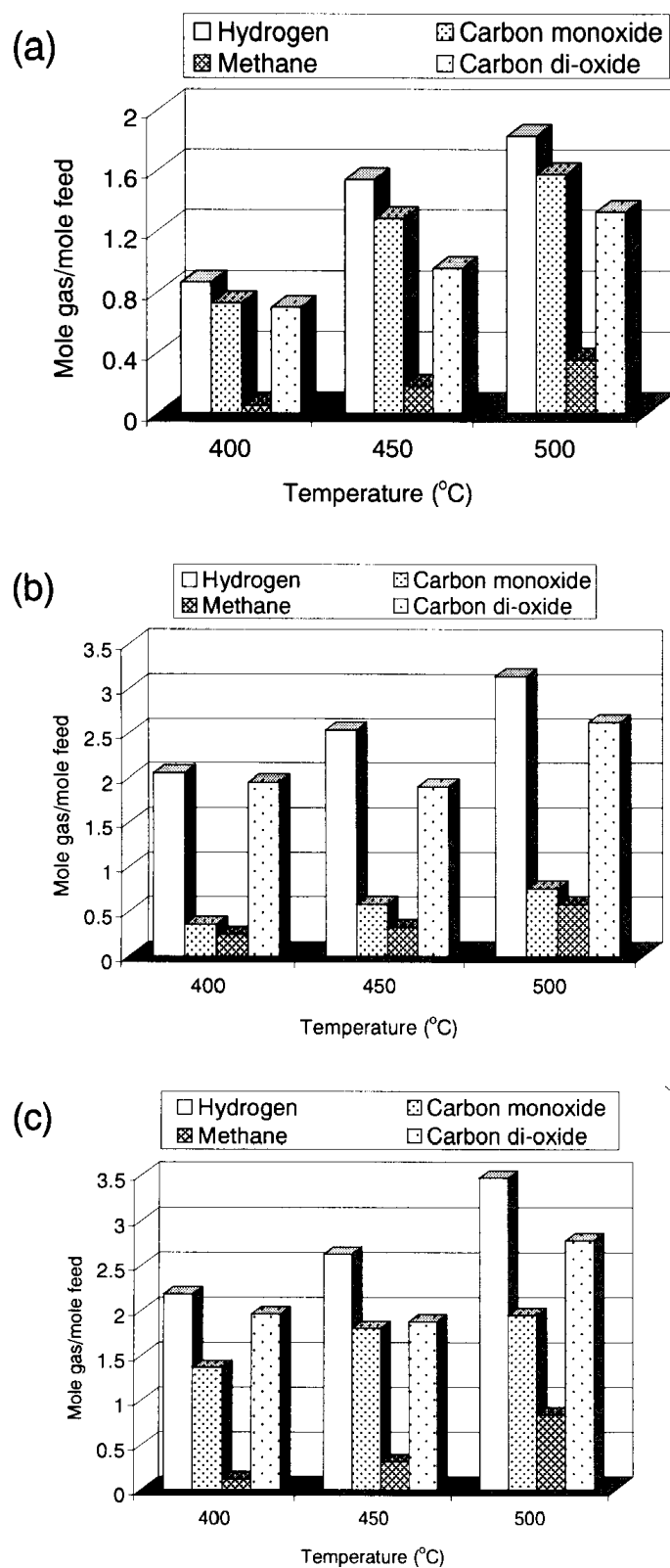


Figure 3.6. Temperature effect on product distribution during non-catalytic & catalytic gasification of glucose in supercritical water, (a) without catalyst (b) impregnation catalyst (c) aerogel catalyst; $t=30$ min, Feed= 0.25M Glucose, Catalyst

1.0 gm.

The metals supported on the aerogel catalyst were shown to contain comparatively smaller crystallite sizes and were more homogeneously distributed on the support compared to the impregnation catalyst (as shown by BET, H₂ pulse chemisorption). The smaller crystallite sizes for the aerogel catalyst were better distributed, leading to less agglomeration and better availability of active sites. The reactants as well as the intermediate products formed during the course of the reactions responsible for coke deposition can closely contact with the metal particle sites of the aerogel catalyst which completely decomposed the C-C and C-O bonds present in the intermediate products to produce hydrogen and carbonaceous gases.

As shown in Figure 3.7, the aerogel catalyst gave both the highest carbon gasification efficiency (CGE) and TOC destruction as measured from the liquid products. The maximum obtainable TOC destruction and carbon gasification efficiency at 500°C was 90 & 66.8% for the impregnation and 94 & 92.8% for the aerogel catalyst, respectively. Hence the catalytic performance of the aerogel catalyst was much higher for producing a high yield of carbonaceous gaseous products compared to the impregnation catalyst while also decreasing coke formation.

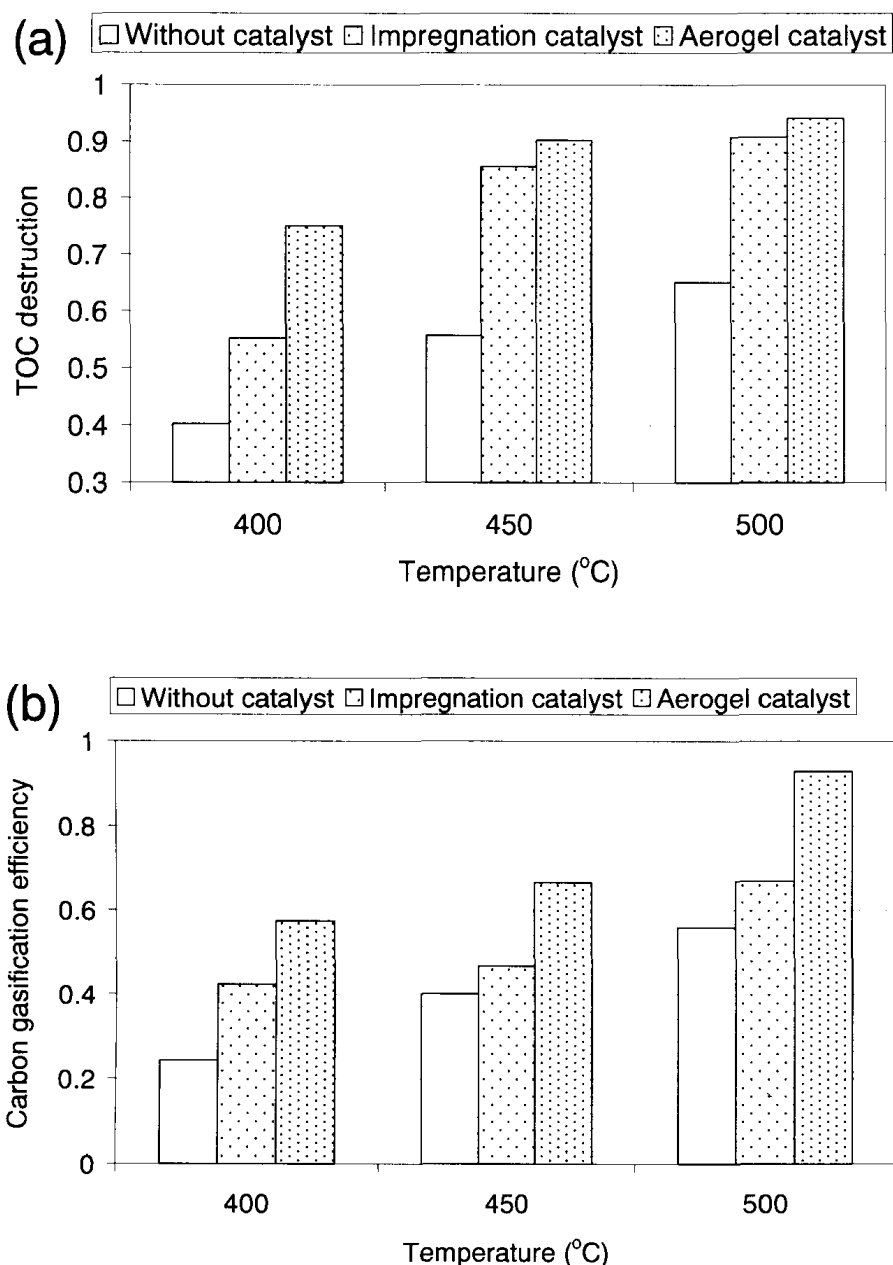


Figure 3.7: Effect of catalysts on (a) TOC destruction and (b) CGE; $t=30$ min, Feed= 0.25M Glucose, Catalyst 1.0 gm.

3.3.4 Characterization of spent catalysts

Most experimental investigations have revealed that catalyst deactivation mainly occurs due to the sintering of Ni particles and carbon deposition on the nickel based catalyst surface [44]. Hao et al. [22] showed that the growth rates of metal particles using an aerogel catalyst were slower than those of an impregnation catalyst containing 10% Ni loading which had a better resistance to sintering by taking

advantage of higher dispersivity and homogeneity. Therefore, metal sintering is not the main reason for the catalyst deactivation but large Ni particles can accelerate the rate of carbon deposition on the catalyst surface.

Carbon deposition could occur on the Ni-based catalysts during SCWG from various forms of carbon including atomic carbon, amorphous carbon and graphitic carbon, which can be gasified at the different temperature ranges of <250 , $250-600$ and $>600^{\circ}\text{C}$, respectively [45]. Generally, both amorphous and graphitic carbon were formed on the catalyst surface because of the required high gasification temperature. The type of deposited carbon on the surface of the spent catalysts was characterized by temperature programmed oxidation (TPO) as shown in Figure 3.8. The TPO curves of the spent catalysts indicate the formation of two kinds of carbon deposition, which correspond to atomic carbon ($<250^{\circ}\text{C}$) and amorphous carbon ($250-600^{\circ}\text{C}$). There was no significant peak observed for the formation of graphitic carbon which mainly deactivates the catalyst. Ruthenium metal itself may play an important role in preventing graphitic coke deposition on the catalyst surface along with enhancing the hydrogen yield as well as increasing the carbon gasification efficiency and TOC destruction. From the TPO peak areas, we can say that the impregnation catalyst was affected by more amorphous carbon deposition rather than the aerogel catalyst which was more resistant to SCWG treatment.

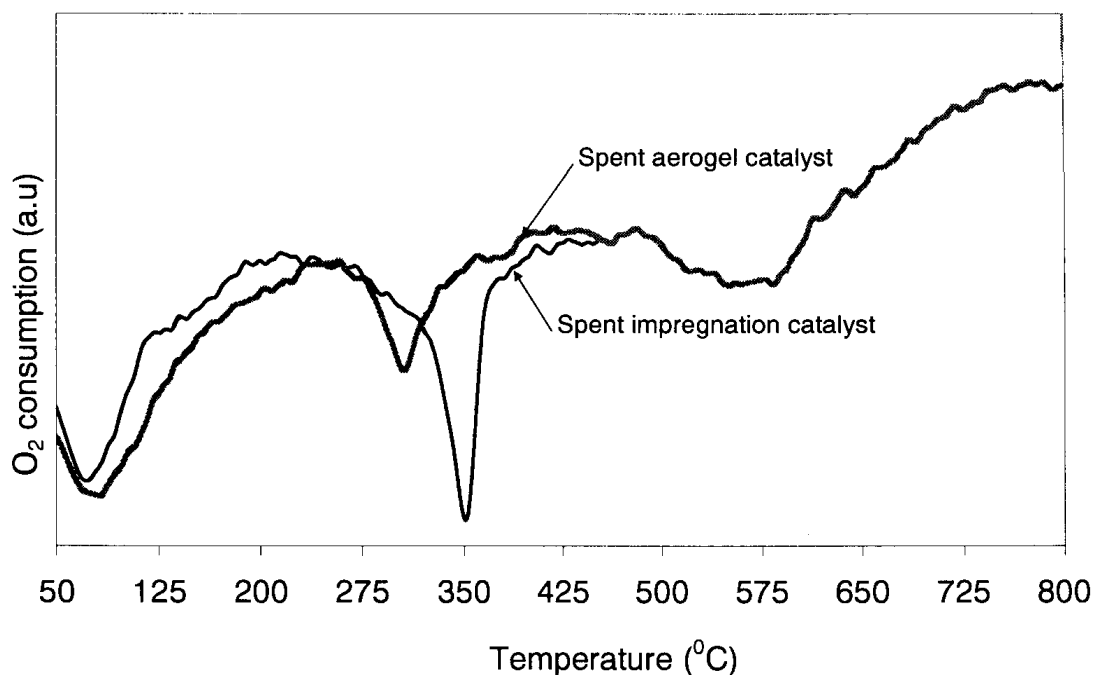


Figure 3.8. TPO profiles of spent catalysts.

The deposited carbon on the catalyst surface was characterized by X-ray diffraction techniques, as shown in Figure 3.9. It can be seen that no distinct diffraction peak of graphitic carbon (usually observed at 26.5° [21]) appeared in the XRD pattern of either the impregnation or aerogel catalysts from the SCWG process. The deactivation of both catalysts observed from the XRD pattern is due to the formation of RuO_2 & NiAl_2O_4 indicating that the catalysts were oxidized from the SCWG process. Although larger crystallite sizes enhance carbon deposition on the catalyst surface, the impregnation catalyst also reduced graphitic coke formation because of the presence of ruthenium.

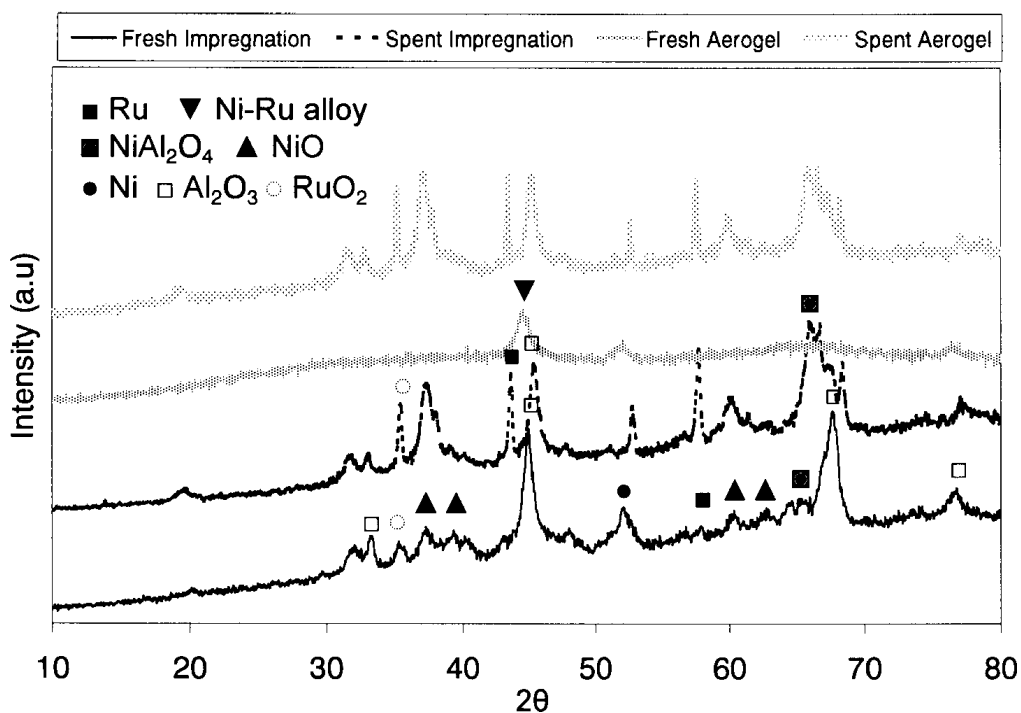


Figure 3.9. Comparison of XRD pattern of fresh & spent catalysts.

The Raman spectrum of graphite in single crystal form shows a single peak at 1580 cm^{-1} , which is called the G band while the spectrum of graphite shows an additional peak at about 1350 cm^{-1} , which is called the D band [46]. No raman shift was observed (not shown) for either the impregnation or aerogel catalysts indicating these catalysts were successful at minimizing graphitic coke. Formation of filamentous carbon is the main characteristic of the graphitic coke [44]. No filamentous carbon was observed from SEM & TEM micrographs of the spent catalysts (Figure 3.10) except agglomeration compared to the fresh catalysts.

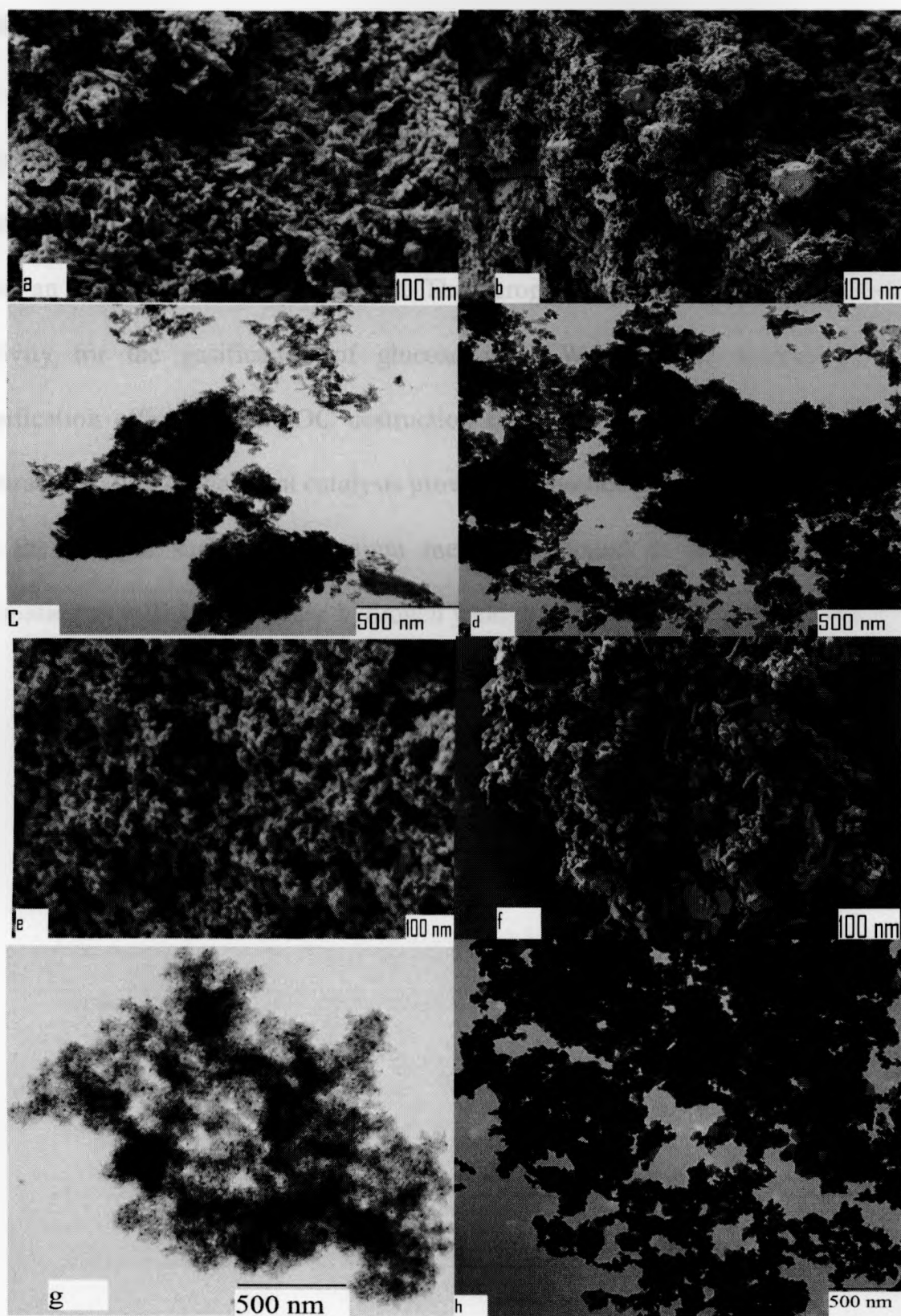


Figure 3.10. SEM & TEM micrographs of catalysts, (a&c) & (b&d): fresh & spent impregnation (crushed) and (e&g) & (f&h): fresh & spent aerogel catalysts respectively.

3.4 Conclusions

Ni-Ru-Al₂O₃ aerogel catalyst was prepared via a sol-gel method combined with a supercritical CO₂ drying, which exhibited a higher BET surface area, smaller catalyst particle sizes, stronger metal-support interaction and higher Ni dispersion degrees than an impregnation based catalyst. The aerogel catalyst showed better catalytic activity for the gasification of glucose in SCW especially increasing carbon gasification efficiency & TOC destruction compared to the impregnation catalyst. Characterization of the spent catalysts proved the absence of graphitic coke deposition on the catalyst surface. Ruthenium metal was found to reduce graphitic coke formation as well as to increase hydrogen yield during the SCWG process.

References:

1. Edwards, P.P., V.L. Kuznetsov, and W.I.F. David, *Hydrogen energy*. Philosophical Transactions of the Royal Society A: Mathematical, Physical and Engineering Sciences, 2007. **365**(1853): p. 1043-1056.
2. Balat, H. and E. Kirtay, *Hydrogen from biomass-Present scenario and future prospects*. International Journal of Hydrogen Energy. 2010. **35**(14): p. 7416-7426.
3. Yoshida, Y., et al., *Comprehensive comparison of efficiency and CO₂ emissions between biomass energy conversion technologies--position of supercritical water gasification in biomass technologies*. Biomass and Bioenergy, 2003. **25**(3): p. 257-272.
4. Guo, L.J., et al., *Hydrogen production by biomass gasification in supercritical water: a systematic experimental and analytical study*. Catalysis today, 2007. **129**(3-4): p. 275-286.
5. Lu, Y., et al., *Hydrogen production by biomass gasification in supercritical water over Ni/ γ -Al₂O₃ and Ni/CeO₂- γ -Al₂O₃ catalysts*. International Journal of Hydrogen Energy. **35**(13): p. 7161-7168.
6. Sato, T., et al., *Gasification of alkylphenols with supported noble metal catalysts in supercritical water*. Industrial & Engineering Chemistry Research, 2003. **42**(19): p. 4277-4282.
7. Yamaguchi, A., et al., *Hydrogen production from woody biomass over supported metal catalysts in supercritical water*. Catalysis today, 2009. **146**(1-2): p. 192-195.

8. Minowa, T., F. Zhen, and T. Ogi, *Cellulose decomposition in hot-compressed water with alkali or nickel catalyst*. *The Journal of Supercritical Fluids*, 1998. **13**(1-3): p. 253-259.
9. Minowa, T. and T. Ogi, *Hydrogen production from cellulose using a reduced nickel catalyst*. *Catalysis today*, 1998. **45**(1-4): p. 411-416.
10. Sato, T., et al., *Effect of water density on the gasification of lignin with magnesium oxide supported nickel catalysts in supercritical water*. *Ind. Eng. Chem. Res*, 2006. **45**(2): p. 615-622.
11. Azadi, P., et al., *Hydrothermal gasification of glucose using Raney nickel and homogeneous organometallic catalysts*. *Fuel Processing Technology*, 2009. **90**(1): p. 145-151.
12. Azadi, P., K.M. Syed, and R. Farnood, *Catalytic gasification of biomass model compound in near-critical water*. *Applied Catalysis A: General*, 2009. **358**(1): p. 65-72.
13. Watanabe, M., H. Inomata, and K. Arai, *Catalytic hydrogen generation from biomass (glucose and cellulose) with ZrO₂ in supercritical water*. *Biomass and Bioenergy*, 2002. **22**(5): p. 405-410.
14. Kruse, A., et al., *Gasification of pyrocatechol in supercritical water in the presence of potassium hydroxide*. *Ind. Eng. Chem. Res*, 2000. **39**(12): p. 4842-4848.
15. Antal Jr, M.J., et al., *Biomass Gasification in Supercritical Water*. *Ind. Eng. Chem. Res*, 2000. **39**(11): p. 4040-4053.

16. Park, K.C. and H. Tomiyasu, *Gasification reaction of organic compounds catalyzed by RuO₂ in supercritical water*. Chemical Communications, 2003. **2003(6)**: p. 694-695.
17. Elliott, D.C., L.J. Sealock Jr, and E.G. Baker, *Chemical processing in high-pressure aqueous environments. 2. Development of catalysts for gasification*. Industrial & Engineering Chemistry Research, 1993. **32(8)**: p. 1542-1548.
18. Hou, Z., et al., *Characterization of Ca-promoted Ni/Al₂O₃ catalyst for CH₄ reforming with CO₂*. Appl. Catal. A, 2003. **253(2)**: p. 381-387.
19. Ronggang, D., et al., *Surface Carbon Depositions on Nickel Catalyst for Carbon Dioxide Reforming with Methane*. Journal of Natural Gas Chemistry, 2001. **10(4)**: p. 273-287.
20. Kim, J.H., et al., *Effect of metal particle size on coking during CO₂ reforming of CH₄ over Ni-alumina aerogel catalysts*. Applied Catalysis A: General, 2000. **197(2)**: p. 191-200.
21. Hao, Z., et al., *Characterization of aerogel Ni/Al₂O₃ catalysts and investigation on their stability for CH₄-CO₂ reforming in a fluidized bed*. Fuel Processing Technology, 2009. **90(1)**: p. 113-121.
22. Hao, Z., et al., *CH₄-CO₂ reforming over Ni/Al₂O₃ aerogel catalysts in a fluidized bed reactor*. Powder Technology, 2008. **182(3)**: p. 474-479.
23. Ponc, V. and G.C. Bond, *Catalysis by metals and alloys*. 1995: Elsevier Science Ltd.
24. Mukainakano, Y., et al., *Surface modification of Ni catalysts with trace Pd and Rh for oxidative steam reforming of methane*. Applied Catalysis A: General, 2007. **318**: p. 252-264.

25. Crisafulli, C., et al., *CO₂ reforming of methane over Ni–Ru and Ni–Pd bimetallic catalysts*. *Catalysis Letters*, 1999. **59**(1): p. 21-26.
26. Wang, W., R. Ran, and Z. Shao, *Combustion-synthesized Ru–Al₂O₃ composites as anode catalyst layer of a solid oxide fuel cell operating on methane*. *International Journal of Hydrogen Energy*, 2011, **36**(1): p.755-764.
27. Youssef, E.A., et al., *Sequential supercritical water gasification and partial oxidation of hog manure*. *International Journal of Hydrogen Energy*, 2010, **35**(21): p.11756-11767.
28. Byrd, A.J., K.K. Pant, and R.B. Gupta, *Hydrogen production from glucose using Ru/Al₂O₃ catalyst in supercritical water*. *Ind. Eng. Chem. Res*, 2007. **46**(11): p. 3574-3579.
29. Youssef, E.A., et al., *Effect of nickel loading on hydrogen production and chemical oxygen demand (COD) destruction from glucose oxidation and gasification in supercritical water*. *International Journal of Hydrogen Energy*. 2010, **35**(10): p. 5034-5042.
30. Richardson, J.T., *Principles of catalyst development*. 1989: Springer Us
31. Choudhury, M.B.I., et al., *Preferential methanation of CO in a syngas involving CO₂ at lower temperature range*. *Applied Catalysis A: General*, 2006. **314**(1): p. 47-53.
32. Schneider, M. and A. Baiker, *Aerogels in catalysis*. *Catalysis Reviews*, 1995. **37**(4): p. 515-556.
33. A. Khaleel, K.J. Klabunde, *Characterization of aerogel prepared high-surface area alumina: in situ FTIR study of dehydroxylation and pyridine adsorption*, *Chem. Eur. J.* 2002, 8:p. 3991–3998.

34. Yu, D., M. Aihara, and M.J. Antal Jr, *Hydrogen production by steam reforming glucose in supercritical water*. Energy & Fuels, 1993. **7**(5): p. 574-577.
35. Mizushima, Y. and M. Hori, *Properties of alumina aerogels prepared under different conditions*. Journal of Non-Crystalline Solids, 1994. **167**(1-2): p. 1-8.
36. Tarte, P., *Infra-red spectra of inorganic aluminates and characteristic vibrational frequencies of AlO_4 tetrahedra and AlO_6 octahedra*. Spectrochimica Acta Part A: Molecular Spectroscopy, 1967. **23**(7): p. 2127-2143.
37. Sui, R., A.S. Rizkalla, and P.A. Charpentier, *Synthesis and Formation of Silica Aerogel Particles By a Novel Sol- Gel Route in Supercritical Carbon Dioxide*. J. Phys. Chem. B, 2004. **108**(32): p. 11886-11892.
38. Ji, L., et al., *Synthesis of High-Surface-Area Alumina Using Aluminum Tri-sec-butoxide- 2, 4-Pentanedione- 2-Propanol- Nitric Acid Precursors*. Chem. Mater, 2000. **12**(4): p. 931-939.
39. Slagtern, A., et al., *Specific Features Concerning the Mechanism of Methane Reforming by Carbon Dioxide over Ni/La₂O₃Catalyst*. Journal of Catalysis, 1997. **172**(1): p. 118-126.
40. Chowdhury, M.B.I., *Nickel-based Catalysts for Gasification of Glucose in Supercritical Water*. PhD Thesis 2010.
41. Liu, Y., et al., *In situ Raman study on the partial oxidation of methane to synthesis gas over Rh/Al₂O₃ and Ru/Al₂O₃ catalysts*. Journal of Catalysis, 2008. **256**(2): p. 192-203.

42. Lee, J.H., et al., *Stabilization of Ni/Al₂O₃ catalyst by Cu addition for CO₂ reforming of methane*. Applied Catalysis A: General, 2004. **269**(1-2): p. 1-6.
43. Gadalla, A.M. and B. Bower, *The role of catalyst support on the activity of nickel for reforming methane with CO₂*. Chemical Engineering Science, 1988. **43**(11): p. 3049-3062.
44. Chen, X., K. Honda, and Z.G. Zhang, *A comprehensive comparison of CH₄-CO₂ reforming activities of NiO/Al₂O₃ catalysts under fixed-and fluidized-bed operations*. Applied Catalysis. A, General, 2005. **288**: p. 86–97.
45. Effendi, A., et al., *Steam reforming of a clean model biogas over Ni/Al₂O₃ in fluidized-and fixed-bed reactors*. Catalysis today, 2002. **77**(3): p. 181-189.
46. Darmstadt, H., et al., *Effects of surface treatment on the bulk chemistry and structure of vapor grown carbon fibers*. Carbon, 1997. **35**(10-11): p. 1581-1585.

CHAPTER FOUR

Kinetic analysis for TOC destruction of glucose by supercritical water gasification

4.1 Introduction

Hydrothermal processes have attracted worldwide attention because of the fascinating characteristics of water as a reaction medium at elevated temperatures and pressures [1]. Hydrothermal processes have shown great potential and effectiveness for the treatment of industrial wastewater with high organic concentrations i.e. sewage sludge, agricultural wastes, food processing wastes etc. Among the hydrothermal processes, supercritical water gasification (SCWG) is an economically viable and ecologically safe destruction technology for treating wet biomass waste from agricultural or industrial residues into combustible gases without requiring a feedstock drying procedure.

The physical properties of supercritical water (SCW) are very different from those of liquid water. The dielectric constant of SCW is much lower, and the number of hydrogen bonds is much lower and their strength is much weaker. As a result, SCW behaves like many organic solvents resulting in organic compounds having complete miscibility with SCW. Moreover, gases are also miscible in SCW, thus a SCW reaction environment provides an opportunity to conduct chemistry in a single fluid phase that would otherwise occur in a multiphase system under conventional conditions [1]. Gasification of biomass in SCW has many advantages such as a high gasification efficiency, high molar fraction of produced hydrogen, and no need for a drying process for wet biomass as compared to other biomass conversion methods.

Calzavara et al. [2] evaluated the supercritical water gasification process for hydrogen production. They found that the energy efficiency reached 60% without including energy recovery, while was 90% including energy recovery.

The influence of process variables such as temperature, pressure, residence time, and catalyst on supercritical water gasification of model compounds has been investigated. At high temperatures such as 650°C the best hydrogen yield using SCWG of sawdust and different starches was reached (i.e. 43 to 57%) [3]. The same important effect for temperature has been reported in other publications [4–6]. The pressure was found to have little effect on the glucose gasification efficiency and the fraction of the gas product [5], although a decrease of pressure led to an increase in hydrogen formation [7]. Carbon gasification efficiency (CGE) & total organic carbon (TOC) destruction were found to increase at a longer residence time. The overall gasification efficiency was observed to be decreased at a shorter residence time [4, 5]. Heterogeneous catalysts are preferable over homogeneous alkali catalysts to avoid reactor corrosion problems while being relatively easy to recover [8]. During a study of catalytic phenol oxidation in supercritical water, Oshima et al. [9] showed that external mass transfer resistance was negligible for small size catalysts (size 0.18-0.25 mm), however larger size catalysts posed some mass transfer resistance. Hence, in this chapter crushed catalysts are used rather than using pelletized catalysts to observe their effect on the products.

Total organic carbon (TOC) is the amount of carbon bound in an organic compound and is often used as a non-specific indicator of water quality and has direct implications in the planning of wastewater treatment and drinking water treatment facilities [8]. Organic matter content is typically measured as TOC and dissolved

organic carbon, which are essential components of the carbon cycle. In addition, low TOC can confirm the absence of potentially harmful organic chemicals in water. Hence for this study, we investigated the destruction and rate of TOC during SCWG. A kinetic analysis of the decomposition rate in SCWG is important to design the required reactor system. However, kinetic information describing SCWG is limited especially for longer residence times. Depending on the feed type, gasification increases with increased residence time [5, 10]. Jesus et al. [11] correlated results of gasification of corn silage at 700°C and 25 MPa in SCW with time and developed a linear relationship between carbon conversion (Y_C) and residence time (τ):

$$Y_C = K\tau = 0.11\tau \quad (R^2=1) \quad (4.1)$$

They also proposed a model for corn silage using mathematical approximation based on zero-order kinetics as follows:

$$Y = 10^2 \exp\left(\frac{47.9[KJ]}{RT[K]}\right)\tau(\text{min}^{-1}) + 10^{-2.8} \exp(6.1 \times 10^{-3} T[K]) \quad (4.2)$$

Lee et al. [4] also found that below 600°C, the hydrogen yield increases with increased residence time during SCWG of glucose. They conducted a kinetic analysis assuming pseudo first order reaction and the following first order reaction rate was developed for COD (chemical oxygen demand) degradation as a function of the corresponding concentration C_c :

$$-r_c = 10^{2.95 \pm 0.23} \exp\left(-71.0 \pm \frac{3.9}{RT}\right) C_c \quad (4.3)$$

Although they assumed zero order for water, they agreed that non-first order kinetics would have given a better correlation of the experimental data.

Kinetic studies on supercritical water gasification have been much less studied than supercritical water oxidation of waste materials. One major shortcoming of these studies is the assumption of a first order reaction rate. Considering water as a zero order reactant may also be misleading for a proper understanding of reaction kinetics since the lower feed concentration (i.e. higher water: feed ratio) increases the percent TOC destruction. More than thirty intermediate products were detected by Hologate et al. [12] (425-600°C and 246 bar) and by Williams and Onwudili [13] during SCWG, so development of a kinetic model is difficult considering the gaseous products rather than TOC destruction. We also showed in chapter three that the higher the TOC destruction, the higher the hydrogen and other gaseous product yields (described in chapter 3). Therefore, a global kinetic model for TOC destruction is developed in this chapter with time and temperature dependency. The pressure effect was not studied because there is no great effect on gasification efficiency and the fraction of gas product from 25MPa to 30 MPa at 500°C and 650 °C [5].

4.2 Experimental

4.2.1 Materials

Glucose was used as the model compound under investigation obtained from Sigma–Aldrich (Oakville, Ontario, Canada) and used as received. De-ionized water was obtained from a compact ultrapure water system (EASY pure LF, Mandel Scientific co, model BDI-D7381) to prepare the glucose solutions.

4.2.2 Methods

All of the experiments for glucose gasification in supercritical water at different temperatures and time were conducted using a 600 ml autoclave batch reactor made of Hastelloy C-276 equipped with 1.5 kW electric furnaces for heating (Autoclave

Engineers, Erie, Penn., USA). The schematic diagram and experimental procedure was described in detail elsewhere [14].

Analysis of the product gases was performed using a gas chromatograph (Shimadzu, GC-2014) equipped with a thermal conductivity detector (TCD) and a 120/80 D Hayesep stainless steel packed column (Grace Davidson) having dimensions of 6.2m long, and 3.18mm inside diameter. Helium was used as the carrier gas. Total Organic Carbon (TOC) was analyzed with a TOC-VCPH (Shimadzu Instruments). The TOC decomposition X was used to evaluate the extent of oxidative decomposition, and defined as:

$$TOC \text{ decomposition, } X = 1 - \frac{[TOC]}{[TOC]_0} \quad (4.4)$$

where $[TOC]_0$ is the initial TOC and $[TOC]$ is the residual after reaction.

Gas yield, and carbon gasification efficiency (CGE), were calculated as shown in equation 4.5 and 4.6 as defined by Yu et al [15].

$$yield = \frac{\text{mol of gas produced}}{\text{mol of glucose in feed}} \quad (4.5)$$

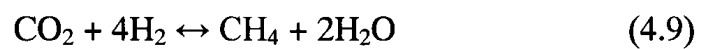
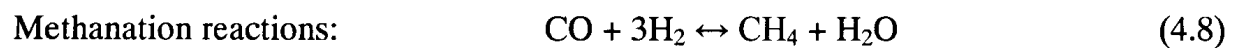
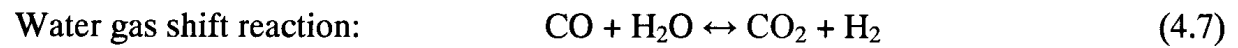
$$CGE = \frac{\text{mol carbon in produced gas}}{\text{mol carbon in feed}} \quad (4.6)$$

4.3 Results & Discussion

4.3.1 Effect of Reaction Time and Temperature

The effect of residence time was studied at 400, 450, 500°C for 0.25M glucose by varying the reaction time from 5 to 60 minutes, as shown in Figure 4.1. It is clear from this figure that increasing the reaction time and temperature directly increases the hydrogen production, while the carbon monoxide concentration decreases with

time. Reduction of carbon monoxide yield with increasing hydrogen yield can be attributed to enhancing the water gas shift reaction (Eqn. 4.7). Also as the methane and carbon dioxide concentration increase with time and temperature, the methanation reactions of carbon oxides along with methane production from the dissociation of intermediate liquid products are increasing (Eqn. 4.8 & 4.9).



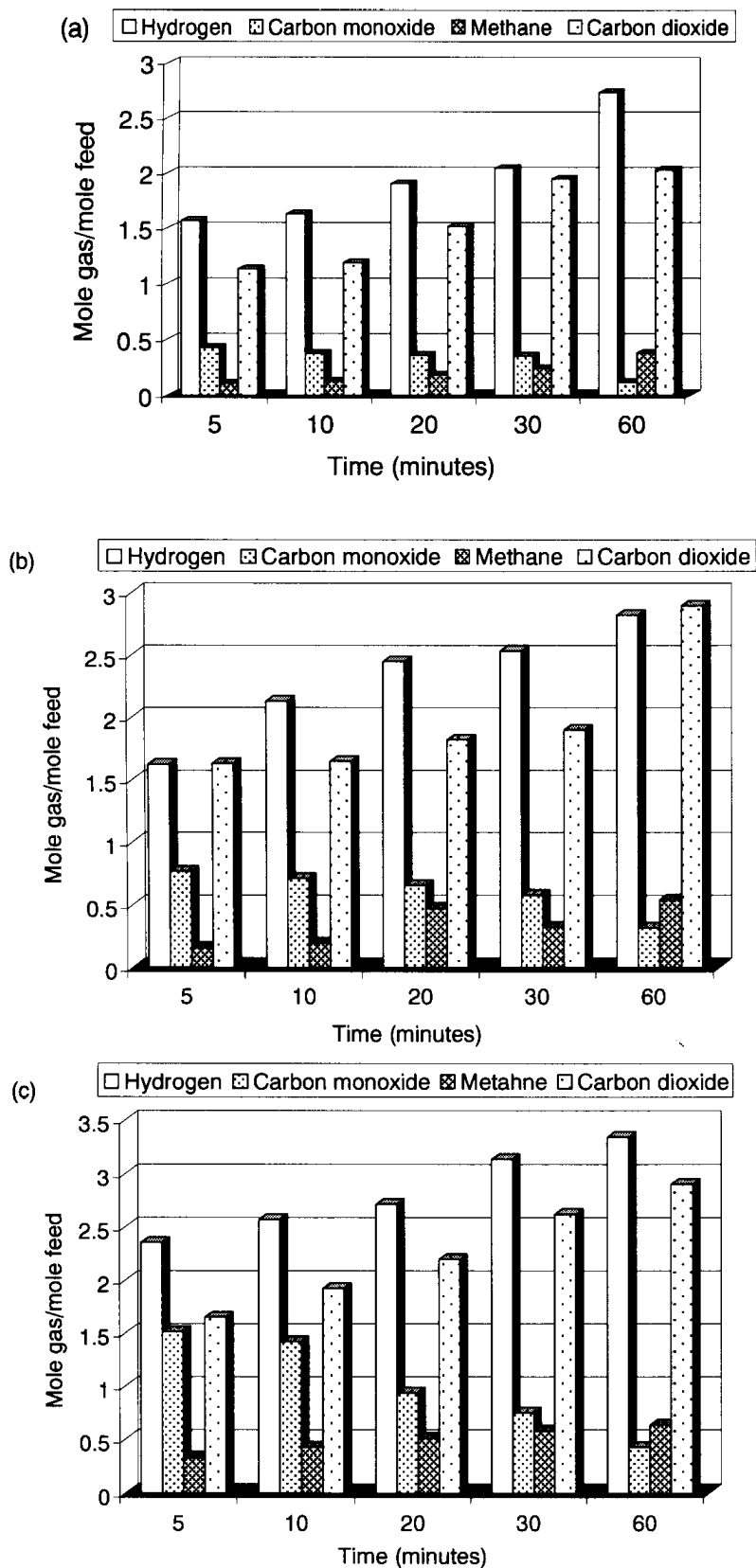


Figure 4.1. Effect of time and temperature on gaseous products. (a) 400°C (b) 450°C (c) 500°C; amount of crushed catalyst (impregnation) = 1 gm, P=25MPa, Feed= 0.25M Glucose.

Figure 4.2 shows that by increasing the reaction time and temperature, the TOC conversion and CGE both increased i.e. the gaseous products increased due to a higher conversion of the liquid intermediates.

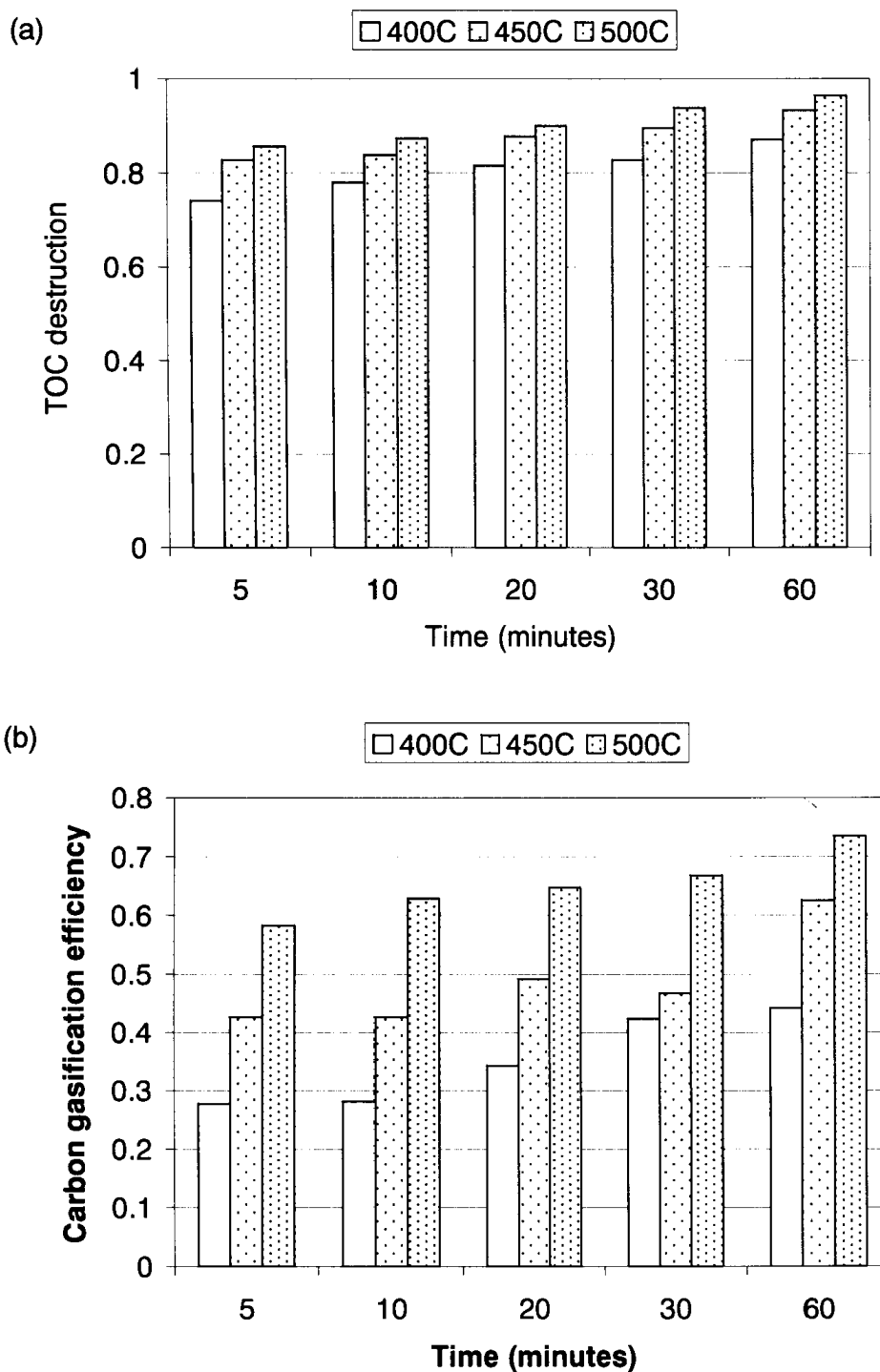


Figure 4.2. Effect of time & temperature on a) TOC destruction and b) CGE; amount of crushed catalyst (impregnation) = 1 gm, P=25MPa, Feed= 0.25M Glucose.

4.3.2 Effect of concentration

Figure 4.3 shows the effect of feed concentration on the gaseous products and TOC conversion and CGE using the impregnation catalysts. The higher feed concentrations lower the hydrogen and carbon dioxide yield, while only a slight increase of carbon monoxide and methane production is observed. Similar experimental results were found by Kersten et al [16], while a thermodynamic analysis by Yan et al. [17] also showed a similar tendency.

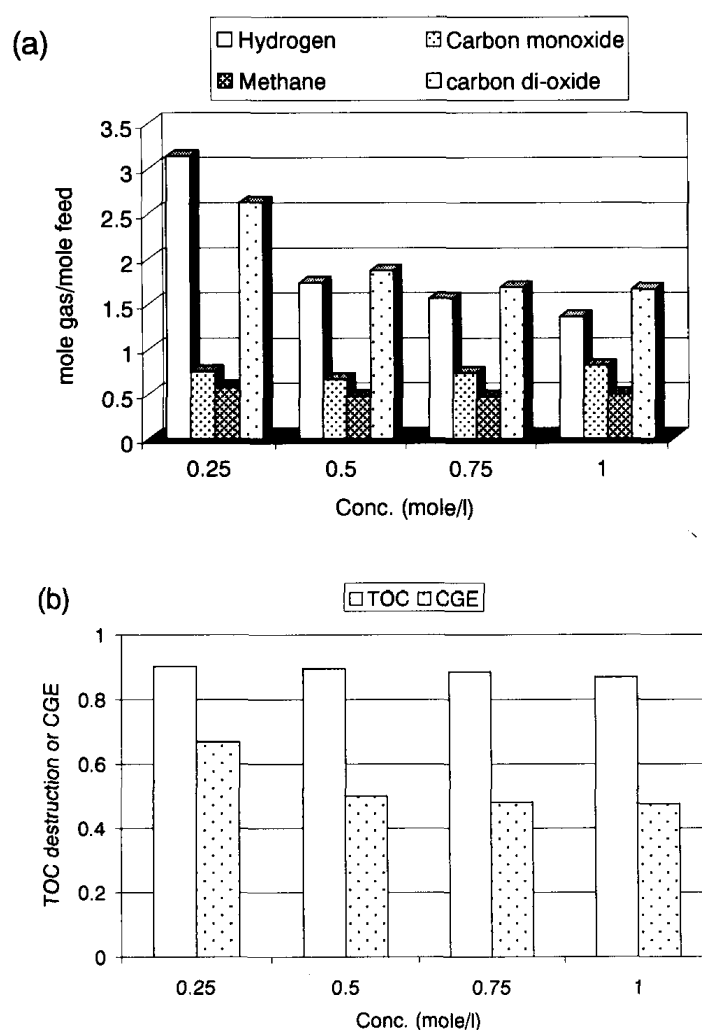


Fig. 4.3. Effect of feed concentration on (a) gaseous products (b) TOC destruction or CGE; amount of crushed catalyst (impregnation) = 1 gm, T=500°C, P=25MPa.

The TOC conversion and carbon gasification efficiency being reduced with increased concentration is attributed to a lower gasification of organic compounds occurring.

From the above observations it is clear that low concentration with increased time and temperature is favorable for the production of hydrogen and higher gasification yields.

Table 4.1 Summary of experimental TOC data.

Reaction Temperature (°C)	Reaction pressure (MPa)	Residence Time (minutes)	[TOC] ₀ mg/L	[TOC] mg/L	TOC conversion, $X=1-([TOC]/[TOC]_0)$
400	25	5	18000	4660	0.741111
400	25	10	18000	3956	0.780222
400	25	20	18000	3310	0.816111
400	25	30	18000	3094	0.828111
400	25	60	18000	2340	0.870000
450	25	5	18000	3090	0.828333
450	25	10	18000	2910	0.838333
450	25	20	18000	2209	0.877278
450	25	30	18000	1878	0.895667
450	25	60	18000	1220	0.932222
500	25	5	18000	2570	0.857222
500	25	10	18000	2278	0.873444
500	25	20	18000	1790	0.900556
500	25	30	18000	1112	0.938222
500	25	60	18000	650	0.963889

4.4 Reaction Kinetics of TOC destruction

In order to develop a reliable reaction rate expression, data were taken under various conditions (Table 4.1). The global power-law reaction rate can be described as follows:

$$r = -\frac{d[C_n]}{dt} = k[C_n]^p[H_2O]^q \quad (4.10)$$

where $[C_n]$ and $[H_2O]$ indicate the concentration of reactants and water, respectively.

p is the order of the reaction with respect to reactant, and q is the order of the reaction with respect to water.

4.4.1 Model one

Considering zero order for water, the global power-law reaction rate can be expressed as:

$$-\frac{d[C_n]}{dt} = k[C_n]^p \quad (4.11)$$

Substituting C_n with $[TOC]$, equation (4.11) becomes,

$$\begin{aligned} &-\frac{d[TOC]}{dt} = k[TOC]^p \\ \Rightarrow &-\ln \frac{[TOC]}{[TOC]_0} = kt \quad [\text{Assuming first order reaction i.e } p=1] \end{aligned} \quad (4.12)$$

The experimental data of TOC at different temperatures are plotted as $-\ln[TOC]/[TOC]_0$ vs time as shown in Figure 4.4.

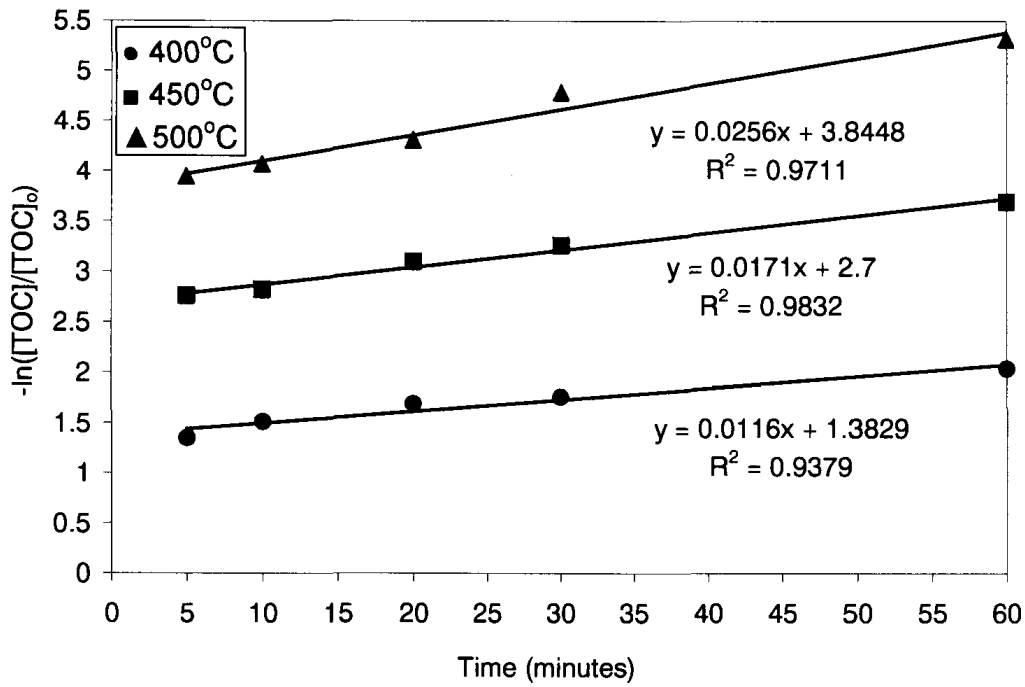


Fig. 4.4. Plot $-\ln([TOC]/[TOC]_0)$ against residence time for TOC decomposition in SCWG.

Figure 4.4 clearly shows a linear relationship with a slow reaction and the assumption of pseudo first order being applied. The slope can be attributed to the reaction rate constant k which has a dependency on temperature, normally expressed using the Arrhenius equation:

$$k = A \exp\left(\frac{-E}{RT}\right) \quad (4.13)$$

where A is the pre-exponential factor, E the activation energy, R the universal gas constant, and T is the temperature in Kelvin. To calculate the activation energy, equation (4.13) was transformed into the logarithmic form, which is plotted in Figure 4.5.

$$\ln k = \ln A - \frac{E}{RT} \quad (4.14)$$

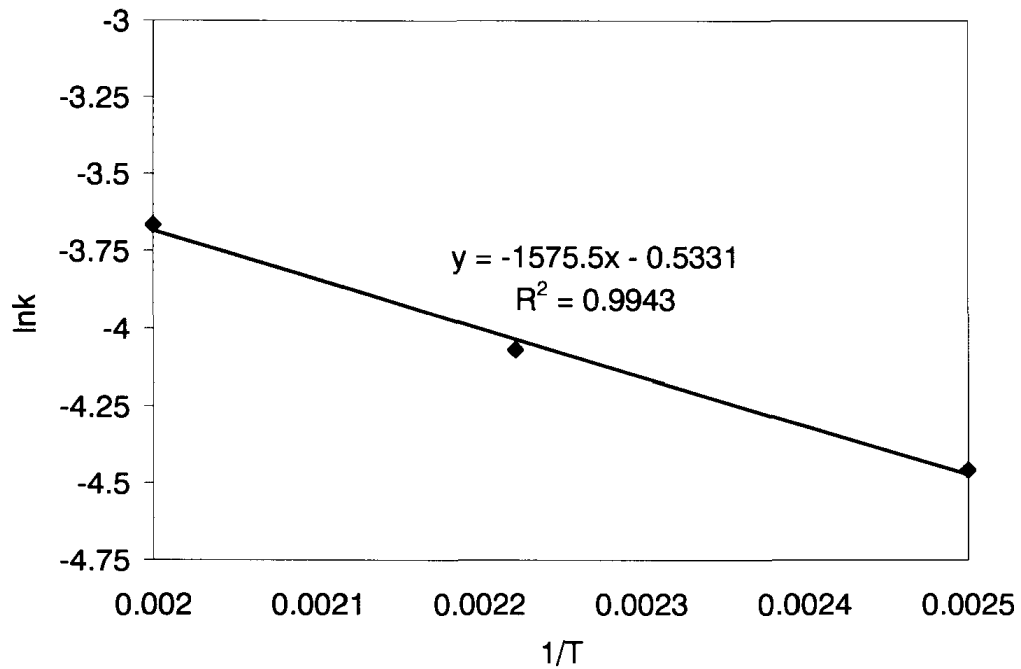


Fig. 4.5. Assumed first order Arrhenius plot for TOC decomposition in SCWG

From the intercept of Figure 4.5 the value of the pre-exponential factor is approximately 0.59 and from the slope, the activation energy E is calculated to be 1.3×10^4 J/mol and corresponding $k_{400\text{ }^\circ\text{C}} = 0.0565/\text{min}$, $k_{450\text{ }^\circ\text{C}} = 0.0664/\text{min}$, $k_{500\text{ }^\circ\text{C}} = 0.0765/\text{min}$. The model equation can be written as,

$$-\frac{d[\text{TOC}]}{dt} = 0.5868 \exp\left(\frac{-13098.71(\text{J/mol})}{RT(\text{K})}\right)[\text{TOC}] \quad (4.15)$$

Table 4.2 Summary of TOC data for model one.

Reaction Temperature (°C)	Reaction pressure (MPa)	Residence Time (minutes)	[TOC] ₀ mg/L	[TOC] mg/L	TOC conversion, $X=1-([TOC]/[TOC]_0)$	Predicted conversion (Eqn. 4.15)
400	25	5	18000	4660	0.741111	0.227500
400	25	10	18000	3956	0.780222	0.398389
400	25	20	18000	3310	0.816111	0.642333
400	25	30	18000	3094	0.828111	0.785222
400	25	60	18000	2340	0.870000	0.953944
450	25	5	18000	3090	0.828333	0.257778
450	25	10	18000	2910	0.838333	0.450167
450	25	20	18000	2209	0.877278	0.701222
450	25	30	18000	1878	0.895667	0.836056
450	25	60	18000	1220	0.932222	0.731667
500	25	5	18000	2570	0.857222	0.294000
500	25	10	18000	2278	0.873444	0.502500
500	25	20	18000	1790	0.900556	0.750444
500	25	30	18000	1112	0.938222	0.874833
500	25	60	18000	650	0.963889	0.984500

The parity plot of this model is shown in Figure 4.6. A large difference in the experimental and predicted model is observed in the parity plot, probably due to the invalid model assumptions. As shown earlier in Figure 4.4, it is evident that the

straight lines drawn for the experimental data do not go through the origin according to equation (4.12). Therefore the experimental reaction does not obey the model predicted, i.e. first order kinetics which means that the concentration of feed i.e. feed to water ratio has a large effect on TOC decomposition. Therefore the effect of water should not be ignored.

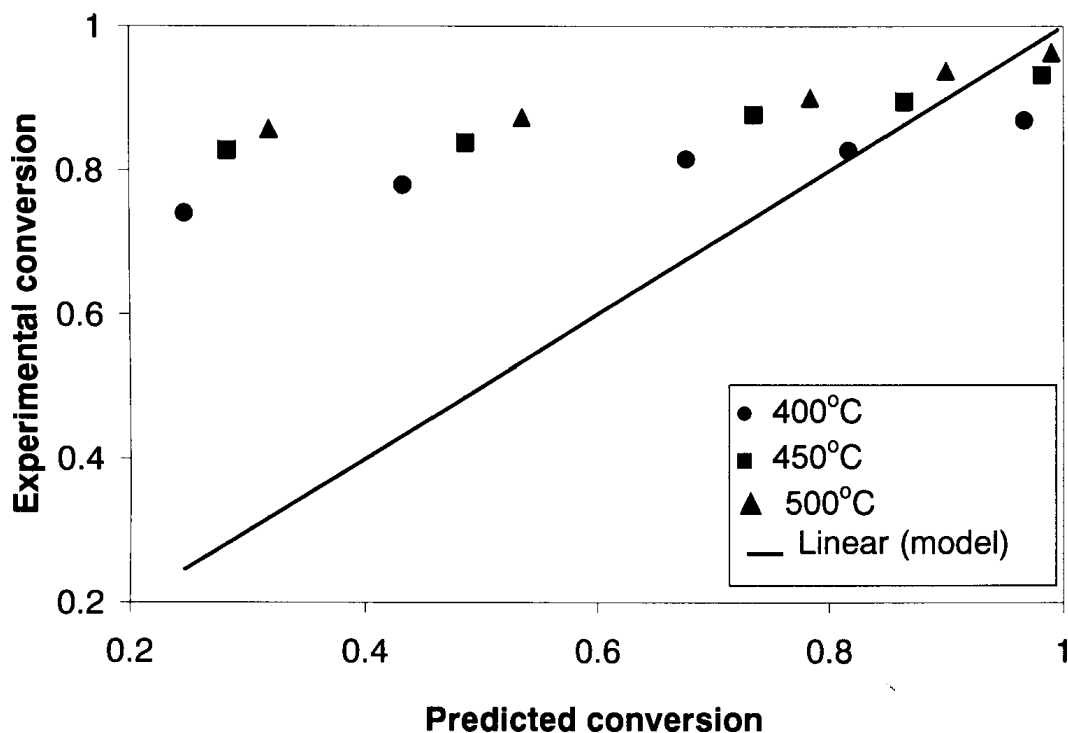


Figure 4.6: Comparison of the TOC conversion between experimental data and predicted values by model one.

4.4.2 Model two

Including the effect of water, the global power-law reaction rate can be expressed as:

$$-\frac{d[TOC]}{dt} = k[TOC]^p [H_2O]^q \quad (4.16)$$

Let's assume at time t, $[TOC] = [TOC]_0 (1-X)$ & $[H_2O] = [H_2O]_0 (1-Y)$

where, $[TOC]_0$ & $[H_2O]_0$ are the initial concentrations, X & Y are the conversion factors of TOC & H_2O respectively.

The relation of Y and X can be written as follows: $Y=aX$, where 'a' is a constant.

Therefore, the water concentration can be written as, $[H_2O] = [H_2O]_0(1-aX)$.

Equation (4.16) becomes:

$$\begin{aligned} -\frac{d[TOC]_0(1-X)}{dt} &= k[TOC]_0^p (1-X)^p (1-aX)^q [H_2O]_0^q \\ \Rightarrow [TOC]_0 \frac{dX}{dt} &= k[TOC]_0^p (1-X)^p (1-aX)^q [H_2O]_0^q \\ \Rightarrow \frac{dX}{dt} &= k[TOC]_0^{p-1} (1-X)^p (1-aX)^q [H_2O]_0^q \end{aligned} \quad (4.17)$$

The reaction rate constant k is a function of temperature described by equation 4.13.

To minimize cross-correlation between parameters, the Arrhenius equation can be rewritten as:

$$k = k_0 \exp\left[\frac{(-E_{app})}{R} \left(\frac{1}{T} - \frac{1}{T_m}\right)\right] \quad (4.18)$$

where, E_{app} is the activation energy and k_0 the pre-exponential factor and T_m being the centering temperature.

Substituting the value of k in equation (4.17),

$$\begin{aligned} \frac{dX}{dt} &= k_0 \exp\left[\frac{(-E_{app})}{R} \left(\frac{1}{T} - \frac{1}{T_m}\right)\right] [TOC]_0^{p-1} (1-X)^p (1-aX)^q [H_2O]_0^q \\ \Rightarrow \frac{dX}{dt} &= k_0 [TOC]_0^{p-1} [H_2O]_0^q \exp\left[\frac{(-E_{app})}{R} \left(\frac{1}{T} - \frac{1}{T_m}\right)\right] (1-X)^p (1-aX)^q \\ \Rightarrow \frac{dX}{dt} &= k' \exp\left[\frac{(-E_{app})}{R} \left(\frac{1}{T} - \frac{1}{T_m}\right)\right] (1-X)^p (1-aX)^q \end{aligned} \quad (4.19)$$

where, $k' = k_0[TOC]_0^{p-1}[H_2O]_0^q$

Equation (4.19) is a differential equation with 5 unknowns containing k' , E , p , q , a . As a non-linear regression is required to fit the rate of reaction, a Matlab program was developed to solve this differential equation by estimating the unknown parameter values.

Table 4.3 Summary of TOC data for model two.

Reaction Temperature (°C)	Reaction pressure (MPa)	Residence Time (minutes)	[TOC] ₀ mg/L	[TOC] mg/L	TOC conversion, X=1- ([TOC]/[TOC] ₀)	Predicted conversion (Eqn. 4.19)
400	25	5	18000	4660	0.741111	0.7227
400	25	10	18000	3956	0.780222	0.7808
400	25	20	18000	3310	0.816111	0.8267
400	25	30	18000	3094	0.828111	0.8489
400	25	60	18000	2340	0.870000	0.8802
450	25	5	18000	3090	0.828333	0.8101
450	25	10	18000	2910	0.838333	0.8498
450	25	20	18000	2209	0.877278	0.8809
450	25	30	18000	1878	0.895667	0.8958
450	25	60	18000	1220	0.932222	0.9168
500	25	5	18000	2570	0.857222	0.8632
500	25	10	18000	2278	0.873444	0.8914
500	25	20	18000	1790	0.900556	0.9134
500	25	30	18000	1112	0.938222	0.9239
500	25	60	18000	650	0.963889	0.9387

Confidence values can be calculated by minimizing the sum of square differences of the experimental and predicted conversions for all data points using the following equation [18]:

$$s^2 = \sum_i^{N_{\text{exp}}} (X_{\text{exp}} - X_{\text{pred}})^2 \quad (4.20)$$

The estimated pre-exponential factor k' and the activation energy are $(8.1 \pm 2)/\text{min}$ and $90.37 \pm 13.13 \text{ kJ/mol}$ respectively. The value of k is found to be $(8.5 \pm 0.32) \times 10^{-6} \text{ min}^{-1} \text{ ppm}^{-2.8}$. The experimental data led to reaction orders of $p=2.35$ for TOC, $q=1.45$ for water respectively. The value of constant 'a' was found to be 1.0199. The uncertainties reported here are 95% confidence intervals. The corresponding correlation coefficient (R^2) is 0.94. Finally the values of the established kinetic parameters were introduced into the power rate-law model equation. The differential equation was solved to predict the TOC conversion at different reaction times and temperatures.

Figure 4.7 shows a parity plot of the TOC conversion predicted from the global power rate law using the parameters derived from the experimental data against the rate obtained experimentally.

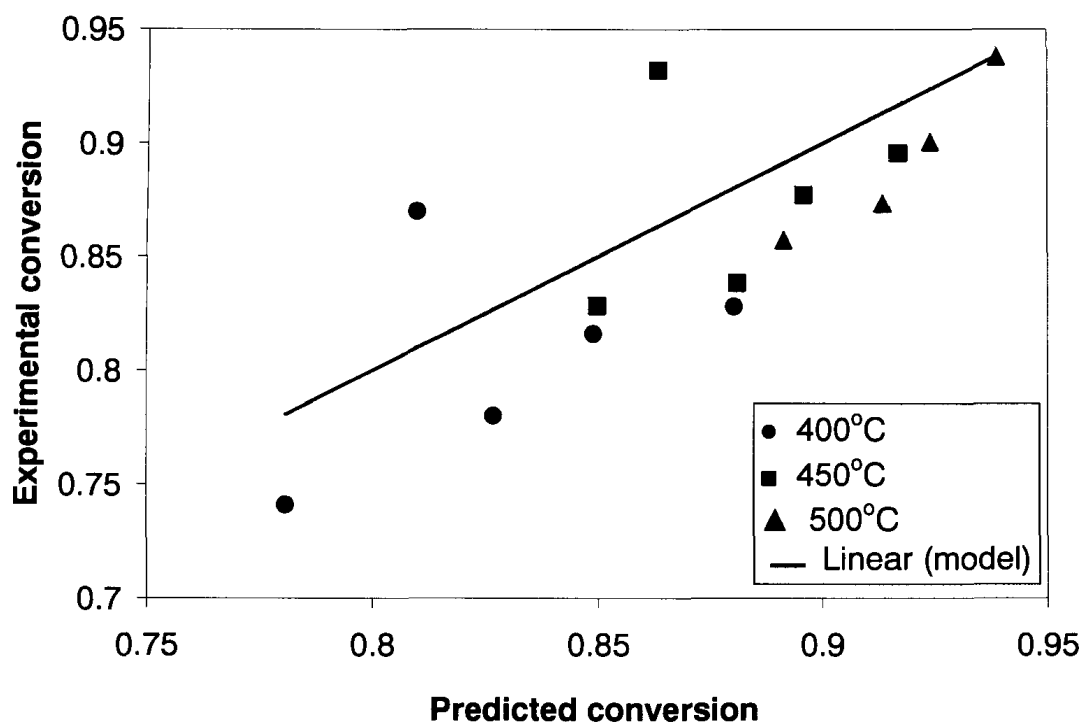


Fig. 4.7. Comparison of the TOC conversion between experimental data and predicted values by the power-law rate expression of the surface reaction (model two).

The predicted values are significantly closer to the experimental values i.e there is no large deviation between the experimental and predicted model in the parity plot (Figure 4.7 & Table 4.3) which is the desired model for TOC destruction of glucose in SCWG process.

4.5 Conclusion

Temperature and concentration have a large effect on TOC destruction and carbon gasification efficiency. Assumption of a first order reaction for TOC destruction of SCWG of glucose and ignoring water concentration due to the large excess led to an erroneous kinetic model development. A global kinetic model for TOC destruction was developed using non-linear regression, which convincingly fit the experimental results.

References:

1. Savage, P.E., *Organic chemical reactions in supercritical water*. Chemical reviews, 1999. **99**(2): p. 603-622.
2. Calzavara, Y., et al., *Evaluation of biomass gasification in supercritical water process for hydrogen production*. Energy Conversion and Management, 2005. **46**(4): p. 615-631.
3. Antal Jr, M.J., et al., *Biomass gasification in supercritical water*. Industrial & engineering chemistry research, 2000. **39**(11): p. 4040-4053.
4. Lee, I.G., M.S. Kim, and S.K. Ihm, *Gasification of glucose in supercritical water*. Industrial & engineering chemistry research, 2002. **41**(5): p. 1182-1188.
5. Hao, X.H., et al., *Hydrogen production from glucose used as a model compound of biomass gasified in supercritical water*. International Journal of Hydrogen Energy, 2003. **28**(1): p. 55-64.
6. Sinag, A., A. Kruse, and J. Rathert, *Influence of the heating rate and the type of catalyst on the formation of key intermediates and on the generation of gases during hydrolysis of glucose in supercritical water in a batch reactor*. Industrial & engineering chemistry research, 2004. **43**(2): p. 502-508.
7. Kruse, A., et al., *Gasification of pyrocatechol in supercritical water in the presence of potassium hydroxide*. Industrial & engineering chemistry research, 2000. **39**(12): p. 4842-4848.
8. Chowdhury, M.B.I., *Nickel-based Catalysts for Gasification of Glucose in Supercritical Water*. PhD Thesis, 2010.

9. Oshima, Y.; Tomita, K.; Koda, S., Kinetics of the Catalytic Oxidation of Phenol over Manganese Oxide in Supercritical water. *Ind. Eng. Chem. Res.* **1999**, *38*, 4183-4188.
10. Williams, P. T.; Onwudili, J., Composition of Products from the Supercritical Water Gasification of Glucose: A Model Biomass Compound. *Ind. Eng. Chem. Res.* **2005**, *44*, 8739-8749.
11. Jesus, P.; Boukis, N.; Czarnetzki, B. K.; Dinjus, E., Gasification of Corn and Clover Grass in Supercritical Water. *Fuel.* **2006**, *85*, 1032-1038.
12. Hologate, H. R.; Meyer, J. C.; Tester, W. J., Glucose Hydrolysis and Oxidation in Supercritical water. *AIChE J.* **1995**, *41*, 637-648.
13. Williams, P. T.; Onwudili, J., Composition of Products from the Supercritical Water Gasification of Glucose: A Model Biomass Compound. *Ind. Eng. Chem. Res.* **2005**, *44*, 8739-8749.
14. Youssef, E.A., et al., *Effect of nickel loading on hydrogen production and chemical oxygen demand (COD) destruction from glucose oxidation and gasification in supercritical water.* International Journal of Hydrogen Energy. 2010, **35**(10): p. 5034-5042.
15. Yu, D., M. Aihara, and M.J. Antal Jr, *Hydrogen production by steam reforming glucose in supercritical water.* Energy & Fuels, 1993. **7**(5): p. 574-577.
16. Kersten, S.R.A., et al., *Gasification of model compounds and wood in hot compressed water.* Ind. Eng. Chem. Res, 2006. **45**(12): p. 4169-4177.

17. Yan, Q., L. Guo, and Y. Lu, *Thermodynamic analysis of hydrogen production from biomass gasification in supercritical water*. Energy Conversion and Management, 2006. 47(11-12): p. 1515-1528.
18. Fogler, H. S., *Elements of Chemical Reactor Engineering*. Prentice Hall International (UK) Limited: London, 2000.

CHAPTER FIVE

Synthesis and characterization of mesoporous alumina with nickel & ruthenium incorporated for use in glucose gasification in supercritical water

5.1 Introduction

Metal supported aluminas are attractive catalysts for biomass gasification processes i.e converting biomass to bioenergy. One of the major problems related to the use of alumina catalysts is the deactivation by coke formation and pore plugging that hinders the diffusion of reactants and products both in and out from the catalyst particles [1]. It is well known that the larger the contribution of micropores to the specific surface area and the wider the pore size distribution, the greater the enhancement in the deactivation rate. Thus, synthesis of alumina catalysts with high mesoporosity properties (having well defined pore structure and size distribution) are of technological interest because of their applications ranging from catalysts, molecular sieves, separation technology and gas sensors, to batteries and electronics [2–3]. With the characteristics of mesoporous materials, such as highly uniform channels, large surface areas, narrow pore-size distributions, tunable pore sizes over a wide range, and so on, alumina with a mesostructure should possess excellent properties. In most applications and particularly catalysis, the pore structure, especially the pore size, size distribution and pore volume have become crucial factors determining the applicability of the porous materials.

Since the first successful synthesis of well-ordered, periodically organized mesoporous silica materials, such as members of the M41S [4] and SBA-15 families [5], efforts have been directed toward extending the group of mesoporous materials to non-silica systems [6]. In this contribution, ordered mesoporous Al_2O_3 has been synthesized which is an interesting and attractive material because of its applications as a catalyst support in heterogeneous catalytic reactions [7]. Although particular attention was previously devoted to the synthesis of mesoporous aluminas, unfortunately disordered structures with amorphous walls were fabricated in most cases because the hydrolysis behaviour of alumina is very complicated and strongly affected by acid, water, temperature, relative humidity, and other factors. This has given rise to rather strict synthetic conditions required for preparing ordered mesoporous aluminas [8-9]. Employing aluminum tri-*tert*-butoxide as the main inorganic precursor and anhydrous aluminum chloride as the pH adjustor and hydrolysis-condensation controller, Tian et al. [10] fabricated partially ordered mesoporous alumina. Zhang et al. obtained pseudo lamellar mesostructured γ -alumina with crystalline framework walls [11]. Niesz et al. first reported the synthesis of ordered mesoporous alumina with amorphous walls through a sol-gel route under strict control of the hydrolysis procedure as well as the condensation of reagents [12]. Kuemmel et al. fabricated ordered nanocrystalline mesoporous γ -alumina powders by aerosol generation of the initial solution using an atomizer [13]. After treatment at 700°C , γ -alumina was obtained which is stable up to 900°C . Liu et al. [14] developed an ordered crystalline mesoporous alumina molecular sieve with CMK-3 as hard template, which presented a new route to obtain ordered mesoporous alumina. However, this synthesis procedure requires multiple steps and is time-consuming.

From the viewpoint of synthesis, it is still a significant challenge to obtain γ -alumina with highly ordered mesostructures via a one-step, convenient, and economic approach. Moreover, the thermal stability and catalytic properties of ordered mesoporous alumina have not been studied in detail yet. The sol-gel route with block copolymers as the soft templates is an easily accessible, reproducible, and high-throughput method to synthesize highly ordered mesoporous aluminas with amorphous and/or crystalline γ -phase framework walls which exhibits a high thermal stability up to 1000°C, possess high surface areas, tunable pore sizes, and a large amount of surface Lewis acid sites [15]. Mesoporous alumina with well-ordered pore structure has also been synthesized by an ionic (anionic, cationic or non-ionic) templating method [16] or by using several different carboxylic acids as chemical templates at room temperature [17].

Since alumina is an important support in catalysis, the successful preparation of ordered mesoporous alumina (OMA) stimulates researchers to extend the templating approach to the synthesis of alumina-supported metal oxides with well-developed mesoporosity, relatively high surface areas, and crystalline pore walls. Supported Ni and Ru are two of the most common catalysts for biomass gasification in supercritical water (SCW). Ni has been identified as one of the best metals for tar elimination by catalyzing C–C bond breakage; as well as being able to catalyze O–H and C–H bond cleavage [18]. Ru is also active for C–C bond rupture and thus is able to catalyze the decomposition of tars and smaller molecules containing C and O [19]. In addition, Ru has been found to promote the water-gas shift reaction, which is important for high-selectivity H₂ production from biomass. The combined effect of Ni & Ru increased

carbon gasification efficiency (CGE) and total organic carbon (TOC) destruction for the gasification of glucose in SCW, as shown earlier in this thesis.

This study investigated the preparation, characterization and catalytic performance of a finely dispersed and thermally stable Ru & Ni catalyst incorporated into mesoporous Al₂O₃ by using different synthesis procedure such as templating and non-templating methods. The properties of the mesoporous catalysts (before & after evaluation) were characterized by means of BET surface area analysis, FTIR analysis, TGA, X-ray diffraction (XRD), Hydrogen temperature programmed reduction (H₂-TPR), Pulse chemisorption, Scanning electron microscopy (SEM), and Transmission electron microscopy (TEM). The catalytic activity and stability of the ruthenium & nickel incorporated mesoporous alumina were compared to those of the conventionally impregnated Ni & Ru catalyst on alumina for glucose gasification in SCW. To the best of our knowledge, this is the first report on an application of mesoporous Ru-Ni-Alumina catalyst to the gasification of biomass in supercritical water.

5.2 Experimental

5.2.1 Materials

Aluminum isopropoxide (C₉H₂₁O₃Al) (98%), Ruthenium (III) acetyl acetonate (C₁₅H₂₁O₆Ru) (97%), Poly(ethylene glycol)-block-poly(propylene glycol)-block-poly(ethylene glycol) (Pluronic P-123, (C₃H₆O.C₂H₄O)_x) were obtained from Aldrich (Mississauga, Canada), Nitric acid (68-70%) was obtained from Caledon Laboratory Chemicals (Georgetown, ON, Canada), Anhydrous isopropanol (purity 99.5%), Nickel nitrate hexahydrate (NiNO₃·6H₂O), Hexadecyltrimethyl ammonium bromide and glucose were obtained from Sigma–Aldrich (Oakville, Ontario, Canada).

5.2.2 Preparation & Characterization

Three different sol-gel synthesis methods using Pluronic P-123, Hexadecyltrimethyl ammonium bromide (surfactant) and without P-123 or surfactant were followed to examine the mesoporosity of the synthesized catalysts.

Synthesis of Ni & Ru incorporated ordered mesoporous alumina (OMA) using Pluronic P-123 was conducted according to the method of Yuan et al. [15]. Pluronic P123 was used as the template, and the alumina source was Aluminum isopropoxide. The required amount of ruthenium precursor, ruthenium (III) acetyl acetonate, the nickel precursor, nickel (II) nitrate hexahydrate and approximately 2 gm of Pluronic P123 were dissolved in 20.0 mL of anhydrous isopropanol and allowed to stir for 4 h. Then, approximately 20 mmol aluminum isopropoxide was dissolved in 3.2 mL of 68-70 wt % nitric acid and 10.0 mL of anhydrous isopropanol. Once dissolved, the two solutions were combined and 10.0 mL of anhydrous isopropanol was used to thoroughly transfer the aluminum isopropoxide solution. The combined solution was allowed to continue stirring for 5 h. Solvent evaporation was performed at 60°C for 48 h in air without stirring. The resulting sample was calcined at 700°C in a horizontal quartz tube furnace with a heating rate of 1°C/min under air and held at the final temperature for 6h.

Nickel and ruthenium incorporated mesoporous alumina by using hexadecyltrimethyl ammonium bromide as a surfactant was synthesized by a post-hydrolysis method at atmospheric pressure and at room temperature [20]. Known amounts of Aluminum isopropoxide (an aluminum source) and Hexadecyltrimethyl ammonium bromide (a surfactant) mixed with ruthenium acetyl acetonate and nickel nitrate hexa-hydrate was separately dissolved in anhydrous isopropanol, and the two solutions were then

mixed. Small amounts of water were dropped into the mixture, until a homogeneous precipitate was formed. The resulting slurry was further stirred for 48 h, and subsequently filtered and dried in air. The crude product was calcined at 700°C for 12 h with an excess stream of air. The temperature was increased to 700°C with a ramping rate of 1°C/min, and maintained at 700°C for 12 h to yield the final form.

For comparison, a nickel & ruthenium catalyst incorporated on alumina was prepared, similar to the preparation of simple metal oxide xerogel [21] without P-123 or surfactant. Aluminum isopropoxide was used as the xerogel support precursor. The required amount of aluminum isopropoxide (i.e. 20 gm for synthesizing 5 gm of catalyst) dispersed in isopropanol (80 ml) was placed in a 250 ml flask and the resultant mixture was kept under vigorous stirring at 75°C for one hour. To the cloudy sol, 0.3 ml of 1M nitric acid was added for peptization (formation of stable dispersion of colloidal particles) and the sol was refluxed with stirring at 75°C for 1h to obtain a clear sol. The appropriate amount of nickel nitrate and ruthenium chloride was dissolved in isopropanol with the individual solutions then added to the clear boehmite sol at 15 minutes intervals, with the resultant mixture refluxed at 75°C for 1 h with vigorous stirring. The sol was kept for three days at room temperature in a sealed flask for aging. After aging, the resultant gel was washed with acetone to remove any traces of solvent, nitric acid, etc. Acetone was removed under ambient drying. The sample was calcined at 700°C after ambient drying.

N₂ adsorption and desorption isotherms (Tristar II 3020, Micromeritics Instrument Corporation) were used to determine the surface area and total pore volume according to the BET and BJH models, respectively. Chemical bonds of the mixed-oxides and functional groups were investigated using an ATR-FTIR spectroscope (Nicolet 6700

FTIR). Thermo gravimetric-differential thermal analysis (TG-DTA) was carried out by a TGA/SDT A851 model gravimetric analyzer to describe the formation process of mesoporous catalyst. The crystalline structure of the supported catalysts was assessed using Powder X-ray diffractometry using CuK α radiation ($\lambda=1.5408 \text{ \AA}$) in the 2θ range from 2° to 82° . Temperature programmed reduction of hydrogen (H_2 -TPR) was performed on a chemisorption apparatus (Micromeritics Autochem 2920) to determine the reducibility as well as the optimum reduction temperature. The morphologies of both the fresh and spent catalysts were obtained from scanning electron microscopy (SEM) micrographs (model LEO1530) and transmission electron microscopy (TEM) images (model JEOL 2010F).

Temperature programmed oxidation (TPO) of the spent catalysts was performed to examine the characteristics of deposited carbonaceous products on the catalysts during reaction. The surfaces of the spent catalysts were also characterized by Raman spectroscopy using a Kaiser Optical Systems RXNI-785 with an excitation wavelength of 785 nm, BET, TG-DTA, SEM & TEM analysis.

5.2.3 Catalyst Testing

The synthesized catalysts were reduced with 5% hydrogen balanced with Ar at 600°C ($3^\circ\text{C}/\text{min}$) for 1 hour for activation. The reduced catalysts (synthesized by templates) were evaluated for glucose gasification in SCW which was carried out in a reactor from Autoclave Engineers, Erie, Penn, U.S.A, which was constructed from Hastelloy C-276 with a capacity of 600 ml with operating pressure of 36 MPa rating at 500°C . The reactor was heated with a 1.5 kW electric furnace that surrounded its main body supplied by the same manufacturer. A detailed description of the experimental setup and procedure was reported elsewhere by Youssef et al. [22]. Briefly, in a typical

experiment the required amount of catalyst was loaded along with 70 ml of deionized water which were injected into the reactor, which was finally purged with He for 10 minutes. The reactor was then pressurized to 0.7MPa with helium in order to prevent water evaporation and then heated to 500 °C. With the increase of temperature the reactor pressure increased to about 25 MPa at 500 °C. The required amount of glucose solution was then pumped into the reactor using a syringe pump (Isco Model 100 DX, Lincoln NE, USA). The initial reaction time (t_0) was started upon injection of the feed into the reactor. After 30 min reaction time, the products were cooled down to ambient temperature using a double pipe heat exchanger and separated by a gas-liquid separator operating by sudden expansion (from 0.635 inner diameter of stainless tube to 3 liter volume vessel). The product gas was then passed through a 2 micron filter to remove any remaining moisture and passed through an OMEGA mass flow meter (FMA 1700/1800 series 0-2 L/min, Laval, Quebec, Canada). The product gases were then collected in a 3L volume Tedlar gas sampling bag for subsequent analysis.

To determine the percent of gasification and hydrogen yield, the product gases were analyzed by gas chromatography (Shimadzu, GC-2014) using a 120/80 D Hayesep stainless steel Nickel packed column (Grace Davidson) with dimensions of 6.2 m x 3.18 mm, a thermal conductivity detector (TCD) and helium as the carrier gas. The gas yield, and carbon gasification efficiency (CGE), were calculated as shown in equations 1 and 2, as reported by Yu et al [23].

$$yield = \frac{\text{mol of gas produced}}{\text{mol of glucose in feed}} \quad (5.1)$$

$$CGE = \frac{\text{mol carbon in produced}}{\text{mol carbon in feed}} \times 100\% \quad (5.2)$$

The liquid effluents from the SCWG experiments were analyzed to measure the Total Organic Carbon (TOC) content using a TOC-VCPH (Shimadzu Instruments). The TOC decomposition X , was used to evaluate the extent of decomposition, as defined by:

$$\text{TOC decomposition, } X = 1 - \frac{[\text{TOC}]_e}{[\text{TOC}]_0} \quad (5.3)$$

where, $[\text{TOC}]_0$ is the initial TOC and $[\text{TOC}]_e$ is the residual TOC after reaction.

5.3 Results & Discussion

5.3.1 Characterization of mesoporous catalysts

Table 5.1 shows the BET surface area, pore volume and pore size of the synthesized mesoporous catalysts after removing the templates (calcined) and reduced at 600°C. The surfactant synthesis shows larger pore volume before and after reduction compared to the other two synthesis methods.

Table 5.1. BET surface area, pore size and pore volume of the synthesized mesoporous materials.

Synthesis method	Sample	Total surface area (BET) (m ²)	Pore volume (cm ³ /g)	Average pore size (nm)
Sol-gel by Pluronic P-123	0.5%Ru-11%Ni-Al ₂ O ₃	388	0.72	3.2
	0.5%Ru-11%Ni-Al ₂ O ₃ (reduced)	310	0.53	2.4
Sol-gel by surfactant	0.5%Ru-11%Ni-Al ₂ O ₃	398	0.74	2.4
	0.5%Ru-11%Ni-Al ₂ O ₃ (reduced)	316	0.55	2.3
Sol-gel without P-123 or surfactant	0.5%Ru-11%Ni-Al ₂ O ₃	296	0.54	2.7
	0.5%Ru-11%Ni-Al ₂ O ₃ (reduced)	15	0.04	---

As shown in Table 5.1, the pore properties of the nickel and ruthenium supported alumina is dependent on the synthesis conditions. The supported aluminas prepared by the investigated synthesis procedures show a narrow pore size distribution centred at 2-3 nm and typical type IV isotherms (Figure 5.1a) according to the Brunauer, Deming, Deming and Teller (BDDT) classification, indicating the presence of mesoporosity [24]. The supported alumina synthesized by P-123 has a much narrower hysteresis loop with nearly parallel adsorption and desorption branches following the H1 type IUPAC classification and suggestive of a highly ordered mesoporous structure with a narrow pore size distribution, as depicted in Figure 5.1(a & b). The location of the hysteresis loop in the N_2 isotherm can be used to determine whether the material possessed regular framework pores or interparticle voids, such as textural pores. The framework porosity at 0.4–0.7 P/P_0 in the N_2 isotherm indicates the porosity is contained within the uniform channels of the templated framework, while the textural porosity at 0.8–1 P/P_0 shows the porosity arising from the non-crystalline intra-aggregate voids and spaces formed by interparticle contacts [25]. The supported catalysts synthesized without template has a type II isotherm after reduction, indicative of a non-porous (or macroporous) structure whereas the other two catalysts still exhibited the similar behaviour even after reduction (Figure 5.1c). Figure 5.1d shows that the pore size distributions were very similar with the non-reduced catalyst, and the templated samples bear mesoporous structure. However, slight hysteresis between adsorption and desorption in the non-templated sample at high pressures is suggestive of the existence of mesopores. According to the pore size distribution analysed by the BJH model (Figure 5.1d), the supported catalyst synthesized by the surfactant method showed the narrowest range of pores size, with the majority around

2 to 4 nm after reduction. The distribution of mesopores in the reduced catalyst synthesized by P-123 was concentrated between 2 and 6 nm.

As shown in Table 5.1 and Figure 5.1a, the catalyst synthesized by surfactant shows a larger surface area with a high textural porosity and micropores than the catalyst synthesized by P-123 with only framework porosity. The H2 type hysteresis behaviour of the supported catalyst synthesized by surfactant implies that the pore size distribution and pore shape were not as well defined as the materials synthesized by P-123 method. The catalyst synthesized without any template shows a uniform pore size distribution, but poorly organized framework porosity due to its textural porosity. This suggests that this material contains irregular porosity that is similar to commercial alumina. Surfactant or P-123 materials show only the effect of the chemical template i.e. a regular pore size distribution.

The well-defined mesoporosity of the supported catalysts synthesized by P-123 or surfactant enabled much higher BET surface areas (i.e. 310 and 316 m²/g, respectively) after reduction than the supported catalyst (15 m²/g) synthesized without template, which proves that the templating synthesis technique strongly controls the mesoporosity of the catalysts. The mesoporous structure provides a different allocation of active sites and thus pathways for mass transfer whereas impregnation or non-templating synthesis causes destruction in the structure which ultimately reduces the surface area and pore volume of the materials.

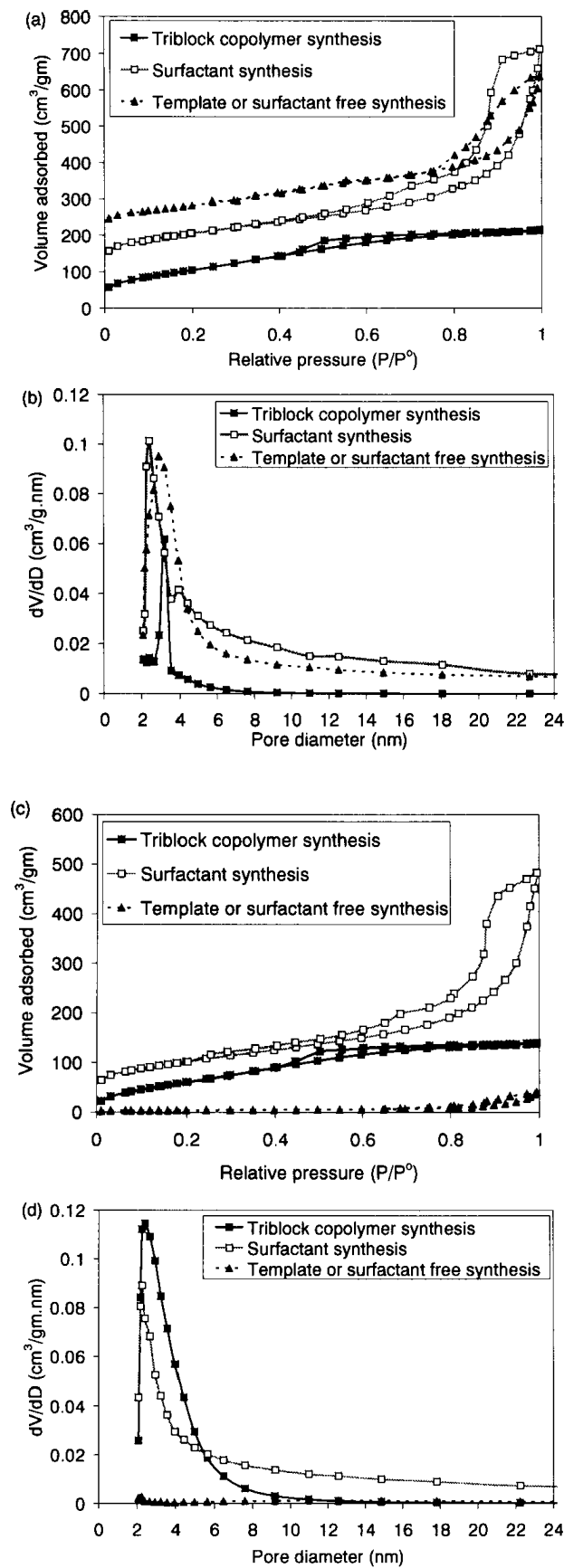
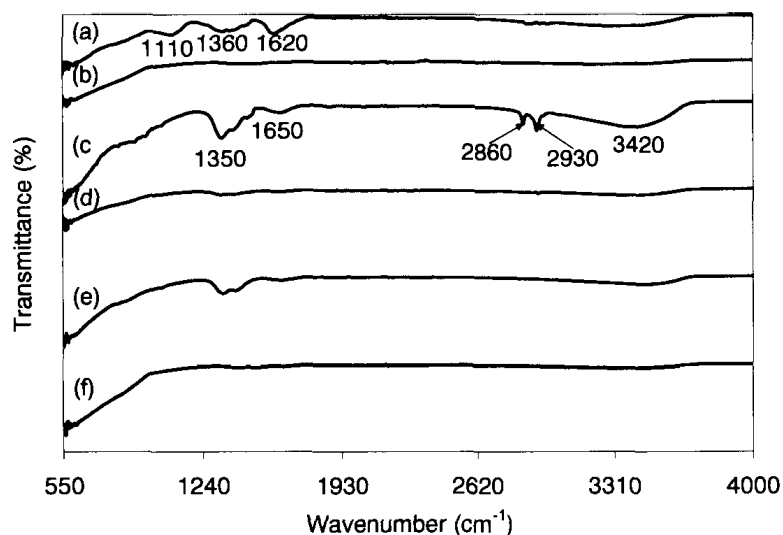


Figure 5.1. N_2 adsorption–desorption isotherms and pore size distribution of mesoporous catalysts: (a) & (b) calcined, (c) & (d) reduced respectively.

Figure 5.2(i) provides the ATR-FTIR traces of both the as-prepared and calcined samples. There was an absorption band for the as-prepared sample synthesized by P-123 at 1110 cm^{-1} which is responsible for alumina hydrate [26] which subsequently disappeared after calcination indicating the hydrolysis of aluminum iso-propoxide. There was a common peak observed at around $1350\text{-}1360\text{ cm}^{-1}$ for all the as-prepared samples. The peak in curve (a) shows symmetric carboxylate ($-\text{COO}^-$) at 1360 cm^{-1} indicating that nitric acid formed bridges between alumina and supported metals i.e metal-metal bonding during sol-gel reactions, in curve (c) shows N-O symmetric stretches at 1350 cm^{-1} indicating the micelle formation when metal solutions were added into the surfactants and in curve (e) shows C-H bending at 1350 cm^{-1} indicating the formation of undesired organic products in the sample respectively. All these peaks disappeared after calcination indicating the removal of P-123, surfactant and undesired organic compounds from the sample respectively. The strong peak in curve (a) at 1620 cm^{-1} and two broad peaks in curve (c) at 1650 & 3420 cm^{-1} are due to a characteristic peak of carboxylic acid ($-\text{COOH}$) and N-H bending & N-H stretching which disappeared after calcination, again indicating the removal of polymer and surfactant respectively. The two sharp peaks in curve (c) at 2860 and 2930 cm^{-1} indicate O-H stretching.

(i)



(ii)

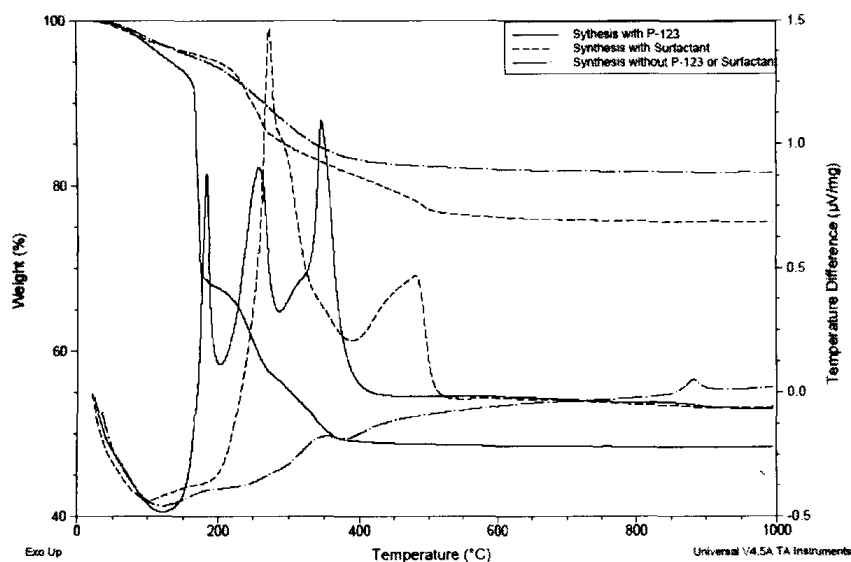


Figure 5.2. (i) ATR-FTIR analysis results of as-prepared and calcined mesoporous catalysts. (a), (c) & (e): as prepared samples and (b), (d) & (f): calcined samples synthesized by P-123, surfactant & without P-123/surfactant respectively. (ii) TG-DTA profiles of as prepared mesoporous catalysts.

Thermo gravimetric-differential thermal analysis (TG-DTA) of the aerogel catalysts was carried out to describe the formation process of mesoporous catalysts, as shown in Figure 5.2(ii). As combined with the IR results, there was only one weight loss observed for the as prepared catalyst synthesized without any template on heating to 400°C, corresponding to an endothermic peak (around 125°C) & two exothermic

peaks (350 & 875°C respectively) in the DTA curve (dotted dash line). Two weight losses were observed for the mesoporous catalysts synthesized by P-123 or surfactant on heating to 500°C, corresponding to one endothermic peak (around 125°C) & three exothermic peaks (180°C, 250°C & 350°C) in the DTA curve (solid line) for the as-prepared catalyst synthesized by P-123, for the as prepared catalyst synthesized by surfactant, one endothermic peak (around 125°C) & two exothermic peaks (300°C & 400-500°C) in the DTA curve (dashed line) are observed. In the case of the catalyst synthesized without P-123 or surfactant, the weight losses in the TG profile and the corresponding broad endothermic peak in the DTA curve resulted from the loss of condensate molecules from the as-prepared sample. The first exothermic peak is attributed to either removal of physically bound adsorbed organic molecules or the decomposition of nitrates. Another exothermic peak observed at 875°C in the DTA profile is attributed to a phase change to δ -alumina [27]. The as prepared sample synthesized by P-123 showed the endothermic and the first exothermic peaks for the loss of condensate molecules as well as residual organic solvents, the second exothermic peak for the removal of polymer and the third exothermic peak for the decomposition of nitrates respectively. Roughly, the weight loss that occurred for the catalyst synthesized by surfactant could be divided into three regions. The weight loss up to ca. 200°C can be attributed to the removal of residual organic solvent, bulk water and physisorbed water. The weight loss starting at ca. 200°C and 400°C can be attributed to the removal of surfactant molecules and the decomposition of ruthenium acetyl acetonates respectively.

H₂ pulse chemisorption analysis (Table 5.2) indicates that the templating synthesis method improves the percent metal dispersion compared to the non-templating

method. Metal dispersion is even much higher for the reduced catalysts synthesized by templates indicating the strong-metal support interactions in the catalyst surface. After reduction at 600°C, the metal particles supported on the reduced mesoporous material synthesized by P-123 were larger than the reduced material synthesized by surfactant, although their metal loading contents were similar. This is attributed to the different starting agents used as chemical templates. As shown in Fig. 5.3(i), the HNO₃ solution used for the P-123 templating synthesis exhibited a characteristic peak of carboxylic acid (–COOH, 1620 cm⁻¹) and a symmetric carboxylate (–COO⁻, 1360 cm⁻¹). The surfactant treated precipitate for the synthesis of mesoporous materials, however, shows an absorption band of N-O symmetric stretches. This indicates the asymmetric and symmetric stretching of carboxyl groups in the HNO₃ treated solution, but in the surfactant treated precipitate, a strong band of N-O symmetric stretches observed which means that when surfactant is used as a chemical template, metal particles may be present in the inner pores as a chemical template, where it then acts as a source of highly dispersed metals. When P-123 was used as the chemical template with HNO₃ solution, metal salts on the outside or near-entrance of the pores act as another metal source because of the rigid structure of P-123. After reduction, this metal source on the outside or near-entrance of the pores will aggregate, thus producing larger nickel particles. Therefore, surfactant synthesis provides more highly dispersed metal particles than P-123 synthesis. The reduced catalyst synthesized by the non-templating method also shows a significant high metal dispersion and small crystallize sizes. However, according to the N₂ adsorption-desorption isotherm and BJH adsorption model, the catalyst lost its porosity after reduction.

Table 5.2. Pulse chemisorption data.

Synthesis method	Sample	Metal dispersion (%)	Active particle diameter (nm)	Cubic crystallite size (nm)
Sol-gel by Pluronic P-123	0.5%Ru-11%Ni-Al ₂ O ₃	0.55	172.2	142.6
	0.5%Ru-11%Ni-Al ₂ O ₃ (reduced)	0.15	214.2	168.5
Sol-gel by surfactant	0.5%Ru-11%Ni-Al ₂ O ₃	0.68	110.5	125.5
	0.5%Ru-11%Ni-Al ₂ O ₃ (reduced)	0.21	158.3	153.6
Sol-gel without P-123 or surfactant	0.5%Ru-11%Ni-Al ₂ O ₃	0.33	108.7	93.9
	0.5%Ru-11%Ni-Al ₂ O ₃ (reduced)	0.07	126.2	106.8

Figure 5.3 shows the wide-angle XRD patterns for the three types of catalysts before and after reduction, allowing a comparison of the nature of the chemical interaction between the Ni & Ru catalyst particles and the support materials. There is no significant peak observed for the catalyst synthesized by the non-templating method, probably due to amorphous phase or small metal particle sizes, which is confirmed by chemisorption experiments. The supported mesoporous alumina prepared using P-123 as a chemical template shows an active alumina phase. On the other hand, mesoporous Ni & Ru supported Al₂O₃ is not a pure alumina material but co-exists with metal oxide. In addition, the active alumina phase overlaps with that of the nickel or ruthenium oxide or nickel aluminate-like material and shows a lower intensity peak compared to pure alumina. The XRD profiles of catalyst samples synthesized from P-123 showed NiO phases at $2\theta = 35.6, 43.6 \text{ \& } 63.5^\circ$ and RuO₂ phases at $2\theta = 28, 37.6$

& 54.6° . The sample prepared by surfactant showed NiO phase at $2\theta = 35.6$ and RuO_2 phases at $2\theta = 28$ & 54.6° , respectively. The reduced catalyst showed only metal phases. This shows that a complete reduction of ruthenium and nickel oxide species to Ru and Ni respectively and reduction temperature of 600°C used for catalyst reduction with H_2 was sufficient to reduce all the nickel and ruthenium oxides to Ni & Ru metals. The peak intensity of nickel in the reduced catalysts (b & d) proved the presence of larger crystallite sizes rather than the fresh catalyst (Table 5.3.2). No NiAl_2O_4 phase, which characterizes a spinel structure, appeared in the XRD profiles of the catalyst samples.

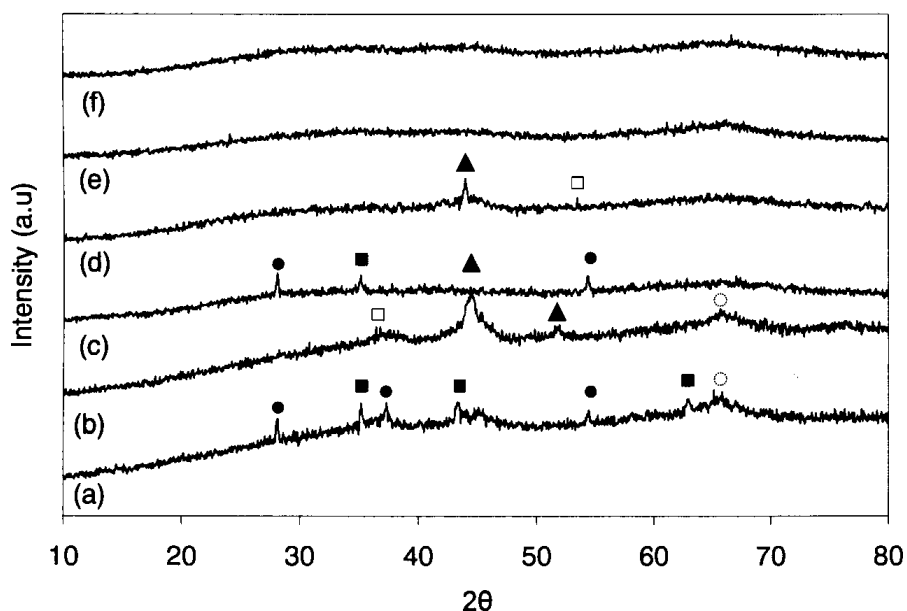


Figure 5.3. XRD patterns of mesoporous catalysts. (a), (c) & (e): fresh and (b), (d) & (f): reduced samples synthesized by P-123, surfactant & without P-123/surfactant respectively. (\circ Al_2O_3 , \blacktriangle nickel, \blacksquare NiO, \bullet RuO_2 , \square Ru).

Temperature-programmed reduction (TPR) has been extensively applied in recent years for characterizing reducible catalysts including metal and metal oxide systems. This technique allows the visualization of a profile of catalyst reduction which is required for studying low loading and highly dispersed systems whose characteristics

are beyond the limits of detectability by other direct structural analysis methods (e.g., X-ray diffraction). The TPR profiles of the synthesized catalysts are shown in Figure 5.4. The three calcined catalysts exhibit quite different peaks for H₂ uptake whereas the reduced catalysts showed a similar trend for H₂ uptake indicating that the metal species produced from metal–support interactions vary depending on the chemical and physical properties of the support and also the preparation conditions.

The catalyst synthesized by P-123 shows a main reduction peak centered at 120°C with a shoulder on the high temperature side at around 136°C, which likely denotes a bimodal dispersion of the RuO₂ phase [28]. The peak at around 200°C indicates the catalyst contains bulk RuO₂ species. In case of nickel species, the reduction peaks found at below 500°C show an easy-to-reduce Ni species with weak metal-to-support interactions, while above 800°C, the reduction peak shows a hard-to-reduce Ni species (i.e., nickel aluminate-like species) [29]. Therefore, the peak at around 650°C represents a strong nickel alumina interaction without forming any nickel aluminate like species since there is no peak between 750-812°C [30]. The reduced catalyst shows four reduction peaks at around 84, 200, 300 & 700°C. It has been reported that the low temperature reduction peak between 81-96°C can be assigned to the reduction of well-dispersed RuO_x species containing mainly RuO₂. The peak at 300°C represents the reduced catalyst which contains a small amount of bulk NiO. The peak intensity in the reduced catalyst at around 200 & 700°C indicates the presence of more bulk RuO₂ species rather than the calcined sample and maximum amount of nickel oxides have been reduced to nickel respectively.

The catalyst synthesized by surfactant shows different reduction peaks at 100, 190, 220, 290, 415, 700°C. The peak around 100 & 190°C indicates the reduction of well

dispersed & bulk RuO₂ species on the catalyst surface. The peak below 500°C indicates easy to reduce nickel species and the peak at around 700°C represents the strong nickel support interaction on the catalyst surface. The reduced catalyst also shows the bulk RuO₂ at around 155°C and bulk NiO at around 200 and 300°C. The intensity of the reduction peak at 600°C represents the reduction of nickel oxides species to nickel.

The template free synthesized catalyst (calcined and reduced) shows the bimodal dispersion of ruthenium oxide phase. The calcined one contains a small amount of bulk NiO. This non-templated catalyst also has a strong nickel-support interaction on the surface.

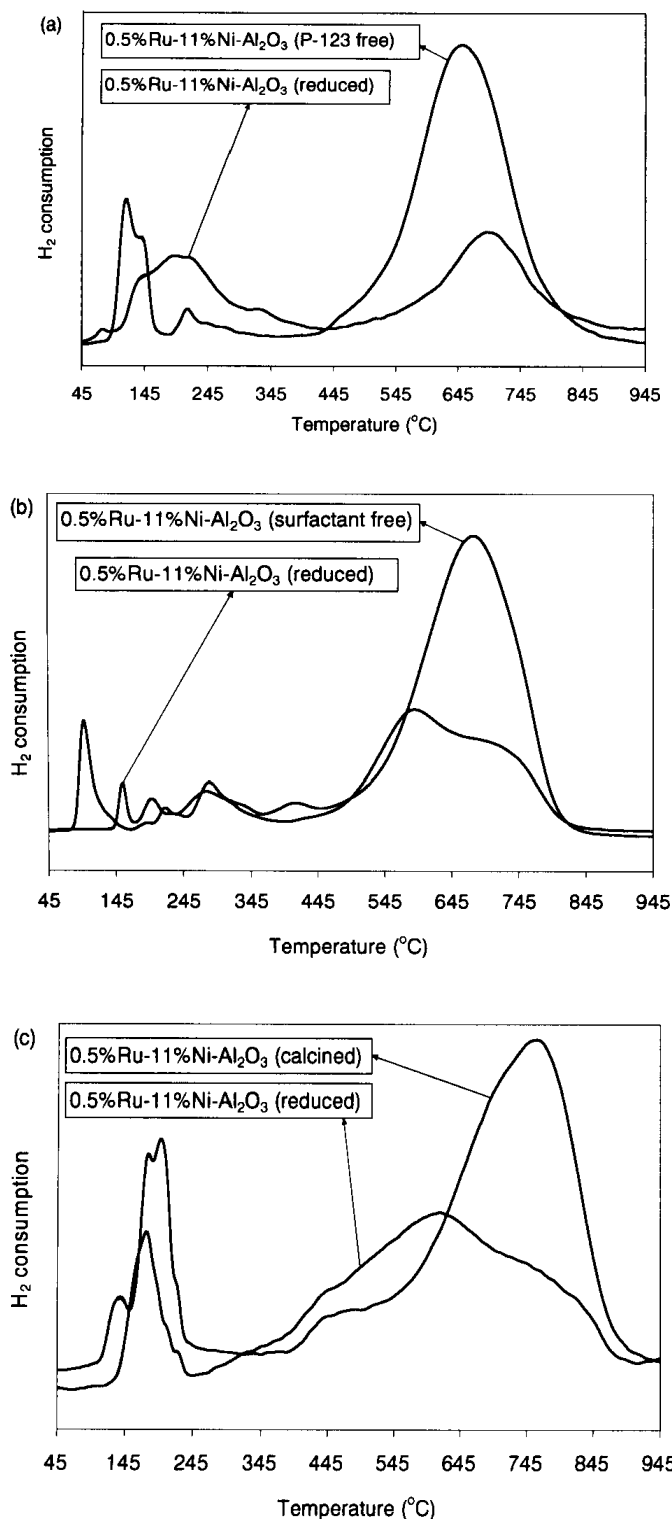


Figure 5.4. TPR curves of synthesized catalysts by (a) P-123 (b) surfactant (c) non-templating respectively.

The reducibility of the support is most likely related to the abundance of mobile oxygen. In ruthenium-promoted Ni catalysts, the position of the high-temperature peak shifts toward a lower temperature compared to that of the monometallic catalyst.

This suggests a promoting effect of Ru on the reduction of NiO particles, probably by the spillover of hydrogen dissociated on Ru to NiO [31]. In the TPR studies of mixed oxides, it has been reported that the two different metal oxides reduce independently in two stages because of the difference in the reduction temperature of the oxides [28]. However, in the presence of interaction between two metal oxides, the reduction of easily reducible metal oxide may enhance the reduction of the other metal oxide, depending on the degree of interaction between them. In the extreme case, both metal oxides may be reduced in a single stage. The present observations indicate that the catalysts behave as a mixture of nickel and ruthenium oxides as the reduction is mainly in two stages.

Figure 5.5 & 5.6 show the SEM & TEM images of the calcined and reduced catalysts. SEM and TEM images show the well ordered structure and less aggregation and small metal particles in the catalysts synthesized by P-123 or surfactant rather than that of non-templated synthesis, respectively. TEM images of the non-templated catalysts show agglomeration because of probably the low metal dispersion although the catalysts containing small metal particles. The TEM results coincide with the chemisorption and XRD results.

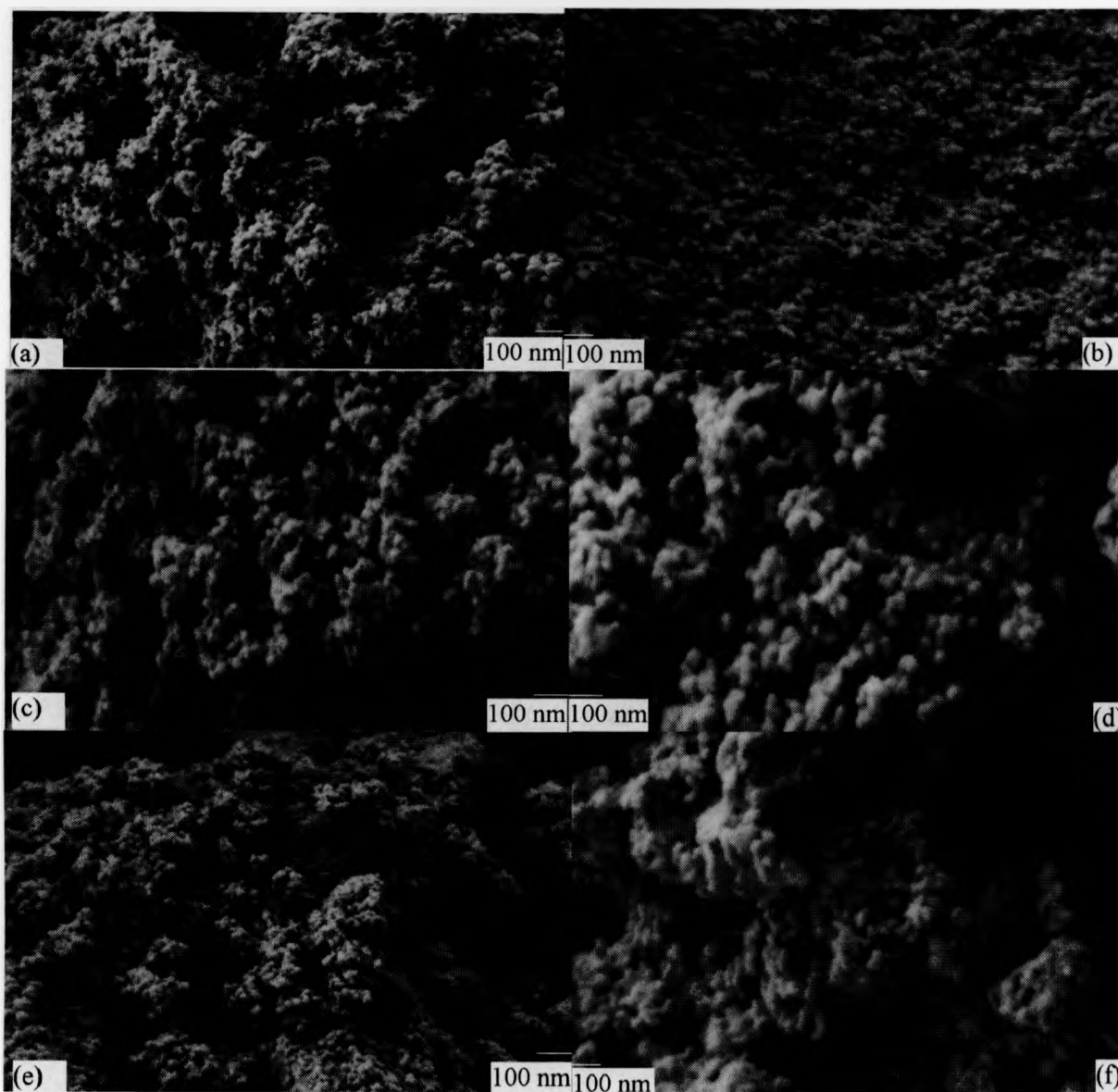


Figure 5.5. SEM images of mesoporous catalysts. (a), (c) & (e) and (b), (d) & (f): fresh & reduced catalysts synthesized by P-123, surfactant and without P-123/surfactant.

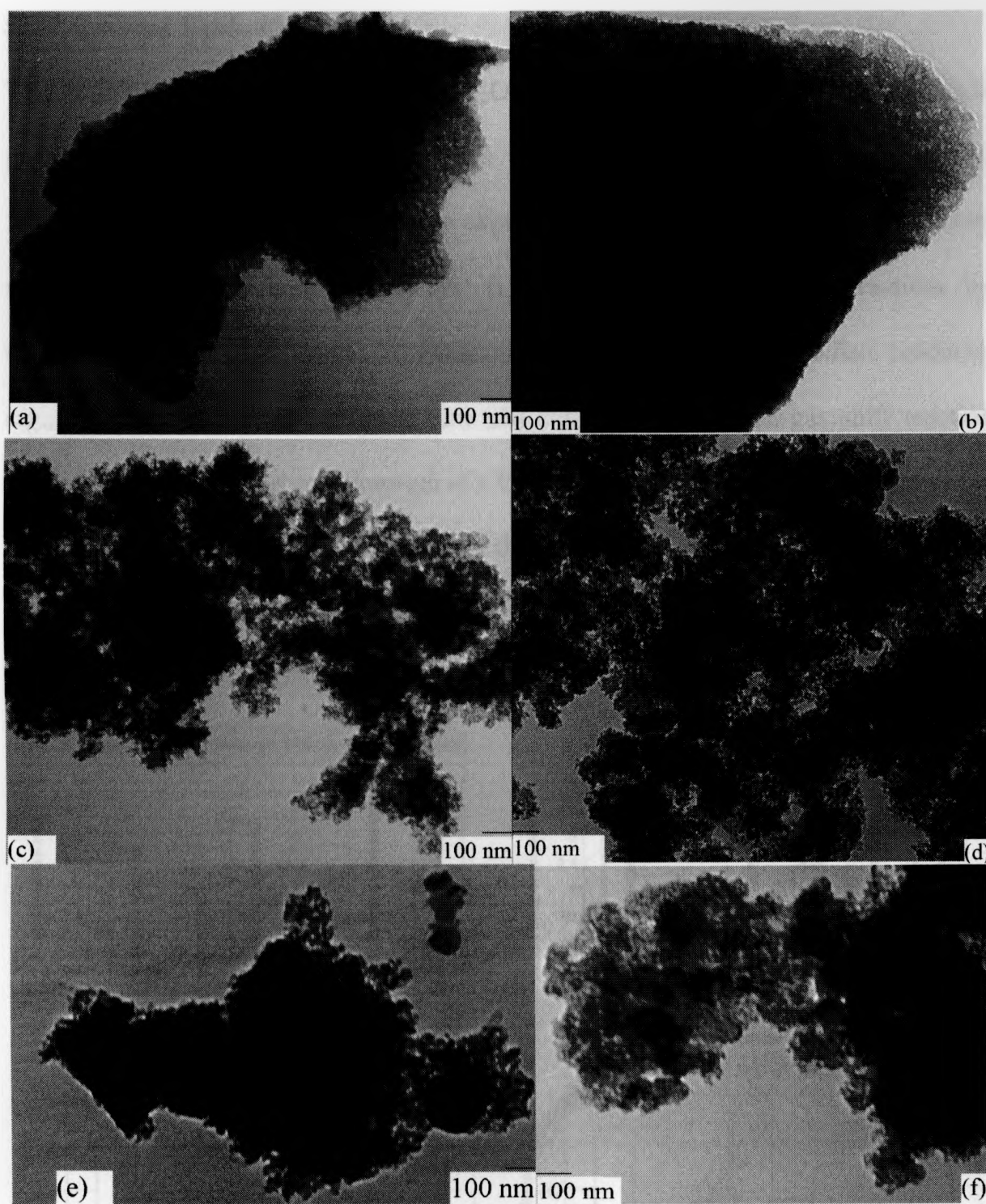


Fig. 5.6. TEM images of mesoporous catalysts. (a), (c) & (e) and (b), (d) & (f): fresh & reduced catalysts synthesized by P-123, surfactant and without P-123/surfactant.

5.3.2 Catalyst Evaluation

The activity of the supported Ru-Ni-Al₂O₃ catalysts in supercritical water glucose gasification at 400-500°C temperatures and 25 MPa pressure was evaluated. Mesoporous Ni-Ru-Al₂O₃ catalysts are expected to influence the product gas quantity and composition in three main ways: (i) improving coke cracking reactions by catalyzing C–C bond cleavage; (ii) enhancing the reforming of intermediate products, e.g., breaking C–O & C–H bonds; and (iii) enhancing the water–gas shift reaction towards maximizing the consumption of CO. Figure 5.7 compares the influence of the novel supported mesoporous catalysts on the accumulative H₂ yields as well as TOC destruction & carbon gasification efficiency measured during hydrothermal decomposition from 400 to 500°C in SCW, respectively.

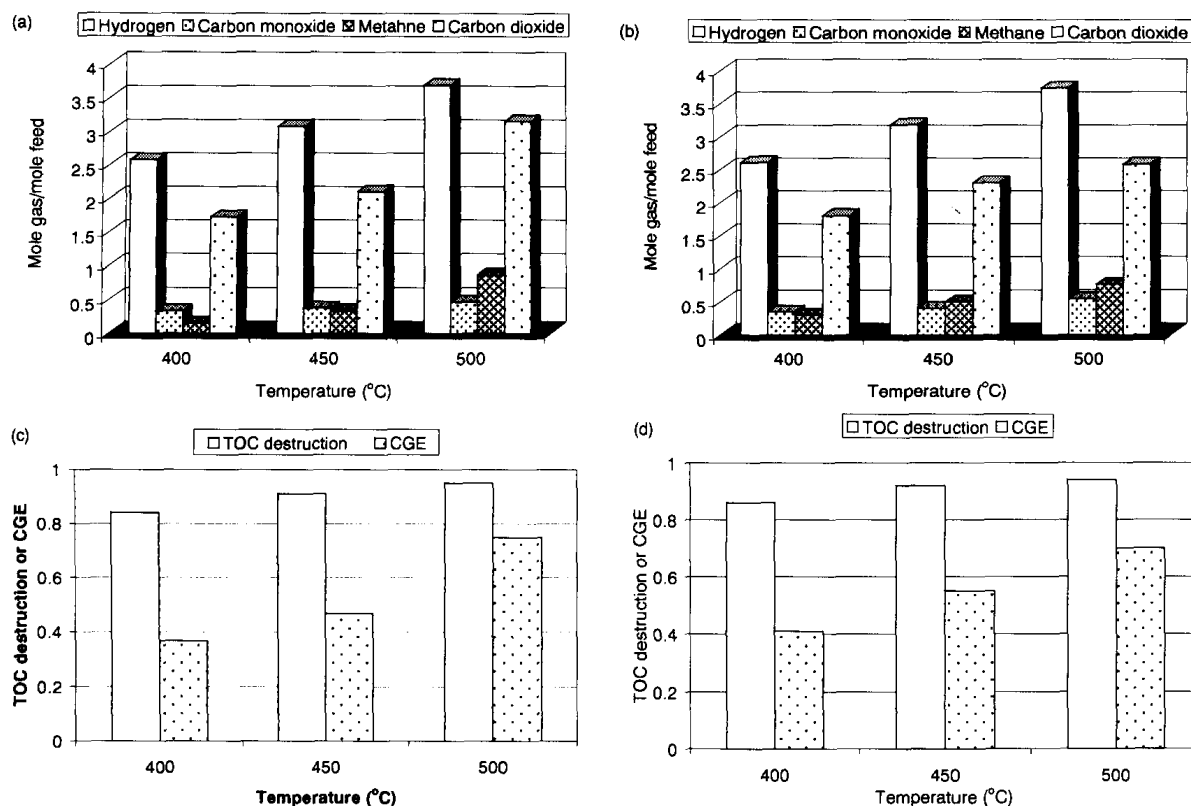


Figure 5.7. Gasification of glucose in supercritical water using mesoporous catalysts,

(a) & (c) synthesized by P-123 (b) & (d) synthesized by surfactant; t=30 min, Feed=

0.25M Glucose, Catalyst 1.0 gm.

Table 5.3 shows a comparative diagram of different synthesized catalysts. A significantly greater increase in H₂ production observed using mesoporus nickel and ruthenium supported catalysts compared to the impregnation & aerogel catalysts. The mesoporous catalysts greatly enhanced the water gas shift reaction by decreasing the carbon monoxide yield to produce high hydrogen yield, subsequently reducing the TOC value and increasing the carbon gasification efficiency.

Table 5.3. Comparing different catalysts activity for producing hydrogen & carbon monoxide yield, TOC destruction and CGE at 500°C.

Name of Catalyst	H ₂ yield (mole H ₂ /mole feed)	CO yield (mole CO/mole feed)	TOC destruction (%)	CGE (%)
None	1.82	1.57	65	60
11%Ni- θ Al ₂ O ₃ (impregnation)	2.60	0.93	80	65
0.5%Ru-11%Ni- θ Al ₂ O ₃ (impregnation)	3.14	0.75	96	80
0.5%Ru-11%Ni-Al ₂ O ₃ (aerogel)	3.47	1.79	97	99
0.5%Ru-11%Ni-Al ₂ O ₃ (P-123)	3.69	0.47	95	75
0.5%Ru-11%Ni- θ Al ₂ O ₃ (surfactant)	3.74	0.55	94	70

The nature of the metal-support interaction has a significant effect on the final catalytic activity. Metal supported catalysts that interact strongly with the alumina support exhibited good resistance against deactivation (discussed in chapter 3). Chu et al. [32] investigated the activity and stability of Ni-modified hexaaluminate for methane partial oxidation; concluding that the stable activity of the prepared catalyst resulted from an enhanced interaction of nickel species with the supporting material. In the TPR measurements shown in Figure 5.4, the reduction peak for the mesoporous catalysts prepared by the templating method appeared at a higher temperature than that for the impregnation method, indicating stronger metal-support interactions in the catalyst. The catalysts synthesized by different templating methods have also well ordered structures and little agglomeration which facilitate the observed high surface areas i.e closer contact between the reactants and catalyst sites giving high reaction rates.

Several possible factors need to be considered to explain the different metal-support interactions of the supported metal catalysts, including metal loadings, calcination conditions, and the surface properties of the support. It has previously been reported that hydroxyl-rich alumina derived from a sol-gel method exhibited a strong metal-support interaction and led to the formation of surface nickel aluminate, even at a relatively low temperature of 230°C [33]. In our experiments, mesoporous Ru-Ni-Al₂O₃ and impregnation Ru-Ni-Al₂O₃ (chapter 3) having almost the same level of ruthenium & nickel loading were prepared under the same calcination process. Therefore, we tentatively conclude that the strong metal-support interaction of the alumina based catalyst results from the surface properties of the alumina and the co-condensation process. The co-condensation step is presumed to provide an easier

route for providing strong metal-support interactions, which have significant effect on the final activity of the catalyst. In high temperature reactions, the catalytic stability toward deactivation results from carbon deposition and/or metal sintering and closely related to the extent of metal-support interaction. It is known that the stability of a catalyst is consistently enhanced with increasing metal-support interaction [32]. This result was clearly confirmed by the catalytic performance test, as shown in Figure 5.7. Although the impregnation catalyst exhibited a high hydrogen yield, it also showed a lower catalytic activity at higher temperature than the mesoporous catalysts. Therefore, it is concluded that the mesoporous catalysts maintained a more stable catalytic activity than the impregnation catalyst (Chapter 3).

Figure 5.3 shows the XRD patterns of the catalysts reduced at 600°C. Compared to the mesoporous catalysts, the impregnation catalyst showed the characteristic peaks of well-developed nickel crystallites (Chapter 3). The TEM images shown in Figure 5.6 are also consistent with the above result; finely dispersed nickel particles in the mesoporous alumina and partially aggregated large nickel particles in the impregnation alumina were observed. The latter case clearly indicates a low dispersion of nickel particles.

From the following discussion we can also understand why the synthesis procedure is important for catalysts, especially when required for use at high temperature. The first is related to the shapes of the catalysts themselves. The commercially available alumina examined in this work is composed of small nanoparticles. After calcination, the metal particles are doped uniformly on the alumina surface to an extent unobservable by XRD. Although metal particles are also formed homogeneously in the mesoporous catalysts, they are separated by a number of small pores because of

the steric effect. Therefore, it would be expected that metal particles on the impregnation catalyst are more easily aggregated than those on the mesoporous alumina during the catalyst pre-treatment step. Small pores of mesoporous alumina can serve as a barrier to prevent migration of metal particles. The second involves metal-support interactions. As evidenced by the TPR result, metal particles in the mesoporous alumina catalysts had a stronger interaction with alumina than that in the impregnation catalyst. This strong interaction in the mesoporous alumina is presumed to prevent aggregation of metal particles. Due to the strong metal-support interaction, the mesoporous alumina catalyst was difficult to be reduced. Thus, it is likely that the supported nickel catalyst with a smaller metal particle size maintained stable catalytic activity.

5.3.3 Characterization of spent catalysts

One of the major problems in using Ni-based catalysts is catalyst deactivation from carbon deposition and metal sintering [34]. Many efforts have been published in order to reduce the deactivation of Ni-based catalysts. The addition of a second metal to the Ni catalyst was reported to be one of the most efficient methods for maintaining catalytic activity [34, 35]. Our previous study (chapter three) also proved that incorporation of ruthenium into a nickel based catalyst reduced graphitic coke formation on the catalyst surface. It is also known that strong metal-support interactions inhibit carbon deposition and metal sintering [32].

Three types of carbon deposition may occur during high temperature gasification or reforming reactions i.e. atomic carbon, amorphous carbon and graphitic carbon. These three forms can be gasified at different temperature ranges of <250, 250-600 and >600°C, respectively [36]. The type of deposited carbon on the surface of catalysts

was characterized by temperature programmed oxidation (TPO) and Thermogravimetric-Differential Thermal Analysis (TG-DTA) as shown in Figure 5.8. There was only one weight loss observed for the spent catalyst synthesized by P-123 on heating to 300°C, corresponding to an endothermic peak (around 100°C) in the DTA curve (solid line), indicating the formation of atomic carbon on the catalyst surface. A similar peak was also present in the TPO curve of the spent catalyst further indicating the presence of atomic carbon. There was no other peak present in the DTA curve for amorphous or graphitic carbon whereas the TPO shows two different peaks at 260 and 560°C, which indicates the formation of a small amount of amorphous carbon, only identifiable by TPO. There was three significant weight losses observed for the spent catalyst synthesized by surfactant on heating to 300°C, corresponding to two endothermic peaks (around 80 & 160°C) and a small exothermic peak around 260°C in the DTA curve (broken dashed line). The first two peaks indicate the formation of atomic carbon and the small exothermic peak represents the formation of amorphous carbon on the catalyst surface. Similar peaks are also observed by TPO. TPO also shows another peak for amorphous carbon around 560°C. There was no significant peak observed for the formation of graphitic carbon which mainly deactivates the catalyst. Ruthenium metal itself along with the mesoporosity of the catalysts may play an important role in preventing graphitic coke deposition on the catalyst surface to enhance the hydrogen yield as well as to increase the CGE and TOC destruction. From the peak areas (TG-DTA & TPO), we can say that the mesoporous catalyst synthesized by surfactant was affected by more atomic carbon deposition compared to the catalyst synthesized by P-123 whereas the reverse

occurred for amorphous carbon. The combined effect may have slightly deactivated the corresponding catalysts.

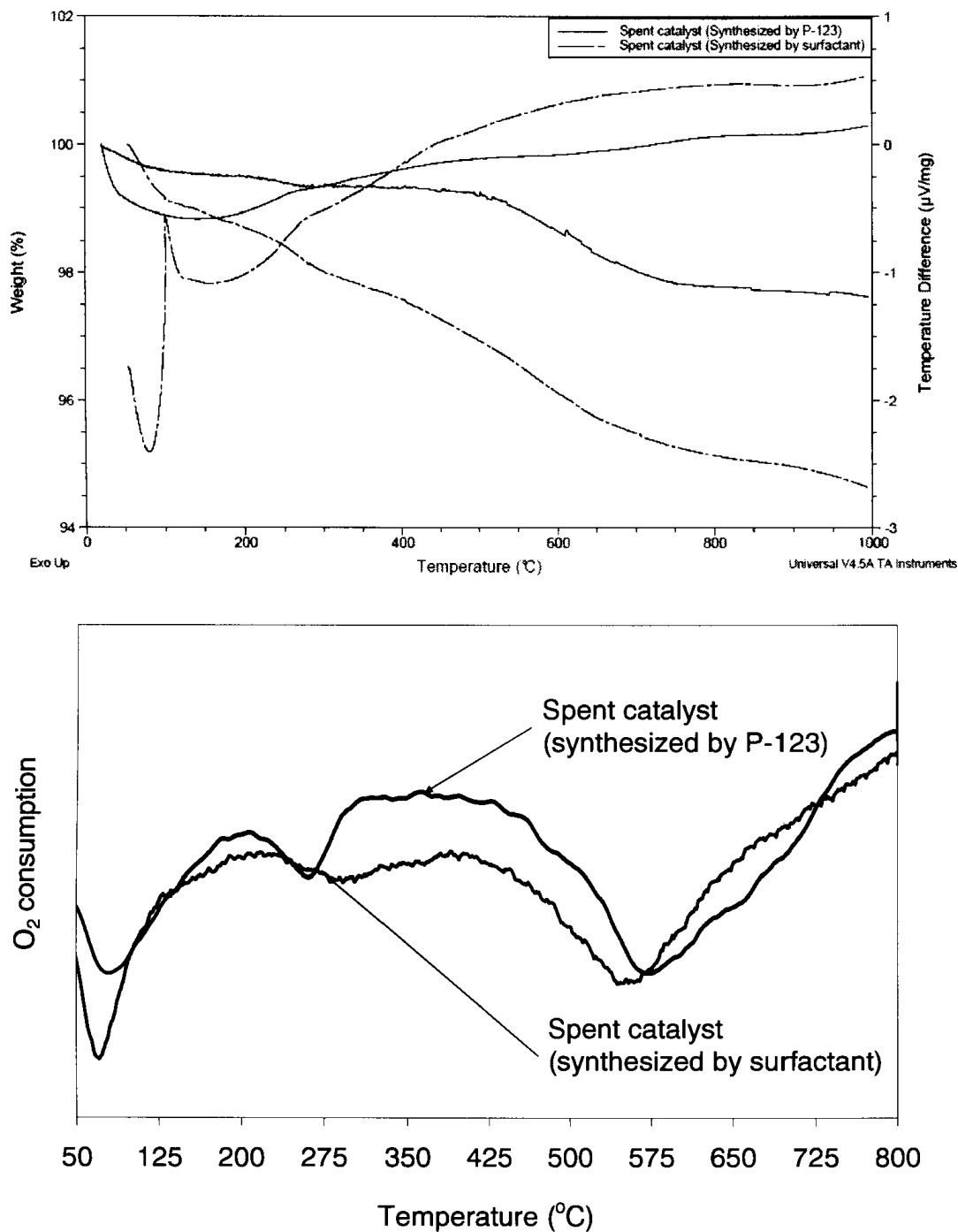


Figure 5.8. TG-DTA & TPO curves of spent catalysts.

No distinct diffraction peak of graphitic carbon (usually observed at 26.5° [37]) appeared in the XRD pattern for both mesoporous catalysts (Figure 5.9). There was no Raman spectrum observed for graphite in single crystal form (1580 cm^{-1}), which is

called the G band and polycrystalline, imperfect graphite & other types of carbon (1350 cm^{-1}), which is called the D band [38] (Figure 5.9).

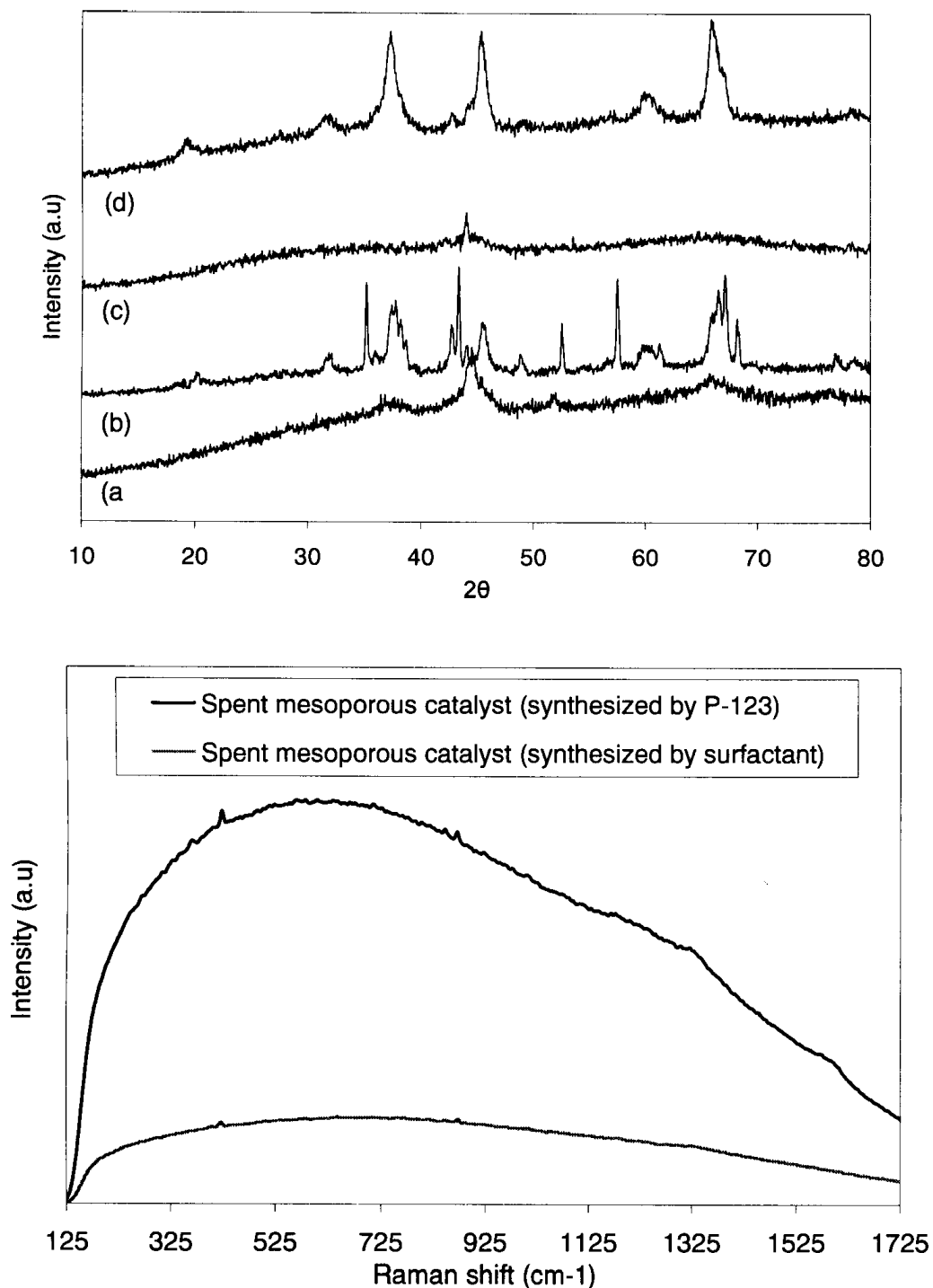


Figure 5.9. XRD (a&c: fresh reduced and b&d: spent mesoporous catalysts synthesized by P-123 & surfactant respectively) & Raman spectra of spent catalysts.

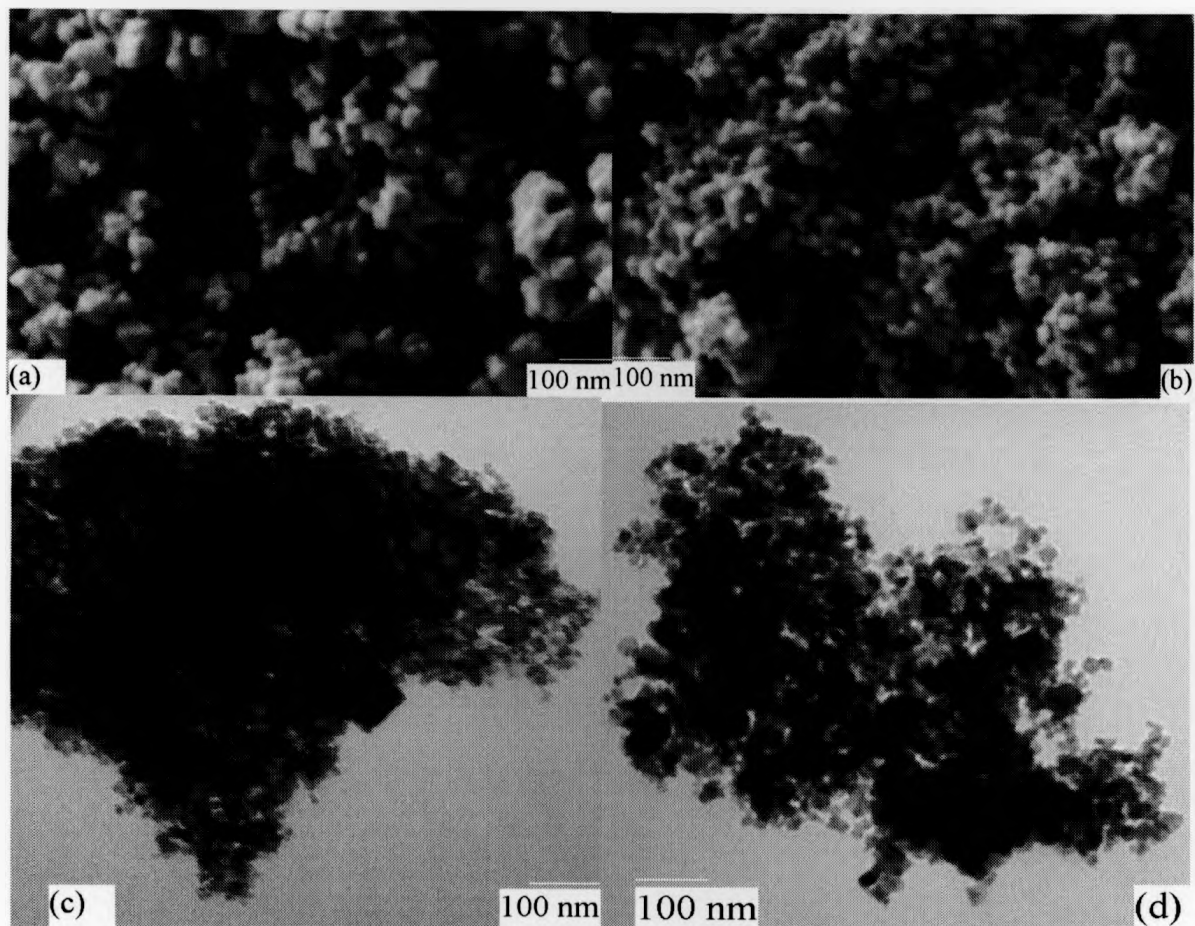


Figure 5.10. SEM & TEM images of spent catalysts (a&c: reduced catalyst synthesized by P-123 & b&d: reduced catalysts synthesized by surfactant).

SEM & TEM images (Figure 5.10) of the spent mesoporous catalysts show less agglomeration after supercritical water gasification. The spent catalysts exhibit the same mesoporosity like the fresh catalysts (Figure 5.11 & 5.1). The TPR profile of the spent catalyst synthesized by the surfactant method is similar to the profile of the fresh calcined catalyst although the spent catalyst synthesized by P-123 showed a negligible amount of hydrogen consumption indicating catalyst deactivation had occurred. The spent catalysts synthesised by the surfactant method can be reused by simply following oxidation for removing atomic and amorphous carbon and reduction steps, respectively.

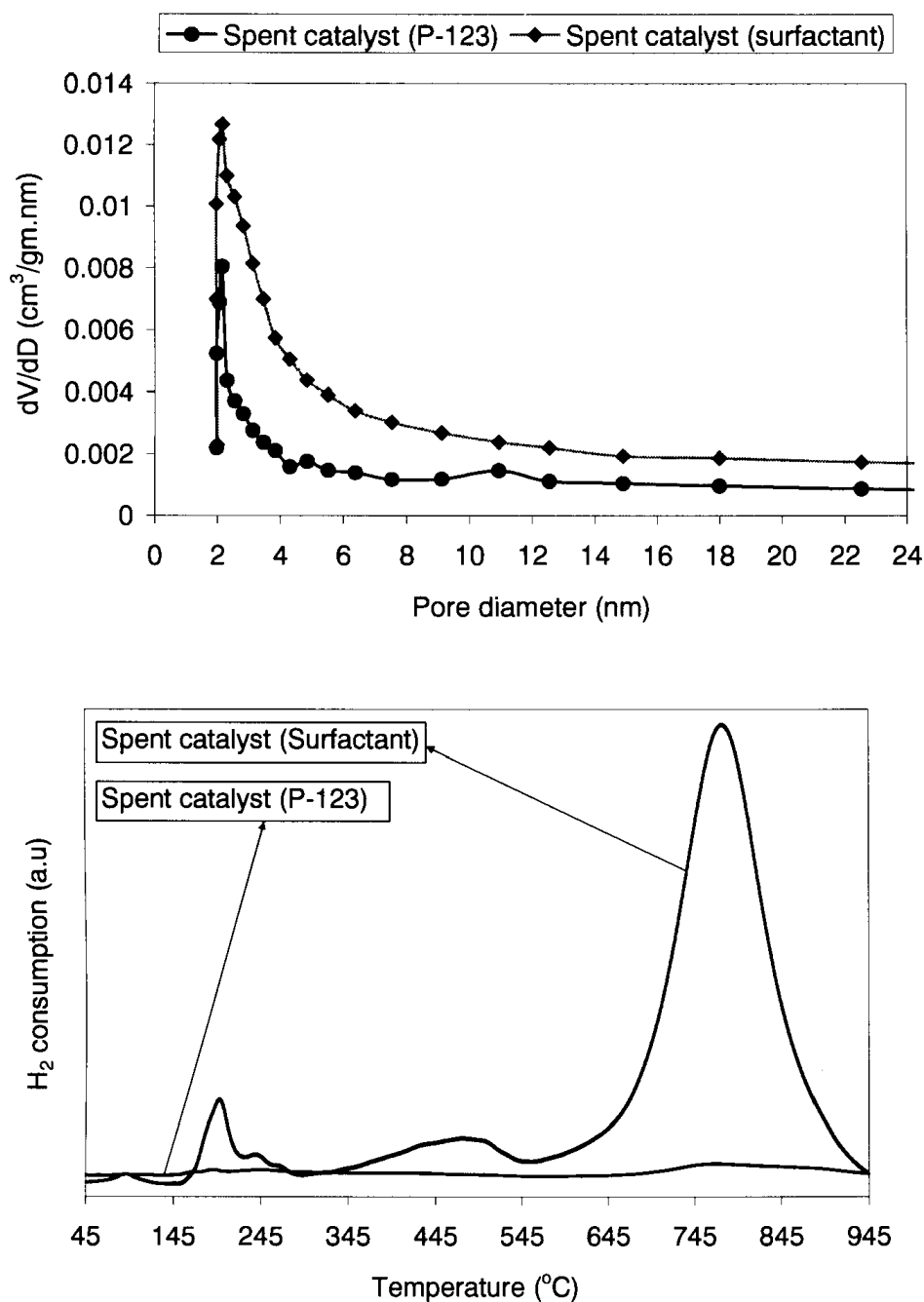


Figure 5.11. Pore size distribution & TPR curves for spent catalysts.

5.4 Conclusion

Mesoporous alumina catalysts that incorporate nickel and ruthenium (Ru-Ni-Al₂O₃) with 11% Ni & 0.5% Ru were synthesized by a one-step sol-gel method using Pluronic P-123 or hexadecyltrimethyl ammonium bromide as the templating agent. The catalyst prepared using P-123 showed well-developed framework porosity and a regular pore distribution, while the catalyst prepared using the surfactant showed a

developed framework and textural porosity and higher surface area than that of P-123. The prepared mesoporous Ru-Ni-Al₂O₃ supports could be used as catalysts only after a reduction step. Results showed that the mesoporous catalysts retained a relatively strong interaction of nickel and ruthenium species with alumina support, leading to finely dispersed nickel & ruthenium particles on the catalyst surface which reduced the graphitic coke formation during supercritical water gasification of glucose. The surfactant synthesized catalyst showed a better catalytic activity compared to that of P-123 and remained almost the same characteristics after gasification which makes the catalyst reusable. In addition, some feature of the catalysts, such as the surface area, pore volume, mesoporosity, metal particle sizes, metal dispersion etc were found to significantly affect the catalytic activity.

References:

1. Devi, L.; Ptasinski, K. J.; Janssen, F. J. J. G. *Pretreated olivine as tar removal catalyst for biomass gasifiers: Investigation using naphthalene as model biomass tar*. *Fuel Process. Technol.* **2005**, *86*, 707–730.
2. Davis, M.E., *Ordered porous materials for emerging applications*. *Nature*, 2002. **417**(6891): p. 813-821.
3. Kavan, L., et al., *Mesoporous thin film TiO₂ electrodes*. *Microporous and Mesoporous Materials*, 2001. **44**: p. 653-659.
4. Kresge, C.T., et al., *Ordered mesoporous molecular sieves synthesized by a liquid-crystal template mechanism*. *Nature*, 1992. **359**(6397): p. 710-712.
5. Zhao, D., et al., *Triblock copolymer syntheses of mesoporous silica with periodic 50 to 300 angstrom pores*. *Science*, 1998. **279**(5350): p. 548-552.
6. Soler-Illia, GJAA, Sanchez, C., Lebeau, B. & Patarin, J. *Chemical strategies to design textured materials: from microporous and mesoporous oxides to nanonetworks and hierarchical structures*. *Chem. Rev.* 2002. **102**: p. 4093–4138.
7. ejka, J., *Organized mesoporous alumina: synthesis, structure and potential in catalysis*. *Applied Catalysis A, General*, 2003. **254**(2): p. 327-338.
8. Bagshaw, S.A., E. Prouzet, and T.J. Pinnavaia, *Templating of mesoporous molecular sieves by nonionic polyethylene oxide surfactants*. *Science*, 1995. **269**(5228): p. 1242.

9. Bagshaw, S.A. and T.J. Pinnavaia, *Mesoporous alumina molecular sieves*. *Angewandte Chemie International Edition in English*, 1996. **35**(10): p. 1102-1105.
10. Tian, B., et al., *Fast preparation of highly ordered nonsiliceous mesoporous materials via mixed inorganic precursors*. *Chem. Commun.*, 2002(17): p. 1824-1825.
11. Zhang, Z. and T.J. Pinnavaia, *Mesostructured- Al_2O_3 with lathlike framework morphology*. *Journal of the American Chemical Society*, 2002. **124**(41): p. 12294-12301.
12. Niesz, K., P. Yang, and G.A. Somorjai, *Sol-gel synthesis of ordered mesoporous alumina*. *Chem. Commun*, 2005. **15**: p. 1.
13. Kuemmel, M., et al., *Thermally Stable Nanocrystalline Alumina Layers with Highly Ordered 3D Mesoporosity*. *Angewandte Chemie International Edition*, 2005. **44**(29): p. 4589-4592.
14. Liu, Q., et al., *Ordered crystalline alumina molecular sieves synthesized via a nanocasting route*. *Chemistry of materials*, 2006. **18**(22): p. 5153-5155.
15. Yuan, Q., et al., *Facile synthesis for ordered mesoporous γ -aluminas with high thermal stability*. *Journal of the American Chemical Society*, 2008. **130**(11): p. 3465-3472.
16. Yang, P., et al., *Block copolymer templating syntheses of mesoporous metal oxides with large ordering lengths and semicrystalline framework*. *Chemistry of materials*, 1999. **11**(10): p. 2813-2826.

17. Kim, Y., B. Lee, and J. Yi, *Synthesis of mesoporous -alumina through pre-and post-hydrolysis methods*. Korean Journal of Chemical Engineering, 2002. **19**(5): p. 908-910.
18. Sutton, D., B. Kelleher, and J.R.H. Ross, *Review of literature on catalysts for biomass gasification*. Fuel processing technology, 2001. **73**(3): p. 155-173.
19. Byrd, A.J., K.K. Pant, and R.B. Gupta, *Hydrogen production from glucose using Ru/Al₂O₃ catalyst in supercritical water*. Industrial & Engineering Chemistry Research, 2007. **46**(11): p. 3574-3579.
20. Kim, P., et al., *Synthesis and characterization of mesoporous alumina with nickel incorporated for use in the partial oxidation of methane into synthesis gas*. Applied Catalysis A: General, 2004. **272**(1-2): p. 157-166.
21. Schneider, M. and A. Baiker, *Aerogels in catalysis*. Catalysis Reviews, 1995. **37**(4): p. 515-556.
22. Youssef, E.A., et al., *Effect of nickel loading on hydrogen production and chemical oxygen demand (COD) destruction from glucose oxidation and gasification in supercritical water*. International Journal of Hydrogen Energy. 2010, **35**(10): p. 5034-5042.
23. Yu, D., M. Aihara, and M.J. Antal Jr, *Hydrogen production by steam reforming glucose in supercritical water*. Energy & Fuels, 1993. **7**(5): p. 574-577.
24. Everett, D.H., et al., *Reporting Physisorption Data for Gas/Solid Systems*. Pure Appl. Chem, 1985. **57**: p. 603.

25. Tanev, P.T. and T.J. Pinnavaia, *Mesoporous silica molecular sieves prepared by ionic and neutral surfactant templating: a comparison of physical properties*. Chemistry of materials, 1996. **8**(8): p. 2068-2079.
26. Mizushima, Y. and M. Hori, *Properties of alumina aerogels prepared under different conditions*. Journal of Non-Crystalline Solids, 1994. **167**(1-2): p. 1-8.
27. Ji, L., et al., *Synthesis of High-Surface-Area Alumina Using Aluminum Tri-sec-butoxide- 2, 4-Pentanedione- 2-Propanol- Nitric Acid Precursors*. Chem. Mater, 2000. **12**(4): p. 931-939.
28. Das, P.C., et al., *Carbon monoxide hydrogenation over various titania-supported Ru-Ni bimetallic catalysts*. Fuel processing technology, 2004. **85**(13): p. 1487-1501.
29. Kim, Y., et al., *A novel method for synthesis of a Ni/Al₂O₃ catalyst with a mesoporous structure using stearic acid salts*, J. Mater. Chem., 2003. **13**: p. 2353–2358
30. Lee, J.H., et al., *Stabilization of Ni/Al₂O₃ catalyst by Cu addition for CO₂ reforming of methane*. Applied Catalysis A: General, 2004. **269**(1-2): p. 1-6.
31. Jozwiak, W. K.; Nowosielska, M.; Rynkowski, J. *Reforming of methane with carbon dioxide over supported bimetallic catalysts containing Ni and noble metal: I. Characterization and activity of SiO₂ supported Ni-Rh catalysts*. Appl. Catal., A 2005, **280**: p. 233–244.
32. Chu, W., W. Yang, and L. Lin, *The partial oxidation of methane to syngas over the nickel-modified hexaaluminate catalysts BaNi_yAl_{12-y}O_{19-δ}*. Applied Catalysis A: General, 2002. **235**(1-2): p. 39-45.

33. Kharat, A.N., et al., *Decomposition of nickel formate on sol-gel alumina and characterization of product by x-ray photoelectron and TOF-SIMS spectroscopies*. Journal of Catalysis, 2002. **205**(1): p. 7-15.
34. Morioka, H., et al., *Partial oxidation of methane to synthesis gas over supported Ni catalysts prepared from Ni-Ca/Al-layered double hydroxide*. Applied Catalysis A: General, 2001. **215**(1-2): p. 11-19.
35. Basile, F., et al., *Rh-Ni synergy in the catalytic partial oxidation of methane: surface phenomena and catalyst stability*. Catalysis Today, 2002. **77**(3): p. 215-223.
36. Effendi, A., et al., *Steam reforming of a clean model biogas over Ni/Al₂O₃ in fluidized-and fixed-bed reactors*. Catalysis today, 2002. **77**(3): p. 181-189.
37. Mizushima, Y. and M. Hori, *Properties of alumina aerogels prepared under different conditions*. Journal of Non-Crystalline Solids, 1994. **167**(1-2): p. 1-8.
38. Darmstadt, H., et al., *Effects of surface treatment on the bulk chemistry and structure of vapor grown carbon fibers*. Carbon, 1997. **35**(10-11): p. 1581-1585.

Chapter Six

Conclusion

This thesis examined the development of new catalysts for the hydrogen production from model biomass compound glucose in supercritical water through different processes, such as impregnation, sol-gel process with supercritical CO₂ drying & sol-gel process with various templates. The most important factors for considering a material as catalyst are surface area, pore volume, mesoporosity, metal particle sizes, metal dispersion and metal support interactions etc. All these properties depend on how the catalysts are synthesized. Our studies have shown how all these properties vary depending on their different synthesis conditions and enhance the supercritical water gasification of glucose.

Non-noble metal catalysts such as Ni are most familiar for use in hydrothermal gasification because of their low cost but these catalysts lead to coke deposition during the gasification process. This thesis has shown that addition of small amounts of noble metal like Ru onto non-noble catalysts greatly reduces the graphitic coke deposition for supercritical water gasification of glucose. The synthesized catalysts improved the overall gasification efficiency (hydrogen & carbon gasification) as well as TOC destruction at moderate temperatures (400-500°C).

The detailed characterizations (fresh & spent catalysts) of all the synthesized catalysts open a new window for using them for gasification of real biomass at laboratory or an industrial scale. The kinetic modelling will also help to the researchers for understanding the reaction mechanism of real biomass gasification in SCW.

Future Works:

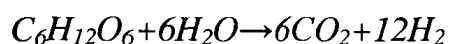
(i) Hydrogen is one of the alternatives of fossil fuel because of its environmental concern. A mixture of gases (mainly H₂, CO, CO₂, and CH₄) has been produced during biomass gasification in supercritical water. Metal organic frameworks (MOF's) might be used after supercritical water gasification for selective adsorption of gases to facilitate green fuel production including pure H₂ or syngas (CO+H₂) which can be used as a synthetic fuel.

(ii) Chowdhury, M.B.I [1] showed that lanthanum modified nickel based catalysts were found to inhibit the methanation reaction, along with graphitic coke formation and enhance the water gas shift reaction. Ru-La-Al₂O₃ catalyst can be evaluated for glucose gasification in supercritical water.

(iii) Titania or Zirconia can be used as the catalyst support instead of alumina as they have better corrosion resistant and could be more stable in the harsh SCW conditions.

(iv) Other model compounds (cellulose, lignin, hemicellulose, cystine etc.) and real life agricultural/industrial wastes, sewage sludge should be investigated at lower temperatures using catalysts.

(v) Since the goal of biomass gasification in SCW is to produce hydrogen rich gas, kinetic modelling should be developed considering hydrogen concentration. The following reaction may be the model reaction for supercritical water glucose gasification ignoring all other side reactions:



(vi) A continuous process should be developed with a few seconds residence time for evaluation of real life industrial viability.

Reference:

1. Chowdhury, M.B.I., *Nickel-based Catalysts for Gasification of Glucose in Supercritical Water*. PhD Thesis 2010.

APPENDIX

Selective Gas adsorption & Separation onto metal Organic Frameworks

7.1 Introduction

Release of harmful chemicals into our environment is a growing national security concern. A number of industrial chemicals produced in excess of 1 million tons/year worldwide are also highly toxic and can be obtained with relative ease. Effective capture of these chemicals is of great importance both to the protection of the environment and to those who are at risk for being exposed to such materials [1]. General-purpose filters are often composed of activated carbon impregnated with copper, silver, zinc, and molybdenum salts [2]. Although such filters have proven to be effective in containing a range of toxic gases, they are not adequately effective against all potential threats [3-4]. The current applications of activated carbons and any needed improvements towards its current performance are largely limited by lack of control over the metrics and functionality of the pores because of the highly amorphous nature of its carbon network. Such obstacles must be overcome if materials are to be developed to address any conceivable harmful chemical.

Over the past two decades, a new type of functional material called Metal-organic frameworks (MOFs) have emerged [5-8]. These are a new class of crystalline porous materials, the structure of which is composed of metal-oxide units joined by organic linkers through strong covalent bonds [9-10]. The flexibility with which these components can be varied has led to an extensive class of MOF structures with ultrahigh surface areas (up to 5900 m²/gm), far exceeding those achieved for porous

carbons [9]. They exhibit high thermal stability, with decomposition between 350°C and 400°C in the case of MOF-5 [11], ensuring their applicability across a wide temperature range. The unprecedented surface area and the control with which their pore metrics and functionality can be designed provide limitless potential for their structure to be tailored to carry out a specific application, thus suggesting the possibility of being superior to activated carbons in many applications.

Metal-organic frameworks (MOFs), also known as coordination polymers or coordination networks, are highly crystalline inorganic-organic hybrids constructed by assembling metal ions or small metal-containing clusters with multidentate organic ligands (such as carboxylates, tetrazolates, sulfoxolates) via coordination bonds (Figure 7.1). They can be one, two, or three dimensional infinite networks. Of these, three-dimensional MOFs with permanent porosity, which can also be termed as porous MOFs, are of the greatest interest because the voids inside the frameworks can accommodate guest molecules for a number of applications [7, 12].

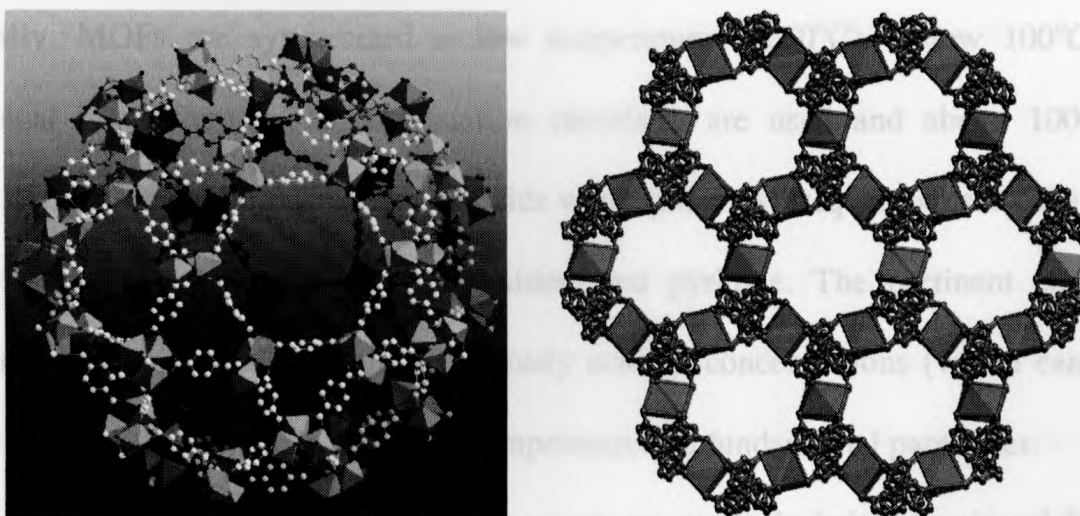


Fig. 7.1. Chromium-based MOF, MIL-101, at 5900 m²/g [13] & Mg-based MOF, at 714 m²/g [14].

Concerns about greenhouse gases in the atmosphere have led to significant interest in removing CO₂ from the exhaust streams of fossil fuel combustion as the first step in carbon sequestration [15, 16]. For flue gas, the high temperature and low CO₂ partial pressure makes this separation particularly challenging. Separations involving CO₂ are also important in a variety of other applications such as upgrading of natural gas and hydrogen purification. Adsorption and membrane based separation technologies hold many advantages for these problems, particularly because of their low energy requirements. Therefore, many materials have been investigated for CO₂ adsorption, including zeolites, other inorganic molecular sieves, and carbon-based materials [17-19]. MOFs are synthesized using organic linker molecules and metal joints that self-assemble to form materials with well-defined pores, high surface areas, and desired chemical functionalities [6, 7, 10, 12]. Because of these attractive properties, MOFs are promising candidates for CO₂ capture.

7.2 Synthesis Strategy of MOF's

Usually, MOFs are synthesized at low temperature (<250°C). Below 100°C, the classical ways familiar to coordination chemistry are used and above 100°C, a solvothermal procedure is required. Beside water (the most frequently used), the main solvents are alcohols, dialkyl formamides, and pyridine. The pertinent chemical parameters of the synthesis are pH (mostly acidic), concentrations (which can vary over a large range) and temperature. Temperature is a fundamental parameter.

Beside the classical methods, four new routes are currently being developed for the synthesis of MOFs. The first [20] uses a mixture of non miscible solvents for the hydrothermal synthesis (heavy alcohols and water, for instance). The solid forms at

the interface of the biphasic mixture and most of the time, provides single crystals of the desired phase.

The second approach represents the first trial for synthesizing MOFs using an electrochemical route [21]. Bulk copper plates (thickness 5 mm) are arranged as the anodes in an electrochemical cell with the carboxylate linker dissolved in methanol as solvent and a copper cathode. After a period of 150 mn at a (voltage: 12–19 V, current: 3 A), the greenish blue precipitate is formed.

The third concerns the microwave synthesis for MOFs. The microwave method has attracted growing attention for the synthesis of nanoporous inorganic materials which normally require several days for their hydrothermal crystallization. This provides an efficient way to synthesize them with short crystallization times, narrow particle size distributions, facile morphology control, and efficient evaluation of process parameters, etc [22]. However, the microwave method has rarely been applied to the synthesis of porous hybrid materials [23].

Finally, the richness of the possibilities of isolating new MOFs and the race for describing them has incited some authors to develop a dedicated application of high throughput synthesis to MOFs systems [24, 25]. High-throughput (HT) methods imply four major steps: design of experiment, synthesis, characterization, and data evaluation which have to be integrated in a workflow in order to reach a maximum of productivity and innovation. While HT-methods can produce a tremendous amount of data in a very short time, their success depends on proper application. Thus, the design of experiment is a step of paramount importance. Statistical methods in combination with data evaluation programs, genetic algorithms and neural networks have been shown to be powerful tools [26]. The number of reactions must also be

minimized by including chemical data and chemical knowledge into the synthesis set-up. In addition, investigations are most often limited to certain parameters, mainly composition, but can also process parameters such as temperature, time and pressure. MOF's contain two central components, connectors and linkers. These are defined as starting reagents with which the principal framework of the MOF's is constructed. In addition, there are other auxiliary components, such as blocking ligands, counteranions, and nonbonding guests or template molecules (Figure 7.2). The important characteristics of connectors and linkers are the number and orientation of their binding sites (coordination numbers and coordination geometries).

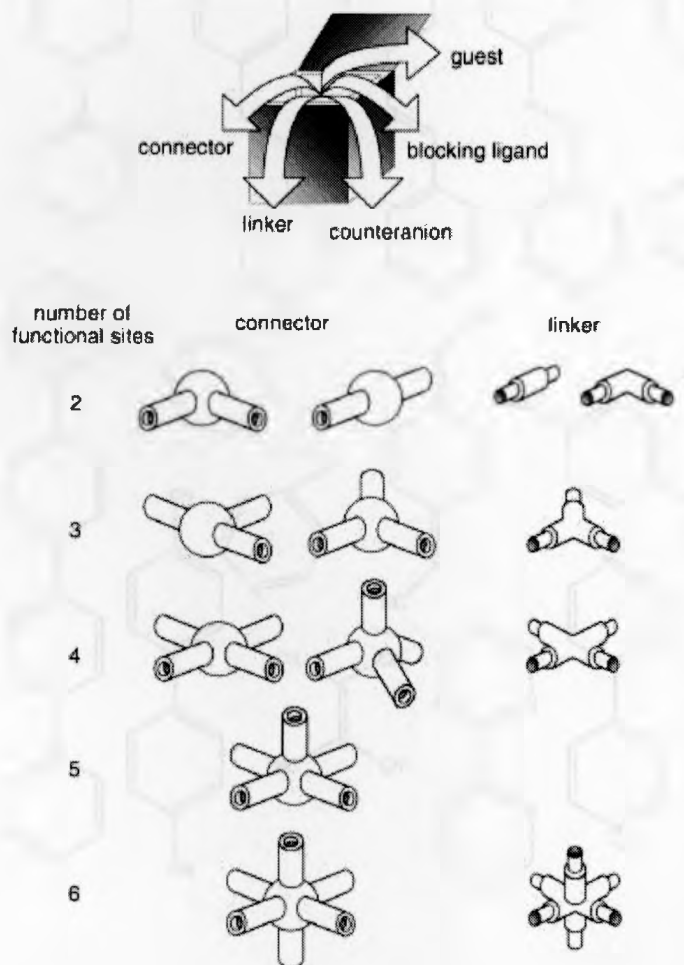


Fig. 7.2. Components of MOF [7].

Transition-metal ions are often utilized as versatile connectors in the construction of MOF. Depending on the metal and its oxidation state, coordination numbers can range

Linkers afford a wide variety of linking sites with tuned binding strength and directionality (Figure 7.3).

Various combinations of the connector(s) and linker(s) afford various specific structural motifs. Figure 7.4 shows representative motifs of frameworks constructed from various types of connectors and a linear linker.

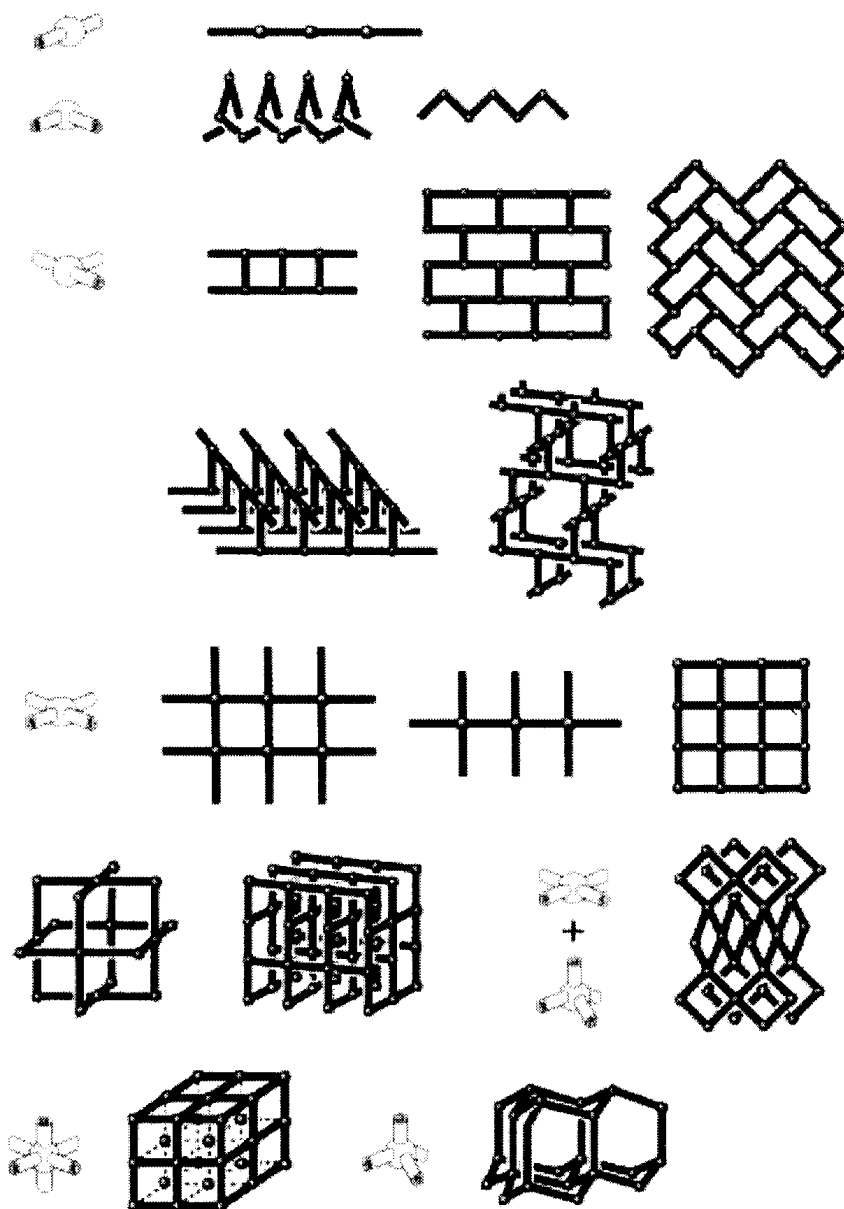


Fig. 7.4. The structural frameworks that can be constructed by using different connectors and linear linkers [7].

7.3 Experimental

7.3.1 Materials

All chemicals were obtained commercially and used without further purification. Anhydrous DMF (N,N-Dimethyl Formamide, 99.8%), HPLC grade CH₃OH (99.9%), Zn(NO₃)₂·6H₂O (99%), Mg(NO₃)₂·6H₂O (99%) from Sigma–Aldrich (Oakville, Ontario, Canada) & Chloroform (99.8%) from Caledon Laboratories Ltd., Georgetown, ON, Terphthalic acid (98%) & 2,5- Dihydroxy terphthalic acid (98%) from Aldrich, Mississauga, Canada, Anhydrous ethanol from Commercial Alcohols, Brampton, Ontario, HPLC grade H₂O from EMD Chemicals Canada.

7.3.2 Synthesis of MOF-5

MOF-5 crystals were synthesized by using terephthalic acid and zinc nitrate and anhydrous dimethylformamide (DMF, as the organic solvent. The MOF-5 was synthesized following the procedure described by Panella et al. [27]. In synthesis, the solvent DMF was first degassed by N₂ for 60 min, and then Zn(NO₃)₂·6H₂O (1.664 g, 5.60 mmol) and terephthalic acid (H₂BDC, 0.352 g, 2.12 mmol) were dissolved in 40 mL of degassed DMF solvent. The mixture was quickly transferred to a 50 mL glass vial and sealed. The vial was then heated to 130°C and held for 2 h under autogenous pressure by solvothermal synthesis. After the reaction, the vial was taken out of the oil bath and cooled down to the room temperature naturally. The cubic-like crystals of colorless powder were isolated by filtration and washed thoroughly with DMF in order to remove the unreacted zinc nitrate. After that, the crystals were immersed in chloroform (50 mL), sealed tightly, and put into the oven at 130°C for 3 days. During the heating process, the solvent was decanted and replenished every day. Finally, the

sample was dried under vacuum at 90°C overnight and stored in a desiccator until it was used.

7.3.3 Synthesis of Mg-MOF-74

Mg-MOF-74 was synthesized following the procedure described by Britt et al. [28]. In a solution of 135 mL dimethylformamide, 9 mL ethanol, and 9 mL water were dissolved 0.337 g 2,5-dihydroxyterephthalic acid and 1.4 g $\text{Mg}(\text{NO}_3)_2 \cdot 6\text{H}_2\text{O}$ with sonication. The resulting stock solution was decanted into fifteen 20 mL vials, which were capped tightly and heated at 125°C for 26 hrs. The mother liquor was then decanted, the products washed with methanol, then immersed in methanol. The products were combined and exchanged into fresh methanol daily for 4 days. They were then evacuated to dryness and heated under vacuum at 250°C for 6 hrs.

7.4 Results

The morphology of MOF-5 & Mg-MOF-74 were studied by scanning electron microscopy (SEM). Figure 7.5 shows SEM images of three dimensional cube-like microcrystals of MOF-5. Its morphology was consistent with the literature [27].

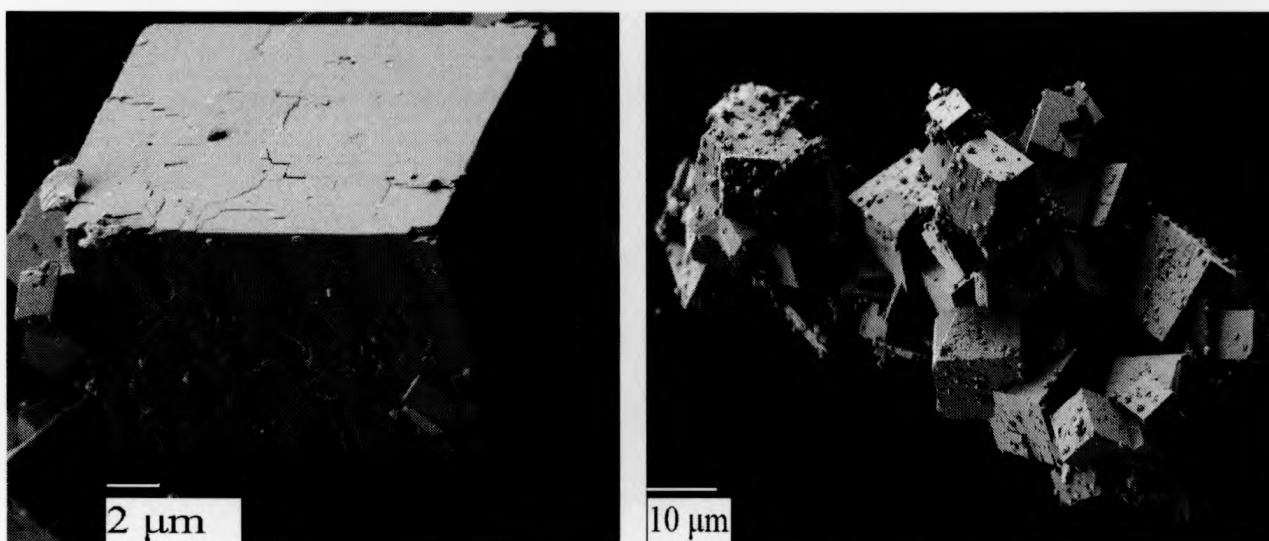


Fig.7.5. SEM images of MOF-5

Figure 7.6 shows rod like structure of Mg-MOF-74.



Fig. 7.6 SEM images of Mg-MOF-74

References:

1. McAtee M, et al., *Chemical Exposure Guidelines for Deployed Military Personnel*, eds Hauschild V, Johnson J (US Army Center for Health Promotion and Preventive Medicine, Aberdeen Proving Ground, MD), Reference document 2003. 230: pp 96–113.
2. Peterson, G.W., et al., *H-ZSM-5 for the removal of ethylene oxide: Effects of water on filtration performance*. *Industrial & engineering chemistry research*, 2008. **47**(1): p. 185-191.
3. Petit, C., et al., *Interactions of ammonia with the surface of microporous carbon impregnated with transition metal chlorides*. *The Journal of Physical Chemistry C*, 2007. **111**(34): p. 12705-12714.
4. Wood, O., *Activated carbon adsorption capacities for vapors*. *Carbon*, 1992. **30**(4): p. 593-599.
5. Kitagawa, S., R. Kitaura, and S. Noro, *Functional porous coordination polymers*. *Angewandte Chemie International Edition*, 2004. **43**(18): p. 2334-2375.
6. James, S.L., *Metal-organic frameworks*. *Chemical Society Reviews*, 2003. **32**(5): p. 276-288.
7. Eddaoudi, M., et al., *Modular chemistry: secondary building units as a basis for the design of highly porous and robust metal-organic carboxylate frameworks*. *Accounts of Chemical Research*, 2001. **34**(4): p. 319-330.
8. Yaghi, O.M., et al., *Reticular synthesis and the design of new materials*. *Nature*, 2003. **423**(6941): p. 705-714.

9. Li, H., et al., *Design and synthesis of an exceptionally stable and highly porous metal-organic framework*. Nature, 1999. **402**(6759): p. 276-279.
10. Rowsell, J.L.C. and O.M. Yaghi, *Metal-organic frameworks: a new class of porous materials*. Microporous and Mesoporous Materials, 2004. **73**(1-2): p. 3-14.
11. Eddaoudi, M., et al., *Systematic design of pore size and functionality in isorecticular MOFs and their application in methane storage*. Science, 2002. **295**(5554): p. 469.
12. Férey, G., *Hybrid porous solids: past, present, future*. Chemical Society Reviews, 2008. **37**(1): p. 191-214.
13. Férey, G., et al., *A chromium terephthalate-based solid with unusually large pore volumes and surface area*. Science, 2005. **309**(5743): p. 2040-2042.
14. Guo, Z., et al., *Magnesium-Based 3D Metal- Organic Framework Exhibiting Hydrogen-Sorption Hysteresis*. Inorganic Chemistry, 2009. **48**(17): p. 8069-8071.
15. Karl, T.R. and K.E. Trenberth, *Modern global climate change*. Science, 2003. **302**(5651): p. 1719-1723.
16. Keeling, C.D., et al., *Interannual extremes in the rate of rise of atmospheric carbon dioxide since 1980*. Nature, 1995. **375**(6533): p. 666-670.
17. Yazaydn, A.O., et al., *Enhanced CO₂ Adsorption in Metal-Organic Frameworks via Occupation of Open-Metal Sites by Coordinated Water Molecules*. Chemistry of Materials, 2009. **21**(8): p. 1425-1430.

18. Deroche, I., et al., *Adsorption of carbon dioxide in SAPO STA-7 and AIPO-18: Grand Canonical Monte Carlo simulations and microcalorimetry measurements*. *Adsorption*, 2008. **14**(2): p. 207-213.
19. Pawlesa, J., A. Zukal, and J. ejka, *Synthesis and adsorption investigations of zeolites MCM-22 and MCM-49 modified by alkali metal cations*. *Adsorption*, 2007. **13**(3): p. 257-265.
20. Forster, P.M., P.M. Thomas, and A.K. Cheetham, *Biphasic solvothermal synthesis: A new approach for hybrid inorganic-organic materials*. *Chemistry of Materials*, 2002. **14**(1): p. 17-20.
21. Mueller, U., et al., *Metal-organic frameworks-prospective industrial applications*. *Journal of Materials Chemistry*, 2006. **16**(7): p. 626-636.
22. Christmann, U. and R. Vilar, *Monoligated palladium species as catalysts in cross-coupling reactions*. *Angewandte Chemie-International Edition*, 2005. **44**(3): p. 366-375.
23. Kitagawa, S., et al., *An oxalate-linked copper (II) coordination polymer, $[Cu_2(oxalate)_2(pyrazine)_3]_n$, constructed with two different copper units: x-ray crystallographic and electronic structures*. *Inorganic Chemistry*, 1995. **34**(19): p. 4790-4796.
24. Stock, N. and T. Bein, *High Throughput Synthesis of Phosphonate Based Inorganic–Organic Hybrid Compounds under Hydrothermal Conditions*. *Angewandte Chemie International Edition*, 2004. **43**(6): p. 749-752.
25. Serre, C., et al., *Synthesis, structure and properties of related microporous N, N'-piperazinebismethylenephosphonates of aluminum and titanium*. *Chemistry of Materials*, 2006. **18**(6): p. 1451-1457.

26. Corma, A., et al., *A new mapping/exploration approach for ht synthesis of zeolites*. Chemistry of Materials, 2006. **18**(14): p. 3287-3296.
27. Panella, B., et al., *Hydrogen Adsorption in Metal–Organic Frameworks: Cu MOFs and Zn MOFs Compared*. Advanced Functional Materials, 2006. **16**(4): p. 520-524.
28. Britt, D., et al., *Highly efficient separation of carbon dioxide by a metal-organic framework replete with open metal sites*. Proceedings of the National Academy of Sciences, 2009. **106**(49): p. 20637.